May 2014

Characterization of Iron Response in Gynecological Cell Lines

Kyle A. Bauckman
University of South Florida, Bauckman5@aol.com

Characterization of Iron Response in Gynecological Cell Lines

by

Kyle Bauckman

A dissertation submitted in partial fulfillment
of the requirements for the degree of
Doctor of Philosophy
Cancer Biology
College Arts and Sciences
University of South Florida

Major Professor: Meera Nanjundan, Ph.D.
Alvaro Monteiro, Ph.D.
Mark Alexandrow, Ph.D.
Jin Cheng, Ph.D.

Date of Approval:
March 25, 2014

Keywords: ovarian cancer, endometriosis, lysosomes, autophagy, Ras/MAPK, mitochondria

Dedication

I dedicate this work to my fiancée, Kelly. You have been unwavering in your support and unending understanding. You have always been there to help me and lift my spirits. You have made me a better person and I will always be thankful.

Acknowledgments

I would like to extend my deepest appreciation to my mentor, Dr. Meera Nanjundan. I entered the cancer biology program with only basic knowledge of cell biology. Dr. Nanjundan taught me everything I know about cell biology techniques and the proper way to conduct research. I am a better scientist thanks to her guidance.

Dr. Idhaliz Flores also deserves appreciation for her continued insight into the field of endometriosis. She accepted me to intern in her lab at the beginning of my graduate school degree. Without her training, I would never have gained interest or knowledge of endometriosis and its vast involvement in ovarian cancer. I would also like to thank my committee members, Dr. Alvaro Montiero, Dr. Mark Alexandrow, and Dr. Jin Cheng, for their continued advice and support throughout my graduate school education.

Finally, I would like to thank my friends, family, and girlfriend for all their moral support. They have been a never ending source of cheer and have always helped me through any challenge. I am very grateful to have all of you in my life.

Table of Contents

List of Tables

List of Figures

Abbreviations

AP-1: Activator Protein
ATP: Adenosine Triphosphate
BCA: Bicinchoninic Acid Assay
CQ: Chloroquine
CD71: Transferrin Receptor
DMT-1: Divalent Metal Transporter-1
DFO: Desferroxamine
eIFs: Eukaryotic Initiating Factors
EOC: Epithelial Ovarian Carcinoma
FAC: Ferric Ammonium Citrate
FBS: Fetal Bovine Serum
FITC: Fluorescein Isothiocyanate
FTX: Frataxin
GFP: Green Florescent Protein
GSH: Glutathione
H_2DCFDA: 2',7'-Dichlorodihydrofluorescein Diacetate
HES: Human Endometrial Cells
HO-1: Heme Oxygenase-1
HSP: Heat Shock Protein
IRP1/2: Iron Regulatory Protein-1/2
ISC: Iron Sulfur Complex
LDH: Lactate Dehydrogenase
LOH: Loss of heterozygosity
LTF: Long Term FAC treatment
OSE: Ovarian Surface Epithelium
PBS: Phosphate Buffered Saline
PI: Propidium Iodide
Poly-HEMA: Polyhydroxyethylmethacrylate
PVDF: Polyvinylidene Fluoride
ROS: Reactive Oxygen Species
RPPA: Reverse Phase Protein Array
siRNA: Small interfering RNA
STR: Short Tandem Repeats
TBST: Tris Buffered Saline with Tween

TEM: Transmission Electron Microscopy

Abstract

Ovarian carcinoma afflicts over 22,000 women each year with a 5 year survival rate of only 18% for stage IV patients [23]. Current treatment options are limited due to high rates of drug resistance and recurrence. Further, the identity of "precursor lesions" which give rise to various subclasses of epithelial ovarian cancer has been evasive. This is due to discovery of the cancer at already an advanced stage. Interestingly, endometriosis a benign but invasive gynecological disease has been described as a "precursor lesion" in the development of specific subtypes of ovarian cancer. Endometriotic cyst development involves the accumulation of "old blood" components including iron-rich heme. Published evidence implicates excess iron that is involved in the transformation of normal surface epithelial cells inducing morphological characteristics of clear cell ovarian cancer cells [13, 34]. Due to excess iron in endometriotic cysts, this essential element may play a transformative role in the development of clear cell ovarian cancer and possibly other subtypes [13, 35-38]. Further, studies show increased risk of developing ovarian cancer, particularly clear cell and endometrioid ovarian subtypes, in patients diagnosed with endometriosis [36, 37, 39, 40] .

This thesis aims to initiate an investigation regarding the contribution of iron and endometriotic lesions in the development and progression of specific subtypes of epithelial ovarian cancers. Since there is a lack of well-validated and characterized endometriotic cell lines that could be used for endometriosis studies, we sought to develop an immortalized cell line for future endometriotic *in vitro* and *in vivo* studies. Thus, in Chapter 3 we present our efforts in

developing a novel life-span extended epithelial endometriotic cell line. The cells were derived from the endometriotic tissue of a patient with endometriosis. We describe our attempts at immortalization and the characterization of this endometriotic cell line in relation to previously reported/available endometrial/endometriotic cell lines.

In Chapter 4 we investigated the role of iron in modulating functional aspects of various gynecological cell lines. Although our expectation was that iron could transform normal ovarian surface epithelial cells (OSE) to a carcinoma-like phenotype, we instead discovered that ovarian cell lines containing Ras mutations (or with H-Ras overexpression) responded to iron (presented as ferric ammonium citrate (FAC)) with a reduced growth response. Further treatment with iron induced an apoptotic/necrotic death response in the Ras mutated HEY ovarian carcinoma cell line. Interestingly, we identified that iron induced autophagic activation in all ovarian cell lines investigate, although autophagy contributed only modestly to the cell death event. Furthermore, we noted that iron activated the MAPK pathway and its inhibition (via U0126, a MAPK inhibitor) allowed survival of cells.

In Chapter 5, we briefly explore the role of iron in ovarian cell types growing under anchorage-independent conditions. We found that the cell lines displayed increased cleaved PARP and apoptosis when placed under these conditions. Treatment with iron led to a reduction in cleaved PARP suggesting that iron promotes cell survival in anchorage-independent conditions. Further, inhibition of autophagy via chloroquine led to increased cleaved PARP suggesting that autophagy may mediate a protective role against anchorage-independent apoptotic response

In Chapter 6, we attempted to elucidate the downstream mechanism following Ras/MAPK activation in response to iron. This study identified several signaling pathways

including that involved in translational control, iron metabolism, as well as mitochondrial function. The inhibition of the iron regulatory and translation control pathway did not significantly lead to rescue of iron-induced cell death of Ras mutated/overexpressed cells. However, we noted mitochondrial stress and damage including altered expression of mitochondrial markers (TOM20/TOM70, outer membrane transporters) which occurred concurrently with iron-induced cell death. The inhibition of iron import into mitochondria using a calcium uniporter channel inhibitor (Ru360) led to a marked reversal of the cell death response. Collectively, these studies suggest that increased mitochondrial permeabilization may be responsible for the observed iron-induced cell death response.

Overall, the studies presented in this thesis have revealed novel responses to iron in the gynecological cell types investigated. We initially sought to understand the role of iron in precursor lesions which included the development of a novel life-span extended epithelial endometriotic cell type. Remarkably, our findings revealed a Ras driven sensitivity to excess iron. Treatment with iron caused decreased cell growth and increased cell death in cell types containing Ras mutation/overexpression. Further, we found that the mechanism leading to the iron-induced cell death events was mediated via the MAPK pathway. We then determined that the cell death response was associated with mitochondrial permeabilization. Loss of mitochondrial integrity occurred in Ras sensitive cell lines and inhibition of iron import into the mitochondria (via the calcium uniporter channel inhibitor, Ru360) led to reversal of this response. We show herein the cellular response of excess iron and its potential implication in ovarian cancer research.

Chapter 1

Introduction

Ovarian Cancer

Ovarian cancer is the 5th most common cancer affecting over 22,000 women each year and leading to another 14,000 deaths [23]. Tactics to treat the disease include surgical debulking of the tumor including the removal of the ovaries in combination with chemotherapy (paclitaxel/cisplatin) [23, 41, 42]. Unfortunately, the disease often remains asymptomatic until reaching an aggressive phenotype [23]. Since the cancer is detected in late stages, resistance to chemotherapy is frequent and the mortality rate is high [43]. This highlights the critical need to not only study ovarian cancer but to develop novel therapeutics to assist in combating resistance, metastasis, and overall tumorigenesis.

Ovarian cancer is a heterogeneous disease since it is comprised of a large array of cancer subtypes [23, 44]. On a broad scope, three types of ovarian tumors exist: (1) germ cell, (2) stromal, and (3) epithelial [23]. Germ cell tumors develop in the ovary from the ova [23, 45]. These tumors are typically benign and appear early stage in reproductive life (early 20s) [23, 45]. Often these tumors can be removed without re-occurrence or loss of fertility [23]. Stromal-derived ovarian cancers are also typically benign or low grade [23]. These tumors often develop due to hormone dysregulation leading to abnormal stromal cell growth [7]. The frequency of epithelial ovarian carcinoma (EOC) far exceeds that of germ cell or stromal tumors; EOC is

believed to account for over 90% of the malignant ovarian cancer patient population [23]. Unfortunately, EOC also accounts for the highest mortality rate primarily due to being undetected until advanced stages (see Figure 1) [23]. The frequency and mortality rate associated with epithelial ovarian cancers is strikingly high; therefore, we focused our studies on this disease [23].

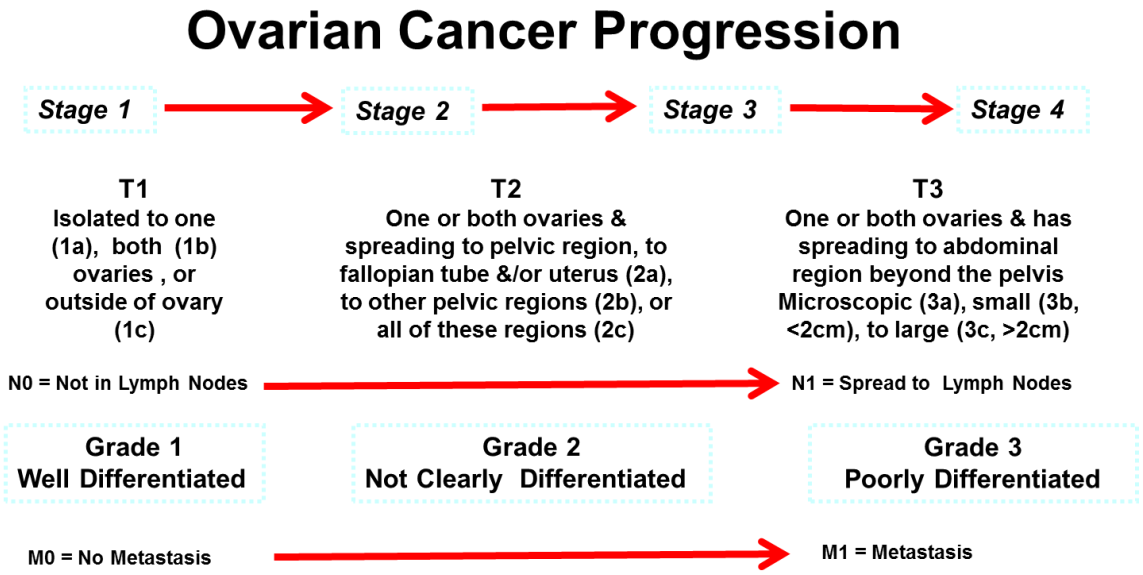

Figure 1: Model of ovarian cancer progression.
Ovarian cancer progression is classified by both grade and location of the disease. The cancer will be graded high if it is more invasive and less differentiated. This chart represents stage and grade information obtained from cancer.gov [23].

As with ovarian cancer, EOC can be broken down into various subgroups which are based on characteristics as well as origin of cancer type [23]. Epithelial ovarian subtypes include (1) serous, (2) endometrioid, and (3) clear cell. Serous carcinoma is the most common form of EOC, comprising ~70% of the patient population [23, 40]. Serous carcinoma can be subdivided into high and low grade states [46]. Low grade serous carcinoma has frequent mutations in K-

Ras and BRAF but lacking in p53 mutations [23, 46]. Low grade serous derives from adenofibromas and/or early stage tumors [23, 40]. This form of serous carcinoma is considered slow growing relative to its high grade counterpart. High grade serous carcinoma is characterized by its high mutation levels along with being multinucleated [23]. Interestingly, a large number of studies have demonstrated that serous carcinoma (specifically high grade) has many morphological similarities to those of the fallopian tube [46, 47]. These studies suggest that the origin of serous carcinoma arises from outside of the ovaries.

Clear cell and endometrioid carcinoma account for about 20% of the EOC patient population [23]. Both subtypes are considered to derive from endometrial lining tissue [36, 38]. One potential explanation for the movement of endometrial tissue to the ovary is retrograde menstruation [36, 39, 40]. This leads to the development of endometriotic lesions; this results from the menstrual lining traveling upward into the fallopian tube and attaching either to the fallopian tube itself, the ovaries, or the peritoneal cavity [38]. Endometriotic tissue then continues and then may eventual lead to the formation of endometriotic cysts [36-38]. The cellular contents of the cysts can develop mutations leading to formation of clear cell borderline tumors and then a more aggressive cancer [13, 17, 18, 34, 35]. A factor that may contribute to this process is the presence of high blood content within the endometriotic cyst [13]. Interestingly, this blood is rich in iron and is marked by the cysts' dark brown coloration which has been termed "chocolate" cysts [13, 34]. Free radical iron promotes the transition of normal cell morphology to clear cell carcinoma phenotype [13]. Although the percentage of clear cell ovarian cancer patients is lower than serous, clear cell is comparatively more chemoresistant and aggressive which makes this rarer form of ovarian cancer a critical area to study [23, 48].

Endometriosis

Endometriosis may be a precursor lesion leading to the development of ovarian carcinoma [36-39, 49]. Studies have shown that women with endometriosis have up to a 40% risk of this ailment developing into ovarian carcinoma [36, 37, 49]. Of this group, the majority of patients had clear cell or endometrioid ovarian carcinoma [36, 37, 49, 50]. Interestingly, endometriosis is a common gynecological disease occurring in millions of women each year with some reports suggesting over 10% of the female population are afflicted [51]. Similarly to ovarian cancer, endometriosis is typically diagnosed after the emergence of abdominal and pelvic pain [51]. Further, endometriosis can also lead to infertility [51].

Classically, endometriosis is believed to derive from the endometrial lining of the uterus [36, 37, 51, 52]. This tissue is sheathed during the estrus cycle allowing for the development of a new lining. In endometriosis, this tissue travels upward into the uterus then into the fallopian tube and then adheres to the ovaries. This phenomenon was first observed by Dr. John Sampson in the 1920s [53]. Since then, these findings have been corroborated and are generally accepted as the primary cause of the disease [51]. Endometriosis can also develop elsewhere; not only in the ovary but outside of the pelvic area, implicating other theories in the development[51]. One leading hypothesis states endometriosis can arise from the ovary itself [52]. This process is called celomic metaplasia which involves the transformation of the ovarian surface epithelial cells (OSE) to endometrial-like cells [52].

Intriguingly, the development of endometriosis parallels that of ovarian cancer and other cancers in general. Endometriosis develops from endometrial cells migrating from its site of origin which grow in a new locations (fallopian tube, ovaries, peritoneal cavity) (See Figure 2) [37].

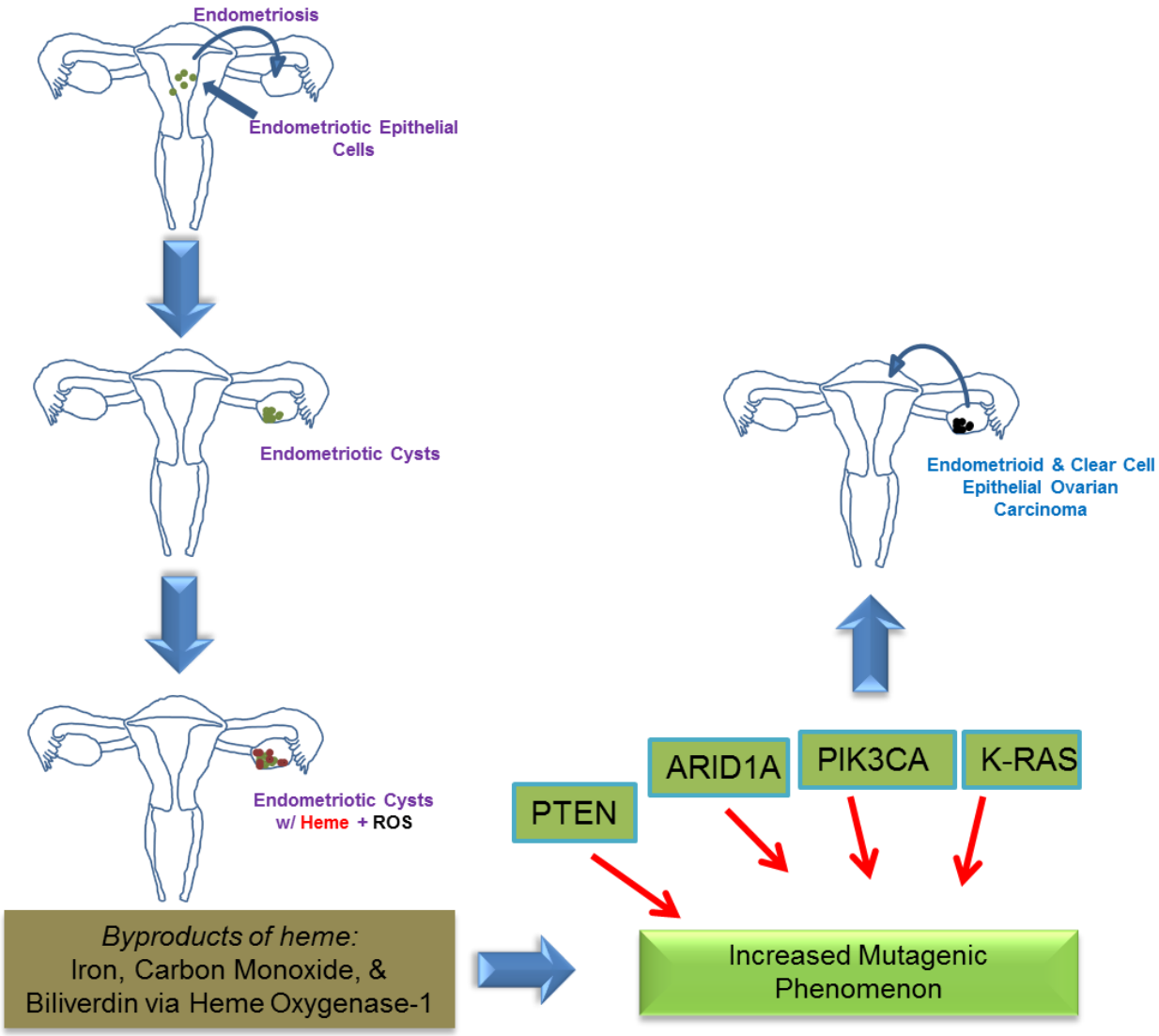

Figure 2: Model of endometriosis progression.
Endometriosis can developed into an endometriotic cyst leading to accumulation of heme. This heme can be broken down via Heme Oxygenase-1 (HO-1) leading to release of free iron and increase of ROS. Consistent exposure to ROS may induce mutations allowing for the development of ovarian cancer [12-18]. *Model created by Kyle Bauckman.

While these lesions are typically limited to gynecological tissue, many studies have shown endometriosis has the ability spread to the pelvic region: abdominal cavity, lung, skin, and colon [36, 37, 50, 52]. Endometriosis, like cancer, also has a staging system with various grades from stage I (minimal) to stage IV (severe) [51]. Interestingly, the only key difference between endometriosis and cancer is the former's retention of cell cycle control [54].

The development of endometriosis is a multifactorial event. While the exact steps required for endometriosis to develop are not fully understood, it is known that a combination of genetic and environmental events are critical (see Figure 2) [51]. Endometriosis can be inherited and is linked to specific genetic mutations including mutations including those in chromosome 7 and 10 [55]. Low levels of the hormone progesterone and decreased progesterone receptors may increase risk of the disease [51]. Environmental factors can also lead to development of this disease. Toxins such as dioxins (found in pesticides) have been connected to increased risk of endometriosis [56]. Interestingly, the risk of endometriosis is greatly reduced after menopause which is converse to ovarian cancer risks [23, 51]. Since endometriosis derives from sheathed endometrial tissue, the advent of menopause halts this process.

Endometriosis is classified into four grades which are based on location, size, and number of lesions [51]. Stage I is considered a minimal level of endometriosis with only one to two small lesions localized to one site [51]. In contrast, stage IV patients have large and numerous lesions located throughout the peritoneal cavity [51]. The tissue growth (size and area) is also quite massive making it difficult to remove. Patients with stage IV often have atypical lesions present within a highly inflammatory environment [33, 36, 37, 51]. These patients are particularly vulnerable to the development of ovarian cancer. Treatment strategies

are dependent on the grade of the disease; this can range from hormone therapy (addition of progesterone or estrogen ablation) and surgery (removal of the endometriotic mass) [51]. Another argued, means of preventing and reducing endometriosis is pregnancy [51]. This likely is due to the increased progesterone produced during pregnancy creating a natural defense against endometriosis.

Strikingly, a large subset of the endometriosis patient population ends up developing cancer. Many studies have shown a large portion (~40%) of the clear cell carcinoma patient population had endometriosis prior to carcinoma development [16-18, 34, 36, 37, 39, 40, 49, 50]. These findings, however, are quite variable due to the difficulty in diagnosing endometriosis and ovarian cancer. Typically, the identification of similar histologic patterns between the malignancy and endometriosis results in positive confirmation of the association [36-38, 50]. Often patients only show symptoms after the cancer has spread from the site of origin and beyond. This makes it challenging to isolate and validate any tissue that might be endometriosis.

Transformation from endometriosis to ovarian cancer can occur via environmental and genetic factors. One hypothesis states that endometriosis develops into an endometriotic cyst in the ovary which leads to cell stress and drives cancer formation [13, 18, 31, 34]. Atypical endometriosis is correlated with the presence of metaplasia, hyperplasia, and cytological atypia [57, 58]. Interestingly, atypical endometriosis is associated with mutations and/or modifications such as increased HNF1β expression, deletion of ARID1a, and increased estrogen receptor expression [14, 59]. These events may lead to atypical lesions formation and appears to be a critical event in the transition to cancer. Further, mutations of p53, K-Ras, and deletion of PTEN are critical for the transition from endometriosis to early forms of ovarian cancer (see Figure 2) [12, 14, 60, 61].

As mentioned, transformation of an endometriotic cyst to aggressive clear cell carcinoma is hypothesized to occur partly due to excessive iron exposure (see Figure 2) [13]. Excess iron present in "chocolate" cysts produces free radical iron which leads to a dramatic increase of ROS [13]. This increased ROS activity then leads to cell stress and subsequent mutations, transforming the benign cyst into one with more aggressive characteristics. Since iron appears to be an important factor in meditating these events, we initiated an investigation into the cellular response of iron in normal gynecological and cancer cell types. Elucidation of the cell signaling pathways triggered by iron in ovarian cells may help to understand its role in modulating cellar transformation.

Iron Signaling Pathway

Iron can be both beneficial and detrimental to cellular survival; it is critical for protein production, protein activity, and ATP production while also increasing oxidative stress [19, 25]. Due to iron's multiple oxidation states, the element is very important in numerous biochemical reactions throughout the body [19, 26]. This includes large scale events such as the transport of oxygen via hemoglobin to micro events such as ATP production [19]. This same oxidative flexibility, however allows for iron to cause oxidative damage and production of reactive oxygen species. Fortunately, evolution has developed mechanisms for strict regulation of iron utilization, storage, and removal that would reduce the detrimental effects of iron exposure [19]. Dysregulation of this iron control pathway could induce negative effects including cell death and/or tumor development [25].

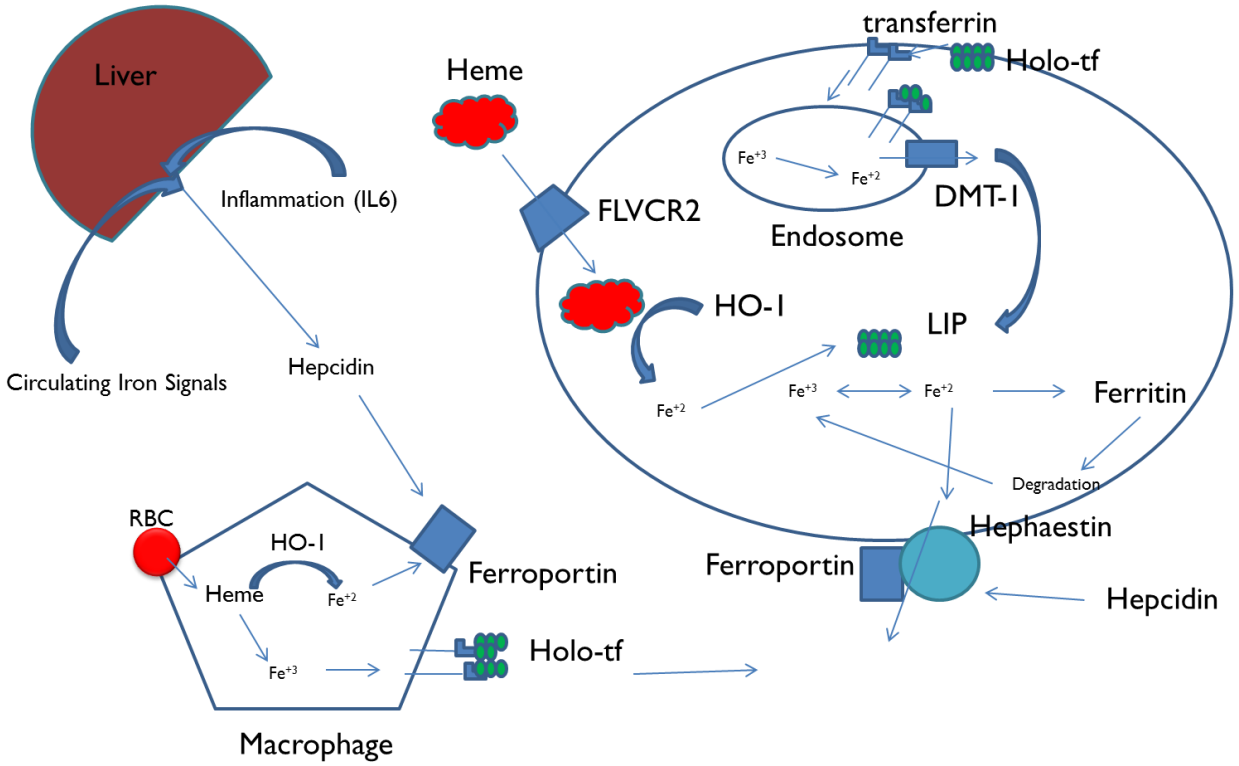

Figure 3: Model of Iron Signaling Pathway.
Iron can enter the cell by interaction with transferrin. Iron can then be shuttled to the transferring receptor. This interaction induces the formation of an endosome in which iron loses association with the transferrin receptor and is converted into its active Fe^{+2} form. This is due to the acidic environment of the endosome. Iron can be shuttled into the cytosol via the Divalent Metal Transporter-1. Once in the cytosol, iron becomes part of the labile iron pool which can be utilized for basic cell functions. Excess iron is stored via ferritin preventing excess iron from creating ROS. Iron may also be shuttle out of the cell via ferroportin [25, 26]. *Model created by Kyle Bauckman.

The iron regulatory pathway is broken down into four functions: intake, storage, utilization, and removal [25]. The primary mechanism of obtaining iron occurs through consumption of products containing iron or through blood containing iron-rich heme. Iron can bind to transferrin (an extracellular protein that recruits and shuttles iron) creating a complex that can associate with the transferrin receptor (CD71) (see Figure 3) [25]. CD71 association with

iron bound to transferrin leads to endosome formation and thus, the cellular internalization of iron (See Figure 3) [25]. Iron is released in the endosome as Fe^{+2} (this occurs via the action of STEAP3 [25]) and can be transferred into the cytoplasm via the divalent metal transporter (DMT-1) (See Figure 3) [25]. This iron is then free to interact in the cell to elicit its effects via protein production, mRNA silencing, or utilization in the mitochondria [19, 25]. Iron can also be stored via the protein ferritin (see Figure 3). This protein binds to iron, converting it to a less reactive state, Fe^{+3}. This iron can be stored in the cell for future use. Ferritin is found in varying levels and consists of heavy and light chain isoforms in different cell types [25]. The heavy and light chains are important in iron storage, but the ratio varies [25]. Some cells express high levels of the heavy chain (i.e. the heart) while others contain higher levels of the light chain (i.e. liver) [25]. It has been speculated that the heavy chain may dominate in cells that utilize iron more for metabolic purposes whereas the light chain may dominate in cells that manage iron toxicity (via iron storage) [25]. If iron bound to ferritin is required for utilization, it will be consumed by lysosomes and free iron (Fe^{+2}) is released. If the cell contains an excess of iron beyond the capacity of ferritin storage, the cell can expel iron extracellularly via ferroportin (See Figure 3) [19, 25]. This transmembrane protein is critical for the expulsion of excess iron preventing accumulation of intercellular free iron. Ferroportin is regulated by the small hormone peptide hepcidin (see Figure 3) [25, 27]. Hepcidin is considered the "master regulator" of iron in the body [27]. It is produced via the liver and acts as an endocrine hormone [27]. Hepcidin promotes the internalization and degradation of ferroportin thus preventing iron from being exported out of the cell [27]. This allows for cells to retain iron under iron scarce conditions.

Mitochondria also have a complex role in iron regulation. Iron can be imported through mitochondrial transport complexes including the calcium uniporter channel (see Figure 4) [62, 63]. Once inside the mitochondria, iron can be utilized for multiple functions including heme biosynthesis, storage (via mito-ferritin), and production of iron sulfur complexes (ISCs) (see Figure 4) [21, 64]. Heme synthesis is mediated by frataxin, a regulatory protein involved of iron-sulfur cluster biogenesis, leading to

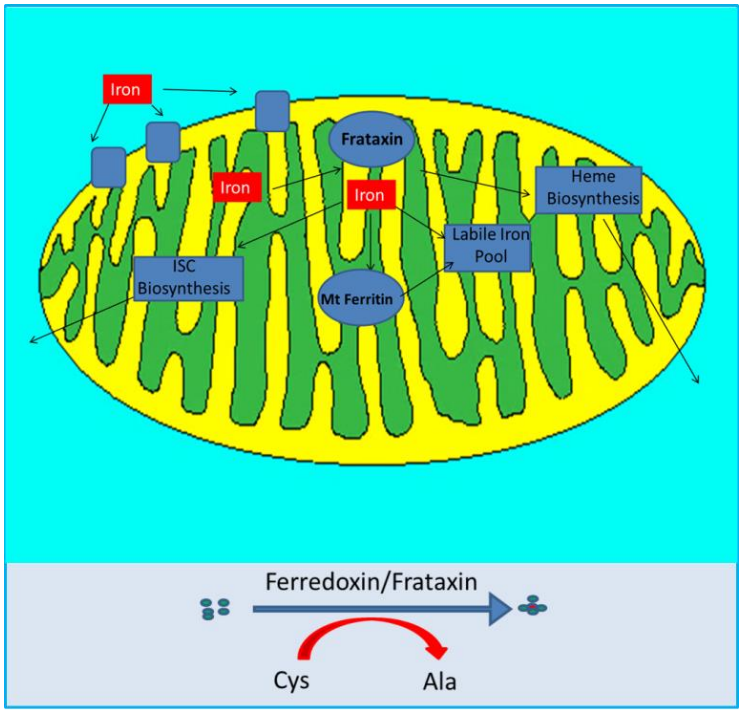

Figure 4: Model of iron regulation in the mitochondria.
Iron can enter the mitochondria through the mitochondrial membrane uniporter channel along with other transport mechanism. Once in the cell, iron is regulated by frataxin to be utilized for heme biosynthesis or iron sulfur cluster formation. Iron may also be stored via mito-ferritin (mt-Ferritin). Iron sulfur clusters are formed via ferredoxin and frataxin. In this process, cysteine donates sulfur leading to four iron particles interacting with one sulfur particle. The donation of sulfur results in cysteine becoming alanine [20-22]. *Model created by Kyle Bauckman.

production and export of the product (see Figure 4) [21, 25]. Mito-ferritin functions similarly to its cytoplasmic counterpart where it stores excess iron safely for future utilization (see Figure 4) [25]. The formation of iron sulfur-complexes is another critical process in mitochondrial functions. Iron-sulfur complexes are utilized for protein regulation and translation [21, 25]. ISCs are created by binding one sulfur molecule with four iron molecules (see Figure 4). ISCs are particularly important in the activity of aconitase. This is an enzyme critical in the regulation of the citric acid cycle and thus important in ATP production and the overall metabolic state of the cell [21, 25].

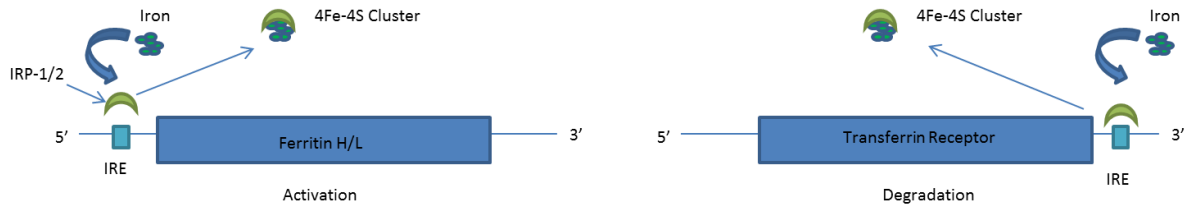

Figure 5: Model of iron regulatory mechanism.
Iron Response Proteins (IRP1/2) interact with Iron Regulatory Elements (IREs) of specific mRNAs. IRPs serve a dual purpose in mRNA regulation. IRPs can interact with IREs in the untranslated regions of mRNA leading to repression of protein production (ferritin H/L) or help to stabilize the mRNA during transcription (transferrin receptor). In the presence of high iron, iron sulfur clusters can interact with IRPs leading to dissociation from the IRE sites. This leads to activation of repressed proteins and destabilization of others [19]. *Model created by Kyle Bauckman.

Multiple proteins (including those important for regulating iron) are transcriptionally controlled by iron regulatory proteins (IRPs) (see Figure 5) [19]. Two types of IRPs regulate transcription [19]. While both play similar roles in regulation, IRP1 is regulated by ISCs whereas IRP2 is not; IRP1 is associated aconitase activity while IRP2 is not. This suggests that IRP1/2 may regulate iron dependent proteins differently, though studies vary on which IRP protein is the most important [19]. Overall, IRPs ability to bind to specific proteins is dependent

on the level of iron in the cell. For example, under low iron conditions, IRPs bind to the 5' untranslated region (UTR) of ferritin suppressing its translation (see Figure 5). When iron is present in high levels, ISCs bind to IRPs preventing its ability to bind to the UTR promoting translation (see Figure 5) [19]. The trend described with ferritin is different in relation to CD71 [19]. IRPs bind to the 3'UTR region of CD71 mRNA in low iron levels, thus promoting its translation (see Figure 5). In contrast, under iron rich conditions, the IRPs are released from the 3'UTR of CD71 leading reduced translation [19].

On a global level, iron can be shuttled throughout the body via heme (in a large complex called hemoglobin) [9, 10, 21]. Heme can be broken down in cells (commonly in macrophages) via the enzyme heme oxygenase-1 (HO-1) (see Figure 6) [9]. HO-1 is a rate limiting enzyme

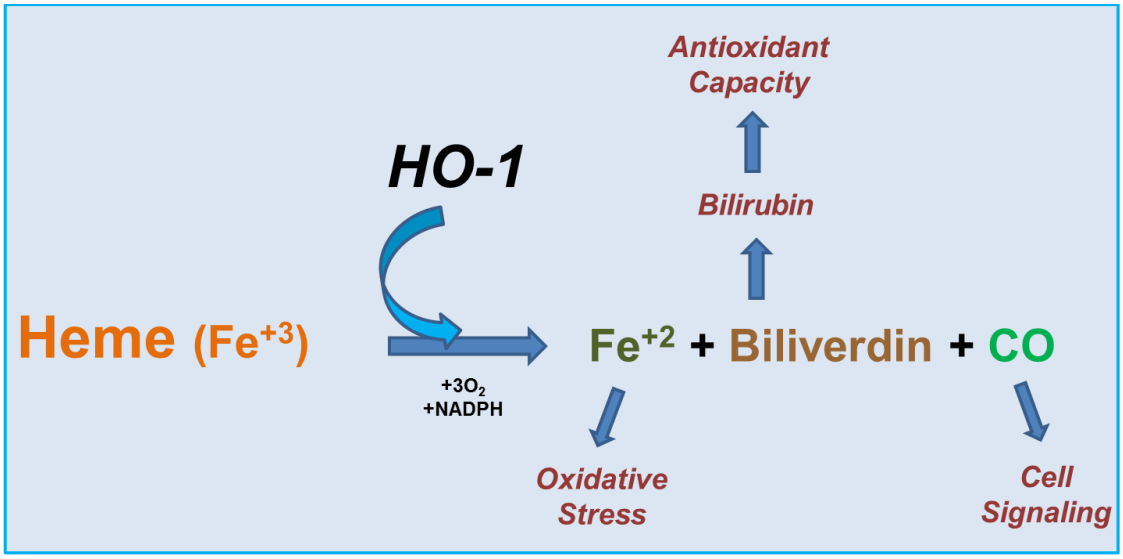

Figure 6: Model of heme regulation.
Heme breakdown is dependent on the rate limiting enzyme heme oxygenase-1. This enzymatic process results in reduced iron (Fe^{+2}), biliverdin, and carbon monoxide as byproducts [9, 10]. *Model created by Kyle Bauckman.

that catalyzes the breakdown of heme into free Fe^{+2}, biliverdin, and carbon monoxide (see Figure 6) [9]. Interestingly, high levels of biliverdin and the degraded byproduct, bilirubin, elicit antioxidant benefits [9, 65]. Some studies even show that high levels of bilirubin lead to increased life span and decreased risk of heart disease [66, 67].

Iron dysregulation is mediated by multiple mutations leading to a variety of cell responses. One of the most common iron associated diseases is Friedreich's ataxia [68]. This is a mitochondrial related disease that specifically involves the mutation of frataxin [68]. Patients are born with a mutation in this gene which leads to metabolic disorders and heart conditions. Iron leads to the development of cancer [68].

Increased presence of iron in normal ovarian cells has been shown to lead to a change to a clear cell like morphology [13, 25, 27, 34, 69, 70]. Indeed, iron is capable of producing ROS due to its free radical nature. Consistent exposure to ROS may increase inflammatory signals and thus induce DNA damage [34]. Further, many reports have shown that cancer cells intentionally acquire high levels of iron [25, 71]. This is likely due to the faster metabolic rate compared to normal cell types. Multiple studies have shown that breast cancer cells utilize iron for beneficial purposes; a mechanism may be hepcidin which promotes for increased intercellular iron [25, 69].

Mechanisms of Cell Death

Though iron plays a tumorigenic role in the body, we have found that iron can adversely affect cell growth in ovarian cell types with Ras mutated/overexpression (see Chapter 4). Similar phenomenon have also been reported in other cell types, but the exact mechanism of iron-induced death is poorly understood [71]. We thus wanted to investigate previously

established mechanisms of iron associated death as well as contribute new knowledge to the field.

Types of programmed cell death mechanisms can be broken down in three major categories. Apoptosis is the most classic form of cell death [72]. This process is activated in response to multiple environmental factors including DNA damage, mitochondrial dysregulation, and cytokine signaling [72]. Apoptotic cells can be easily identified by their distinct membrane blebbing and spherical appearance. Apoptotic cell death can occur in an intrinsic and extrinsic manner [72]. Extrinsic apoptosis may also involve loss of cytochrome c via the mitochondria. Extrinsic apoptosis' striking difference is that death cues occur from outside elements while intrinsic death occurs from internal cell activity. Intrinsic apoptosis is mediated by the mitochondria, particularly due to loss of cytochrome c [72]. This leads to activation of caspases 9 and 3, leading to cell death. In contrast, extrinsic cell death is regulated by external cytokines such as TNF and TGF. These inflammatory signals can induce a caspase 8 dependent cell death. Extrinsic apoptosis may also involve loss of cytochrome c via the mitochondria. Apoptosis can also be induced by detachment from the extracellular matrix; this is termed anoikis, a type of apoptotic cell death [72-75]. Anoikis is particularly interesting since resistance to this death leads to metastasis *in vivo* [73, 74, 76, 77]. While a normal cell would die after becoming detached from its extracellular matrix, a cancer cell can continue to survive. The loss of adhesion allows the cancer cell to travel through the body to a distant site, attach, and continue to divide allowing the secondary tumor to grow.

Macroautophagy (called autophagy herein) is another major regulator of cell death [72, 78, 79]. Unlike apoptosis, autophagy has a dual purpose; inducing cell death as well as promoting cell survival [79]. Autophagosomes are induced to breakdown and recycle damaged

organelles and proteins (see Figure 7). These proteins induce the production of autophagosomes via autophagy regulatory proteins. These regulatory proteins help form the phagophore that

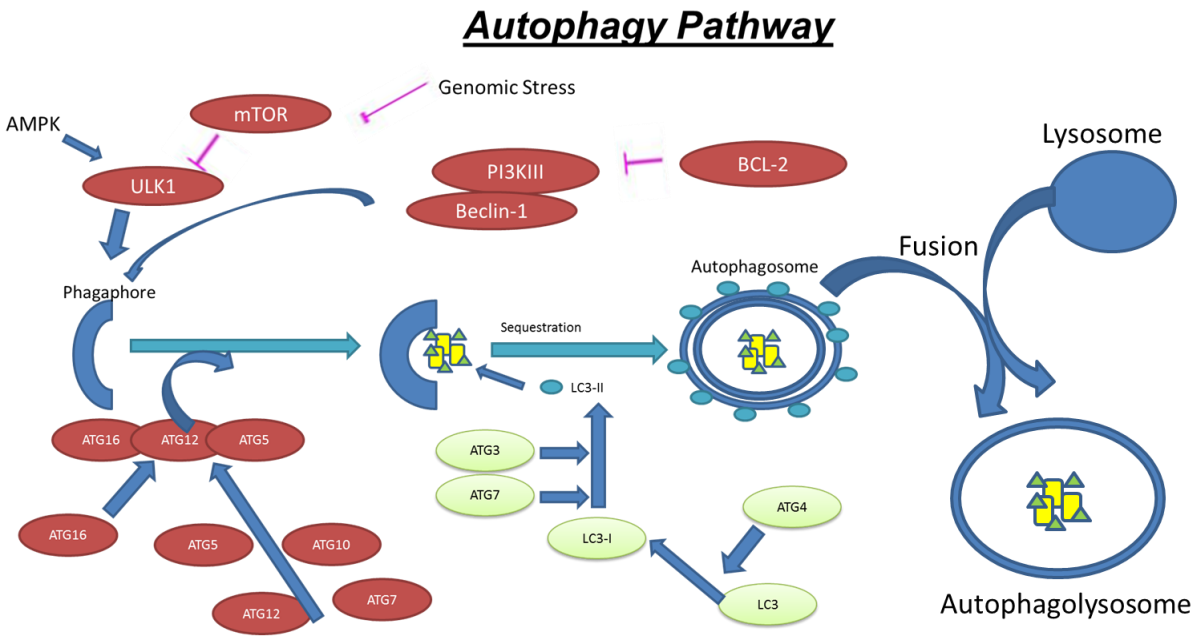

Figure 7: Model of autophagy regulation.
Autophagy can be induced by metabolic signals (AMPK), genomic stress, and modulation of BCL-2. Induction of autophagy leads to the formation of a phagophore that is utilized to sequester damaged organelles and proteins. Autophagy proteins convert LC3 to LC3-I and finally LC3-II. This occurs via lipidation of LC3 by autophagy proteins (ATG4, ATG3, ATG7). This is then recruited to the autophagosome membrane. Finally, the autophagosome fuses with a lysosome to create an autophagolysosome. The fused entity then degrades the damaged contents and recycles them into free amino acids and nutrients [24]. LC3-II is degraded after fusion of the lysosome with the autophagosome via lysosome hydrolases [24]. *Model created by Kyle Bauckman.

engulfs damaged organelles and proteins. Autophagosomes can be easily detected by its double bound membrane using transmission electron microscopy (TEM) [79]. Once a complete autophagosome is formed, it can fuse with a lysosome creating an autophagolysosome (see Figure 7) [72]. This complex degrades the organelles and proteins into free amino acids and nutrients that can be utilized in the cell. In this sense, autophagy is a cell protective mechanism removing unwanted/damaged material from the cell [79]. However, if the cell contains a large amount of organelle and/or protein damage, the cell will produce abundant autophagosomes leading to eventual death of the cell [73, 80].

This dual behavior allows autophagy to illicit tumor suppressor and tumor promoter functions depending on the circumstances [79]. A cell that is under increased stress via ROS can utilize autophagy to remove damaged material allowing it to return to a normal state [48, 73, 79, 81]. However, consistent exposure to ROS can lead to mutations creating a more aggressive cell type [48, 73, 79, 81]. Autophagy can assist in the cells' survival when it otherwise may not be able to tolerate the stress. Further, cancer cells can utilize autophagy to produce nutrients in an environment that is otherwise depleted [48, 73, 79].

The third major programmed cell death mechanism is known as necroptosis [72]. This mechanism has only recently been established [82]. Prior to this, the phenomenon was considered part of a nonprogrammed event known as necrosis. Necrosis involves the loss of plasma membrane integrity leading to cytoplasmic contents entering the microenvironment [72]. This phenomenon can be induced by elevated levels ROS. The mechanism is considered nonprogrammed since it is not cued by a specific signaling pathway. Characteristics or necroptosis are similar to necrosis; however, has been shown to be regulated by RIP proteins [72,

83]. RIP proteins create a scaffold called a ripoptosome that provides the signals that lead to membrane permeabilization [83].

An iron mediated cell death pathway was recently discovered called ferroptosis which can be induced by inhibition of the Ras pathway [3]. Inhibition of the Ras pathway was found to increase ROS levels thus promoting membrane permeability and mitochondrial stress [3, 84]. This mechanism, although intriguing, is yet to be fully understood. Only two articles are currently available on this mechanism; thus there is more to elucidate about the pathway [3, 84].

Concluding Remarks

The overall focus of our project was to further understand the role of endometriosis in the development of ovarian cancer. We divided this study into two components. One section focused on establishing an *in vitro* model to study endometriosis. This involved the development of a novel immortalized epithelial endometriotic cell line and proteomic profiling in comparison to other well-established ovarian cell line subtypes. The second section focused on investigating how high levels of iron (seen in endometriotic lesions [13, 35, 85]) would alter growth and behavior of normal gynecological and ovarian cancer cell types. We wanted to determine if iron could increase cell growth in "normal" cell types which would be suggestive of acquisition of a more aggressive phenotype. In contrast to expected results, we found that iron was detrimental to cell types harboring Ras mutation/overexpression. This directed us to focus on the cell signaling pathways and cell death mechanisms induced by iron treatment. We present herein the characterization of iron treatment in gynecological cells. The hypothesis and specific aims addressed in this thesis are described below.

Specific Aims

The goal of our studies was to understand the role of iron in gynecological cell types. We hypothesized that cells with overexpressed or mutated Ras expression would be sensitive to iron treatment. Moreover, we hypothesized that continuous iron treatment would induce "normal" cells to grow, leading potentially to carcinoma-like characteristics. We addressed these hypotheses in the following aims.

Development and Characterization of a Novel Endometriotic Cell Line (Chapter 3)

Aim 1: Characterize primary endometriotic cell lines

1.1 : Determine if cells are stromal or epithelial

1.2 : Assess markers of growth, survival, cell cycle, and EMT in relationship to existing ovarian cell types

Aim 2: Immortalize and establish a novel endometriotic cell line

2.1: Immortalize cells

2.2: Characterize the immortalized cells to confirm immortalization and the retention of similar proteomic profile expressed in primary cells

Aim 3: Determine the role of autophagy in endometriotic cell survival

3.1 Inhibit autophagy and determine the survival capacity of endometriotic cells

Iron modulates cell survival in a Ras- and MAPK-dependent manner in ovarian cells (Chapters 4, 5, and 6)

Aim 1: Determine the influence of iron in gynecological cell types

1.1: Assess changes in cell behavior (growth, cell survival, migration, wound healing)

1.2: Determine the form of cell death induced by iron treatment

1.3: Effect of iron in an anoikis-induced environment

Aim 2: Validate that Ras- and MAPK- markers are crucial for iron-induced cell death

2.1: Use of inhibitors to reverse cell death

2.2: Investigate the role of iron regulatory pathways to identify the dependence on Ras

Aim 3: Identify cell signaling pathways downstream of Ras/MAPK that are involved in iron-induced cell death

3.1: Determine the role of mitochondrial in iron-induced cell death

3.2: ROS activity in iron-induce cell death

Overall Studies

Chapter 3 concerns the development and characterization of a novel endometriotic cell line. The work presented in Chapter 3 represents unpublished data (Bello *et al.*, unpublished data) performed in collaboration with the laboratory of Dr. Idhaliz Flores. Chapters 4, 5, and 6 focus on the role of iron in gynecological cell growth and function. The data presented in Chapter 4 represents the published work entitled "Iron modulates cell survival in a Ras- and MAPK- dependent manner in ovarian cells" in the journal Cell Death and Disease (2013). Chapter 5 presents in progress studies that will contribute to a yet untitled anoikis paper. Finally, Chapter 6 represents the follow-up to the work presented in Chapter 4 which will be submitted in the near future.

Chapter 2

Materials and Methods

Cell Lines

Serous carcinoma cell line, HEY and normal surface ovarian epithelial cells (T80) were provided by Dr. Gordon Mills at MD Anderson Cancer Center, Houston Texas. Cells were maintained in RPMI media with 8% Fetal Bovine Serum (FBS) and penicillin/streptomycin. T80 + H-Ras and T80 + K-Ras cells were also provided by Dr. Gordon Mills. These cells were also maintained in RPMI media with 8% FBS and penicillin/streptomycin. The endometrioid carcinoma line (TOV112D) was purchased through ATCC, Manassas Virginia and the clear cell carcinoma cell line (TOV21G) provided by Dr. Johnathan Lancaster at Moffitt Cancer Center, Tampa Florida. Both TOV112D and TOV21G were maintained in a 1:1 mixture of Medium 199 and MCDB131 with 8% FBS and penicillin/streptomycin. HES cells were provided by Dr. Douglas Kniss at Ohio State University, Columbus Ohio. HES cells were maintained in DMEM with 8% Fetal Bovine Serum (FBS) and penicillin/streptomycin. All cell lines reported in the following work have been tested and confirmed mycoplasma negative along with STR profiled with the exception of HES cells. HES cells were reported to contain markers of HeLa cells [4]. Experiments were performed only with cells under a passage of 20.

Immortalization of primary endometriotic cells

Primary endometriotic cells were provided by Dr. Idhaliz Flores at Ponce School of Medicine, Puerto Rico. The cells were maintained in 1:1 mixture of Medium 199 and MCDB131 with 8% FBS and penicillin/streptomycin along with insulin/transferrin/selenium (ITS). We utilized large T antigen to immortalize the primary cells. We obtained large T antigen pBABE-puro vector from Addgene. We generated retroviral particles utilizing HEK293T cells. These cells were transfected with pCGP and pVSVG vector. Collections of retroviral media were collected at 48h and 72h post-transfection. These particles were filtered (removal of HEK293T cells) and then used to infect the primary endometriotic cells. After infection, cells were treated with puromycin (2.5 µg/mL) to select for positively infected cells. We isolated 6 colonies that we expanded and validated for future use.

Isolation of genomic DNA

Genomic samples were obtained using the DNeasy blood and tissue kit purchased from Qiagen.

Cloning of HO-1

RNA was extracted from T80 cells utilized an RNeasy kit from Qiagen. The samples were then quantified using Nanodrop (purchased from Thermo Scientific). RT-PCR was performed utilizing the primers below (NCBI NM_002133.2):

Forward primer: 5′-GGAATTC-ACCATG-GAGCGTCCGCAAC-3′

Reverse primer: 5′-G-GAATTC-TCA-CATGGCATAAAGC-3′

Samples were run with PCR conditions of 48 ^{o}C 30mins, 94 ^{o}C for 2 minutes, 40 cycles of denaturation at 94 ^{o}C for 1 min, annealing at 60 ^{o}C for 1 min, extension at 68 ^{o}C for 5 min and a

final extension of 72 ^{o}C for 15 minutes. This PCR product was cloned into a pBabe-puro pTOPO vector (obtained via Invitrogen). To confirm positive clones, EcoRI-HF (from NEB Biolabs, cuts at 5'..,G/AATTC...3' and 3'...CTTAA/G...5") was utilized to digest the plasmid to confirm proper insertion. The primers above are separated by dashes to distinguish between the EcoRI site, start codon, and HO-1 specific region. The insert was gel purified and the vector dephosphorylated utilizing Antarctic acid phosphatase from NEB. After this, the insert was ligated to the dephosphorylated vector using T4 Quick DNA ligase (from NEB). Positive clones were sequenced by the Moffitt Cancer Center, Molecular Biology Core to ensure no mutations occurred in the HO-1 sequence. Once confirmed, the plasmid was made in high quality and quantity via Maxi Large Plasmid preparation (purchased by Qiagen) to utilize for downstream applications.

PCR-sequencing

Genomic sequencing of PIK3CA and K-Ras in the immortalized endometriotic cells was carried out via the following conditions: 94 C for 2 minutes, 40 cycles of 94 ^{o}C for 1 min, 45 ^{o}C for 1 min, 68 ^{o}C for 1 min and a final extension of 72 ^{o}C for 10 minutes. The PCR samples were identified on a 1.5% agarose gel and gel purified with a Qiagen gel purification kit. Purified PCR sample was sequenced by the Moffitt Cancer Center, Molecular Biology Core. Primers below are specific for PI3KCA exons 9 and 12 (NCBI NM_006218.2) and K-Ras exon 1, codon 12 and 13 (NCBI NM_004985.3).

PI3KCA Exon 9:

Forward primer: 5′-GAATCCAGAGGGGAAAAA-3′

Reverse primer: 5′-CCATTTTAGCACTTACCTG-3′

PI3KCA Exon 12:

Forward primer: 5′-TTGATGACATTGCATACATTCG -3′

Reverse primer: 5′-ACCTGTGACTCCATAGAAA-3′

K-Ras:

Forward primer: 5′-GCCTGCTGAAAATGACTG-3′

Reverse primer: 5′-GTTGGATCATATTCGTCCA-3′

Generation of stable cell lines

We generated retroviral stable HO-1 expression in T80 cells. As with primary cell immortalization, we utilized HEK293T packaging cell to generate virus particles. pCGP and pVSVG vectors (containing viral components: gag and pol in pCGP and env in pVSVG) (purchased from Clonetech) using Fugene HD (Roche) were again utilized and 48 hour and 72 hour post-transfection. Retroviral particles were collected and placed in wells to infect the desired cells (T80). This process was similarly used for stable knockdown studies of ATG5. A pSUPER control and two unique ATG5 shRNA (with coding regions of 5′ GGC ATT ATC CAA TTG GTT TA 3' and 5′ GCA GAA CCA TAC TAT TTG CT 3' labeled as H2 and H7 respectively (targeting exon 4 and 3 respectively of ATG5)). These shRNAs were created by Dr. Xiao-Feng Zhu at the State Key Laboratory of Oncology in South China. Endogenous ATG5 was knocked down utilizing these shRNAs in T80, HEY, TOV112D, and TOV21G cell lines. Once infected, the cells were treated with puromycin (2 μg/ml for HEY, 1 μg/ml for T80, 2 μg/ml for TOV112D, and 2 μg/ml for TOV21G) to allow for selection of infected cells (48 hour

treatment with puromycin). Knockdown of ATG5 expression in the stable cell lines were validated via real-time PCR and western analysis.

siRNA knockdown studies

Cells were seeded at 325,000 per 6 well plate and left to adhere overnight. The following day cells were transfected with one of the following siRNA: NRF2 (L-003755-00), ATG6/beclin-1 (L-010552-22), ATG7 (L-020112-00), hVps34 (L-005250-00), H-Ras (L-004142-00), K-Ras (L-005069-00), HSP70 (L-021084-01), or non-targeting ON-TargetPLUS control (D-001810-10) along with Dharmafect I obtained from ThermoScientific. The transfection process started with removal of complete media and addition of warm (37 ^{o}C) serum free media. Cells were placed in incubator while siRNA cocktail was assembled (100 µL serum free media, 5 µL of a 20µM siRNA stock, and 4 µL of Dharmafect). This was added drop-wise to wells and left to incubate for 3 hours. Complete media was overlayed after 3 hours and left overnight. The following day, media was removed and fresh complete media was added. Cells were allowed to recover for 3 hours and then a 2nd transfection was performed following the same process. The 3rd day, media was removed and replaced with fresh complete media and recovered for 3 hours. After the recovery phase, cells were treated or reseeded (followed by treatment). All knockdowns were validated by western analysis; NRF2 knockdown was further validated with qPCR.

Protein isolation, SDS-PAGE, and western blot analyses

All cells following treatment had media removed and were washed with PBS. PBS was removed and cells were lysed with RPPA lysis buffer for 1 hour on ice. Cells were then scraped, lysate collected, and spun down to remove cell pellet. Protein lysate concentration was

determined utilizing a BCA assay (Thermo Scientific). BCA is a colorimetric assay to determine concentration of protein. Dilutions were prepared based on BCA readings and prepared for a total volume of 50 µL. 10 µL of 6x SDS loading buffer was then added to the samples. All samples were run on 8, 10, or 12 % polyacrylamide gels along with molecular weight markers. Samples were run at 100 volts for 2.5 hours. The gel was transferred using a semi-dry apparatus. PVDF membranes were activated utilizing 100% methanol and used to transfer gel contents on. The transfer process lasts 2 hours at 0.11 Watts for one membrane. Membranes were then washed with 1x TBST for 10 minutes followed by a blocking period of one hour. We utilized 5% milk in TBST for the blocking process. Following blocking, cells were briefly washed with 1x TBST and primary antibody was applied overnight. Membranes were then placed on a shaker in a 4 ^{o}C cold room for overnight blocking. The following day, primary antibody solution was removed and the membrane washed with TBST for 1 hour (changing out the wash every 15 minutes). Following the wash, secondary antibody was applied for 1 hour (secondary antibody was added in milk). The concentration of secondary was dependent on the primary antibody. After secondary treatment, the membrane was washed with TBST for 1.5 hours (changing the wash every 15 minutes). After washing, the membrane was treated with ECL luminescent detection reagent and developed utilizing x-ray film. After developing, membranes were regenerated for an hour utilizing stripping buffer. Afterwards, cells were washed, blocked, and primary was applied for another antibody. Primary antibodies are summarized below in Table 1.

RNA isolation and qPCR

Total RNA was extracted utilizing the RNeasy Mini Kit from Qiagen. We utilize the one-step RT-PCR master mix obtained from Applied Biosystems to determine mRNA levels of HO-1

Table 1: List of primary antibodies used for thesis.

Antibody	Company	Product #	Secondary	Dilution
ATG5	Cell Signaling	2630	Rabbit Polyclonal	1 to 1000
ATG7	MBL International	PM039	Rabbit Polyclonal	1 to 1000
β-Catenin	Cell Signaling	9587	Rabbit Polyclonal	1 to 1000
Beclin-1	Cell Signaling	3738	Rabbit Polyclonal	1 to 1000
Caveolin-1	Cell Signaling	3267S	Rabbit Polyclonal	1 to 1000
CD71 (transferrin receptor)	Santa Cruz	sc-51829	Mouse Monoclonal	1 to 100
DMT-1	Novus	2F7	Mouse Monoclonal	1 to 1000
E-Cadherin	Biosciences	610181	Mouse Monoclonal	1 to 1000
EGFR	Santa Cruz	sc-03	Rabbit Polyclonal	1 to 1000
EVI1	Cell Signaling	2593S	Rabbit Polyclonal	1 to 1000
FTH1 (ferritin)	Cell Signaling	3998	Rabbit Polyclonal	1 to 1000
GAPDH	Cell Signaling	2118	Rabbit Polyclonal	1 to 4000
HO-1	Cell Signaling	5061	Rabbit Polyclonal	1 to 100
HSP27	Enzo	SPA-800	Rabbit Polyclonal	1 to 1000
HSP70	StressMarq	SMC-100	Mouse Monoclonal	1 to 1000
hVps34	Cell Signaling	3358	Rabbit Polyclonal	1 to 1000
K-Ras	Santa Cruz	sc-30	Mouse Monoclonal	1 to 100
LAMP-1	Cell Signaling	9091	Rabbit Monoclonal	1 to 1000
Large T Antigen	Pharmingin	554148	Rabbit Polyclonal	1 to 1000
LC3B	Cell Signaling	2775	Rabbit Polyclonal	1 to 1000
N-Cadherin	Cell Signaling	4016S	Rabbit Polyclonal	1 to 1000
NRF2	Cell Signaling	8882	Rabbit Monoclonal	1 to 1000
p-AKT (Ser473)	Cell Signaling	4060	Rabbit Polyclonal	1 to 1000
p-ERK 1/2	Cell Signaling	9101	Rabbit Polyclonal	1 to 1000
p53	Cell Signaling	2527	Rabbit Polyclonal	1 to 1000
p62	BD Biosciences	610498	Mouse Monoclonal	1 to 1000
pp70S6K (Thr389)	Cell Signaling	9234	Rabbit Polyclonal	1 to 1000
pGSK3	Cell Signaling	9331S	Rabbit Polyclonal	1 to 1000
pS6 (Ser235/236)	Cell Signaling	4858	Rabbit Polyclonal	1 to 1000
PARP	Cell Signaling	9542	Rabbit Polyclonal	1 to 1000
PLSCR1	Santa Cruz	sc-59645	Mouse Monoclonal	1 to 500
PTEN	Cell Signaling	9559	Rabbit Polyclonal	1 to 1000
RON	Cell Signaling	2654S	Rabbit Polyclonal	1 to 1000
Shc	Millipore	06-203	Rabbit Polyclonal	1 to 1000
Smad2/3	Cell Signaling	3102	Rabbit Polyclonal	1 to 1000
SnoN	Santa Cruz	sc-9141	Rabbit Polyclonal	1 to 1000
TGFβRII	Cell Signaling	3713S	Rabbit Polyclonal	1 to 1000
TOM20	Santa Cruz	Sc-11415	Rabbit Polyclonal	1 to 7000
TOM40	Santa Cruz	Sc-35467	Mouse Monoclonal	1 to 1000
TOM70	Santa Cruz	Sc-390545	Mouse Monoclonal	1 to 1000
Total AKT	Cell Signaling	4685	Rabbit Polyclonal	1 to 1000
Total MAPK	Cell Signaling	4695	Rabbit Polyclonal	1 to 1000
Total Ras	Cell Signaling	3339	Rabbit Monoclonal	1 to 1000
Vimentin	Pierce	MA3-745	Mouse Monoclonal	1 to 1000

(HMOX, Hs01110250_m1) and NRF2 (NFE2L2, Hs00975961_g1). All results were normalized using *β*-actin and then by comparing treated cells with untreated cells (or HO-1 expressing cells to vector control cells). The fold changes in RNA were calculated using the formula $2^{-\Delta\Delta C_T}$.

Immunofluorescence

Autoclaved glass cover slips were placed in 6-well plates and cells were seeded. Cells were allowed to grow on top of the cover slips overnight prior to treatment. For EGFP-LC3 (obtained from Addgene), cells were transfected and treated the following day (following a 3 hour recovery).

Transmission electron microcopy

Cells were grown to confluence in 100mm dishes and treated with FAC at 0, 6, 18, and 24 h. The samples were fixed in 0.1 M phosphate buffered 2.5% glutaraldehyde overnight, followed by 1 hour in buffered 1% osmium tetroxide, dehydrated in a graded series of acetone, and then embedded in LX 112 epoxy resin. Thin sections obtained from blocks of the samples were stained with 8% aqueous uranyl acetate and Reynold's lead citrate. These samples were viewed and recorded via a FEI Morgagni 268D (FEI Company, Inc. Hillsboro, OR, USA) TEMs were imaged at multiple magnifications. Edward Haller (Department of Integrative Biology, College of Arts and Sciences, University of South Florida) carried out fixation, generation of slider, and imaging of all samples.

Cell cycle analysis

Upon completion of experimental treatment, cells were trypsinized and spun down. Cells were suspended gently with cold PBS and then gradually vortexed 9 mL of 70% ethanol (in PBS). Samples were stored overnight in -20 ^{0}C. The following day, samples were spun down and then washed with 2 ml cold PBS. The PBS was removed and 500 µL of Propidium Iodide (PI) mix was added (20% Triton X, 1.6mg RNase, 500 µg/µL Propidium Iodide (PI). This solution was stored at room temperature for 15 minutes in the dark. Samples were read via flow cytometry at the College of Medicine University of South Florida.

ATP viability assay

A cell titer glo assay as utilized to detect ATP levels. Cells were seeded in 96 white opaque plates. HEY, T80, T80 + H-Ras, T80 + K-Ras were seeded at 2500 cells/well and TOV112D and TOV21G at 5000 cells per/well. After treatment, media was removed and wells washed with PBS. ATP was detected utilizing the ATP viability kit purchased from Promega. Readings were measured via luminescence detection (reported as relative light units, RLU).

Wound healing assay

A cytoselect 24-well plate (purchased from Cell Biolabs) was utilized to perform wound healing. The assay consisted of a 24 well plate with inserts that prevent cells to grow in the area. Cells were seeded at 250,000 (T80), 500,000 (TOV112D, TOV21G, and T80 + H-Ras), 400,000 (T80 + K-Ras), and 200,000 (HEY) cells. These numbers were optimized to ensure cells were confluent upon treatment. Once treatment was added, the inserts were removed and cells were

allowed to grow in the vacant area. After completion of treatment period, cells were imaged and stained to determine growth of wounds.

Colony formation assay

Cells were seeded at 500 cells/well in a 6 well plate and allowed to adhere overnight. The following day the wells were treated and allowed to grow for 2 weeks. Upon completion, cells were stained with crystal violet.

Lysosome detection

Lysotracker was utilized both for immunofluorescence and flow cytometry. For immunofluorescences, cells were seeded on glass cover slips in 6 well plates. The following day cells were given desired treatment. One hour before the end of treatment, cells were treated with Lysotracker Red (Invitrogen). Media was removed and pre-warmed media containing 75nM Lysotracker Red was added. Cells were placed back in the 37 ^{o}C incubator for 1 hour. A similar process was carried out with flow cytometry utilizing 75 nM Lysotracker Green. Adherent cells were trypsinized and combined with the collected media containing the non-adherent population.

Mitochondrial detection

Cells were seeded on glass cover slips in 6 well plates at 250,000 cells/well. The following day cells were given desired treatment. 1 hour before the end of treatment, cells were treated with Mitotracker Red-CMXROS (Invitrogen). Media was removed and pre-warmed media treated with 250nM Mitotracker Red CMXROS was added. Cells were placed back in incubator for 1

hour. After treatment, the media was removed, cells washed with PBS, fixed in 4% formaldehyde/PBS for 30 minutes, followed by two PBS washes.

Lactate dehydrogenase assay (LDH)

Cells were seeded in 96 well plates at 2500 cells per/well. Cells were placed in media with only 1% FBS. Cells were treated the following day for desired treatments. Upon completion of treatment, plates were spun down and 100 µL of media was collected from each well and transferred to a new 96 well plate. 100 µL of LDH reaction mixture (purchased from Fisher Scientific) was added to the wells. The plate was incubated at room temperature for 30 minutes and then read on a plate reader with a wavelength of 490 nm. The relative toxicity was determined by subtracting background from media only controls (0.1% FBS).

Annexin V/PI apoptosis assay

The Annexin V/ PI staining was purchased via Calbiochem. After treatment of cells, media was collected and transferred to a conical tube. Samples were trypsinized and mixed with the collected media. Samples were spun down and the pellet retained. Samples were suspended in 500µL of PBS and transferred to an Eppendorf tube. Samples were treated with 10µL binding reagent followed by 1.25 µL of Annexin V FITC. The samples were then incubated at room temperature for 15 minutes in absence of light. Samples were spun down and supernatant removed and pellet suspended with 500 µL of binding buffer. 10 µL of PI was added and samples were incubated on ice for 30 minutes (in the dark). Samples were analyzed via flow cytometry at the College of Medicine University of South Florida with the assistance of Dr. Karoly Szekeres.

Chemical treatments

Chloroquine (CQ) (Fisher Scientific, Pittsburgh, PA, USA) (12.5 or 25 μM) was dissolved in tissue culture-grade water. Ferric ammonium citrate (Fisher Scientific) was utilized between 5μM to 10mM and dissolved in tissue culture-grade water or PBS. Deferoxamine mesylate (DFO) (Sigma-Aldrich, St. Louis, MO, USA) was used between 1 nM to 250 μM, and dissolved in tissue culture-grade water. Ferrostatin (no. 9065366, $C_{15}H_{22}N_2O_2$, ChemBridge, San Diego, CA, USA) was used at 100 μM and dissolved in dimethylsulfoxide (DMSO). U0126 and LY294002 were obtained from Cell Signaling Technology (Danvers, MA, USA) and used at doses of 10 μM and 75 μM, respectively (dissolved in DMSO). Ru360 (Fisher Scientific) dissolved in de-oxygenated tissue-culture grade water was utilized at a final concentration of 10µM.

Senescence assay

After treatment, media was removed and washed with PBS. A β-galactosidase senescence assay was purchased via Cell Signaling Technology to allow detection of senescence. After a PBS wash, 1 mL of fixative was added to each well for 10 minutes. Fixative was removed and cells were washed twice with PBS. 1 mL of β-galactosidase staining solution was then added and incubated at 37 ^{0}C overnight. The following day the plates were observed under a light microscope for the detection of blue staining. The stain is indicative of β-galactosidase a marker of senescence.

Cell viability

Cells were seeded at 5000 cells/well (IE, HES, TOV112D, and TOV21G) or 2500 cells/well (T80 and HEY) in 96-well plates. Cells were left to adhere overnight and the following day treated as needed. Once treatments finished, cells were stained with crystal violet. Once dry, wells with crystal violet were treated with Sorenson's buffer to dissolve stained samples. Samples were quantified using a plate reader at 570 nm wavelength.

ROS detection assay

Cells were seeded at 5000 cells/well (TOV112D, and TOV21G) or 2500 cells/well (T80, T80 + H-Ras, and HEY) in 96-well plates. Cells were allowed to adhere and grow overnight. The following day, the media was removed from the wells and they were washed with 100 µL PBS. PBS was removed and replaced with warm PBS treated with H_2DCFDA dye at a 10 µM concentration. Cells were incubated with dye for 30 minutes at 37 ^{o}C. Following staining, PBS with dye was removed and replaced with media containing desired treatments (FAC) or with 100 µM hydrogen peroxide (to serve as a positive control). In the presence of ROS, H_2DCFDA becomes cleaved creating fluorescence signal. Signal was measured via a plate reader with an excitation wavelength of 485 nm and an emission wavelength of 530 nm.

Anoikis assay

Poly-HEMA was dissolved in 95% ethanol to generate a 20 mg/mL poly-HEMA stock solution. Poly-HEMA was dissolved overnight on a shaker. Poly-HEMA solution was filtered and then used for cell treatments. 100 µL of solution was added to each 96 well plate and 1mL for each 6 well plate (to ensure full coverage of the well). Plates were allowed to air-dry in a biosafety

cabinet until ethanol evaporated. Another coat of poly-HEMA was then added and allowed to dry to ensure full coating. Plates were left to dry overnight followed by two washed with PBS to remove any remaining ethanol or particulate. Cells were treated upon seeding.

Statistical analysis

All experiments presented were carried out in replicates as specified in the figures. We utilized error bars to represent the standard deviation based on P-values (a standard student's t-test) generated using Prism software. NS symbolizes non-significant p-values ($p>0.05$), * represents $p<.05$, ** represents $p<.01$, and *** represents $p<.0001$.

Chapter 3

Development and Characterization of a Novel Endometriotic Cell Line

Introduction

Endometriosis is a debilitating disease that affects millions of women every year [37]. Patients with endometriotic lesions frequently have debilitating pain and a risk of becoming infertile [86]. Further, there is evidence of increased risk for epithelial ovarian carcinoma [36, 49, 87]. Though modern treatment strategies are in place to diminish and remove the lesions, there still remains a serious risk to patients diagnosed with the disease. Studies have demonstrated a correlation between endometriosis and presence of clear cell/endometrioid ovarian carcinomas [13, 15, 36]. Association of endometriosis to ovarian cancer is classified by identification of the carcinoma and endometriotic lesion in the patient region [12, 13, 68]. Since cancer is more invasive, endometriosis tissue is often overlooked. As a result, current statistics may underestimate the occurrence of ovarian cancer due to endometriosis. Atypical endometriotic lesions are correlated with an increased risk of ovarian cancer development [14, 33, 38]. Multiple groups have shown that the transition from endometriosis to ovarian cancer is mediated by the development of atypical endometriosis [15, 33, 38, 50]. Atypical endometriosis is correlated with the presence of metaplasia, hyperplasia, and cytological atypia [33, 38]. Interestingly, atypical endometriotic lesions contain mutations in HNF1β [59], ARID1a loss of heterozygosity (LOH) [14, 15], and decreased levels of progesterone [14, 15, 18, 33, 38, 51, 59].

These atypical lesions contain multiple aberrations including activating mutations in the catalytic subunit of PI3K (PIK3CA) in exon 9 and exon 20, deletion of ARID1a (LOH i.e. loss of function of an allele on one chromosome), as well as overexpression of HNF1β (a transcription factor involved in increased metabolism) [14, 15, 17, 18, 59]. Further, studies have shown mutations such as p53 inactivation [12], PTEN deletion and/or inactivation [17, 18], and increased K-Ras expression [60, 61]. These mutations are considered critical for the transition from endometriosis to ovarian cancer [12, 14, 60, 61]. One study has even suggested that K-Ras may be a key marker involved in the transition from atypical endometriotic lesions to clear cell ovarian carcinomas [61]. However, since these studies utilized patient samples from advanced stage IV ovarian cancers, the invasive nature of the cancer tissue may have hindered detection of endometriotic lesions.

The transformation from endometriosis to ovarian cancer is a poorly defined process. One hypothesis argues reactive oxygen species (ROS) and inflammatory responses within the endometriotic cyst may promote this transition to cancer [13, 35, 88, 89]. As discussed in Chapter 1, these endometriotic cysts, also known as "chocolate cysts," are filled with "old blood components" including iron-rich heme. Iron inside the cyst can lead to transformation of the surface of the ovary to an ovarian clear cell like morphology [13]. Cysts may release free radical iron, generating ROS throughout the microenvironment leading to increased inflammation and cell stress [13, 35, 90]. Iron production of ROS through Fenton chemistry interactions with ROS producing enzymes (such as NADPH, NOX, and LOX), leads to free radicals that can cause DNA and mitochondrial DNA damage [13, 35, 71, 90]. While this stress often leads to cell death, consistent exposure to ROS may lead to mutations favored for tumorigenesis [13, 35, 90].

The use of patient samples to correlate endometriosis and ovarian cancer has been limiting. As mentioned above, the majority of patient studies derive from cases with advanced stages of ovarian cancer. Thus, these advanced stage ovarian cancer specimen studies could potentially prevent identification of endometriotic lesions leading to an underestimation of associated risks. Secondly, since the process of lesion removal is quite invasive, the patients frequently prefer to undergo non-surgical treatment strategies (i.e. hormone therapy) [45, 51, 52]. As a result, the patient sample size is often limited. In addition, endometriosis may be asymptomatic until it has reached an aggressive and harmful stage. Other research constraints in the field of endometriosis are the limitations with model organisms. Since the development of endometriosis necessitates the presence of an estrus cycle, a system that occurs only in primates, animal models which utilize rodents (i.e. mice and rats) are thus not ideal experimental model organisms [91, 92]. Recently, however, a validated mouse model for endometriosis has been developed [93-95] which involves the implantation of gynecological tissue of a donor mouse into a syngeneic recipient mouse [94]. This implanted tissue eventually develops into endometriotic-like lesions in the peritoneal cavity with characteristics similar to those that develop in women [91, 92]

Currently, the most accepted animal models for the study of endometriosis are baboons and rhesus monkeys [91, 92, 96]. These primates undergo an estrus cycle similar to humans and are ideal for endometriosis studies. However, baboons present difficulties in experimentation due to their time to reproductive maturity, size, and cost [91, 92, 96]. Further, endometriosis in baboons may take several years to develop with only a portion of the animals (<5%) even developing endometriosis [91]. *In vitro* research studies based on the use of cell lines also are faced with limitations. The use of primary cells has limitations with regards to both life span

(passage number) and availability (lack of patient samples from which to derive the primary cells). While a limited selection of immortalized endometriotic cell lines are available for study, their origins and purity have recently come under question (see Table 2) [4]. For example, some endometrial cell types (i.e. HES, EEC) that have been utilized by many prominent endometriosis laboratories have been recently identified to be other cell types (i.e. HeLa and MCF7, respectively) [4]. Moreover, several published endometriotic cells have not been fully validated to confirm either stromal or epithelial origin. None of the published cell lines have been Short Tandem Repeat (STR) profiled publicly [4].

This lack of cells is not without reason. One dilemma with isolating ectopic endometrium for cell line development is its diverse cellular composition. Indeed, the normal endometrial tissue termed "eutopic" (derived from the endometrium) while the cysts termed "ectopic" (growths outside the endometrium) [52] consists of a mixture of stromal and epithelial cells. In this respect, we would be required to isolate epithelial cells from the total cell population. Lastly, endometriotic cysts are not monoclonal in nature, suggesting the isolation of a selected subpopulation of cells may not represent the cysts in its entirety [97]. Due to a dire need to develop a fully validated and immortalized endometriotic cell line, we attempted to

Table 2: Table of endometriosis related cell lines.
Table provides description of endometriosis cell types available in literature along with their origin, characteristics, and reported problems [4-8].

Cell Line	Claimed Cell Type	Characteristics	Contamination
HES	Endometrial	Epithelial	HeLa
EEC	Endometrial	Epithelial	MCF7 cells
FbEM-1	Endometriosis	Epithelial	None Reported
Z-12	Endometriosis	Epithelial	Unknown
ESC	Endometriosis	Stromal	Unknown
CRL-7566	Endometriosis	Epithelial	Unknown

develop such a cell line derived from primary endometriotic cells. We obtained two primary endometriotic cell lines (called Primary C and Primary D) from the laboratory of Dr. Idhaliz Flores (Ponce School of Medicine, Puerto Rico) which was isolated from endometriotic cysts of a patient. Herein, we attempt to develop a novel endometriotic cell line that we characterize for specific markers (i.e. stromal, epithelial, EMT, tumor suppressor, cell growth, and cell cycle regulators) prior to and following retroviral infection with SV40 large T antigen. It has previously been observed that endometriotic cells express a honeycomb morphology along with expression of epithelial marks (cytokeratin) and the absence of stromal characteristics (vimentin) [5]. We believe that this novel endometriotic cell line (termed "IE" cells) will contribute toward future *in vitro* studies of endometriosis.

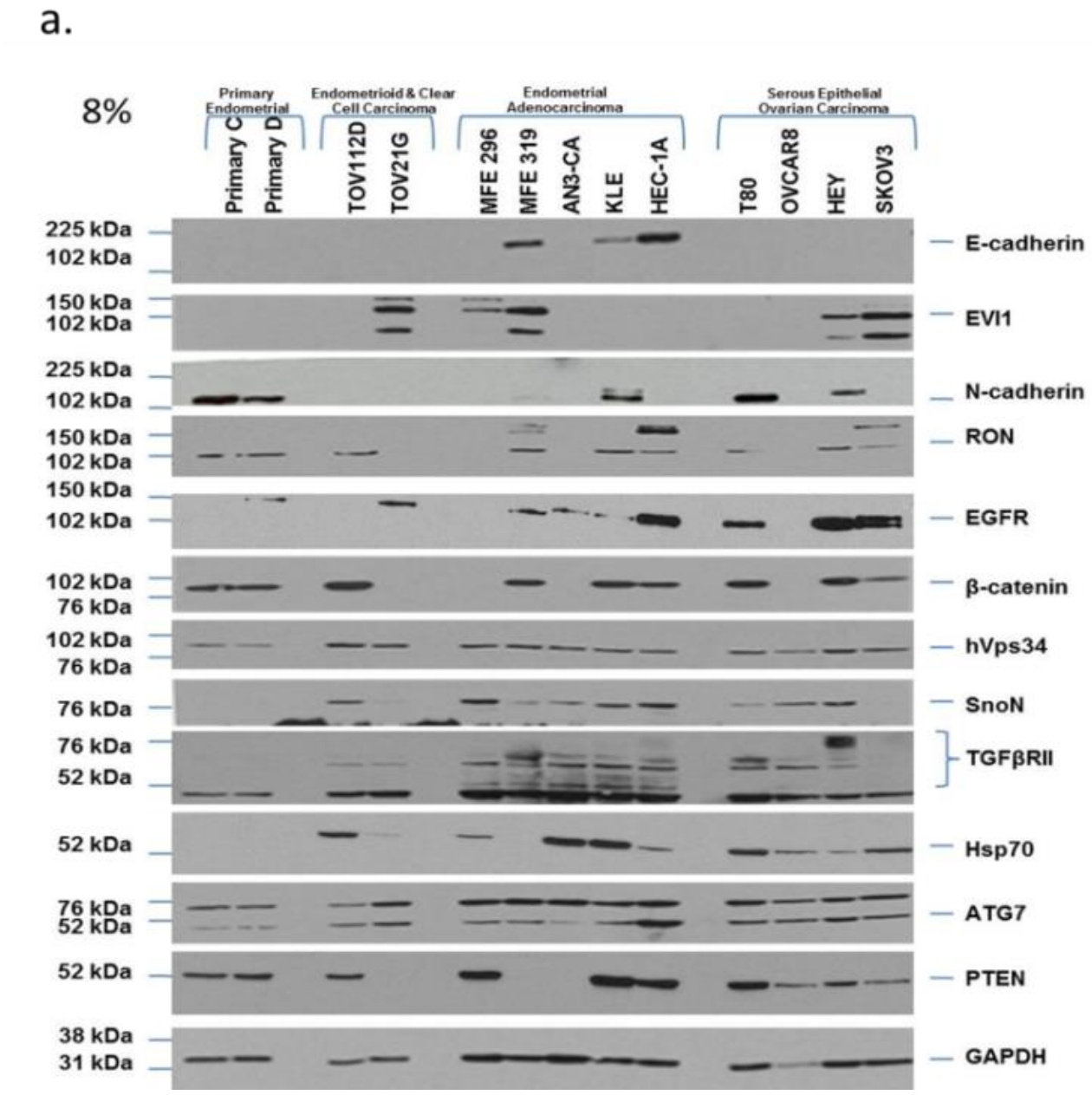

Figure 8: Cell profile of primary endometriotic cells.
Continued on following page.

b.

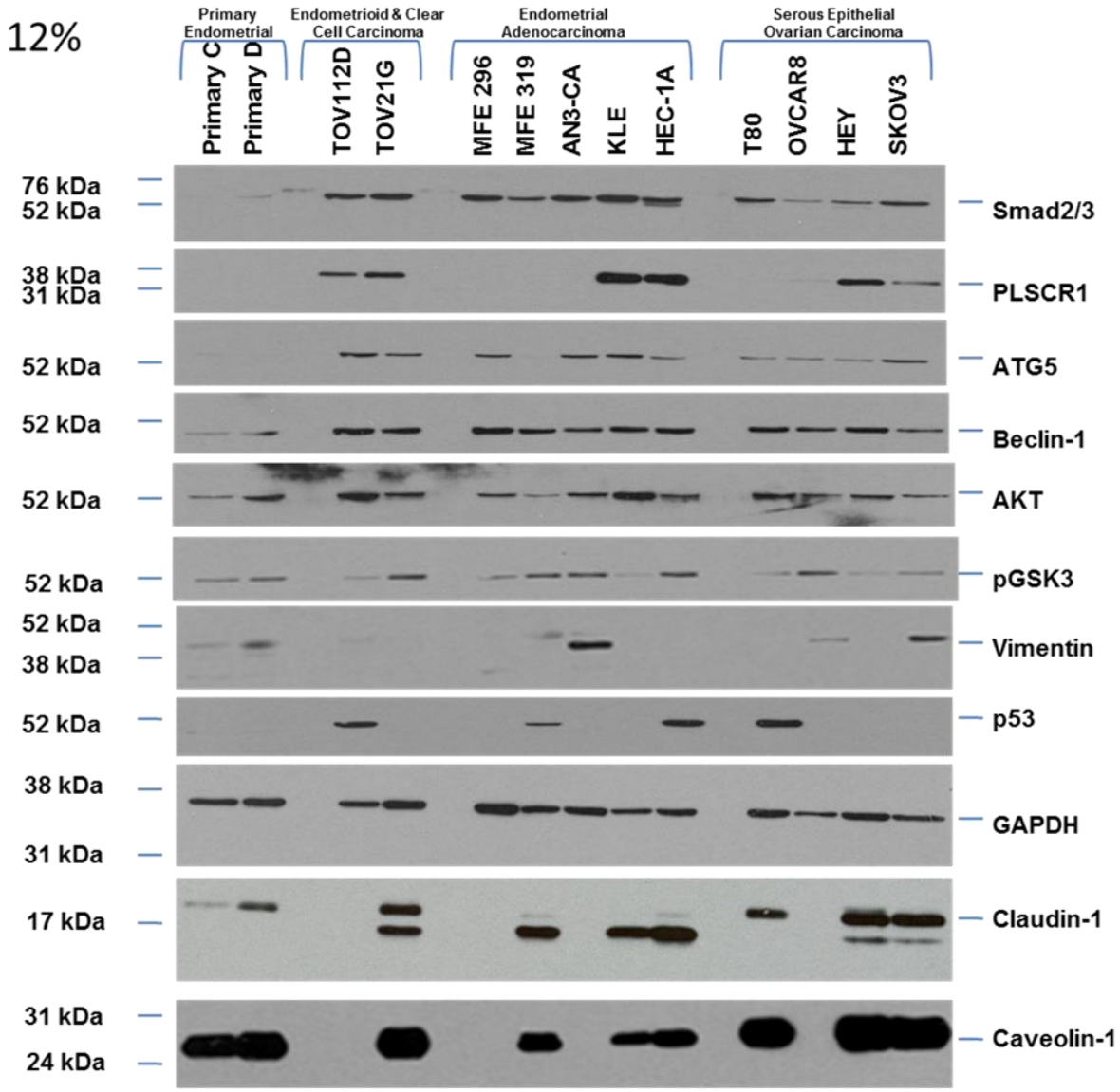

Figure 8: Cell profile of primary endometriotic cells.
Primary endometriotic cells were compared to endometrioid, clear cell, adenocarcinoma, and serous carcinoma cell lines to determine the expression patterns of tumor promoters (EVI1, RON, EGFR, SnoN, AKT), tumor suppressors (TGFβRII, Smad2/3,PTEN), autophagy markers (ATG5, ATG7, beclin-1, hVps34), epithelial markers (E-cadherin), and Stromal Markers (N-cadherin, vimentin).

Results

Basal protein expression analyses of primary endometriotic cells reveals markers of epithelial and stromal cells

Since the characteristics of the primary C and D endometriotic cells have not previously been delineated, we performed an in-depth protein analysis of markers important in cell growth, migration, regulation, and survival. The primary cells were derived from endometrial tissue of a patient with endometriosis. We wanted to investigate if the protein expression of primary cells (EMT, growth, cell cycle markers, tumor suppressors, autophagy proteins) were similar to that of any available gynecological cell line (see Figure 8). Thus, we performed western blot analyses of primary endometriotic cell C and D together with a large array of ovarian carcinoma cell lines (see Figure 8). The gynecological cancer cell lines included endometrioid ovarian cancer cell line (TOV112D), clear cell ovarian cancer cell line (TOV21G), endometrial adenocarcinoma (MFE296, MFE319, AN3-CA, KLE, HEC-1A), and serous epithelial ovarian cancer (OVCAR8, HEY, SKOV3) cell lines (see Figure 8). Along with these cell lines, a normal immortalized ovarian surface epithelial cell (T80) was also analyzed. When we carried out this cell profile, all of the cells were tested to be mycoplasma-negative and STR profiled (data not shown). This is of importance as recent reports revealed that multiple gynecological cancer cell lines have been mis-identified or contaminated by rapidly growing cell lines including HeLa [4]. Fortunately, one study performed STR analysis on HEC-1A, KLE, and AN3-CA and have found they all contain a unique profile [4]. In addition, we have validated our HEY, TOV21G, and TOV112D cell lines via STR profiling and authenticated their identity (data not shown).

We next surveyed an array of proteins critical in cell growth, regulation, and survival to determine global expression patterns. First, we assessed whether the cells were epithelial or

stromal in origin. We investigated the expression of epithelial markers including E-cadherin as well as stromal markers including N-cadherin and vimentin (see Figure 8). Next, we assessed the proliferative capacity of the primary cells relative to ovarian cancer cell lines. To address this, we investigated the expression of tumor promoters including EVI1 and SnoN/SkiL (a TGFβ co-repressors amplified at the 3q26.2 locus in ovarian cancers) (see Figure 8) [98]. We then assessed the expression of tumor suppressors including p53, PTEN, and Smad2/3 (see Figure 8). We also assessed markers of autophagy (ATG5, ATG7, beclin-1) in the primary cell types relative to ovarian cancer cells since some studies have implicated autophagy in influencing cell survival, possibly endometriotic and endometrial cell survival (see Figure 8) [78, 81].

As shown in Figure 8, the primary cells expressed tumor suppressors PTEN and Smad2/3 with undetectable levels of the tumor promoters EVI1 and SnoN/SkiL. We were unable to detect E-cadherin expression in both the primary C and D cell lines although we did detect low level expression of the stromal markers, vimentin and N-cadherin. These results suggest that the primary cell lines contain characteristics of stromal cells. Indeed, visual observation of the primary cells under the light microscope clearly demonstrates the presence of two distinct cell types, one with honeycomb morphology representative of an epithelial-like endometriotic cell population with another cell type of a more elongated, fibroblast-like morphology (data not shown). Furthermore, after several passages in culture, the population shifted greatly in favor of the stromal-like morphology suggesting that the stromal-like cell population were capable of outgrowing the slower growing epithelial population (data not shown). In addition, we noted that the cell line growth capacity slowed markedly after 10 passages in culture, which hindered long-term studies.

Retroviral infection with SV40 large T antigen extends lifespan of IE cells

Due to the limited passage number inherent with the primary cell line, we proceeded with immortalization. In brief, immortalization can occur through the expression of large T and small T antigens thus leading to inactivation of p53 [99, 100]. The expression of hTERT is also required to prevent the shortening of telomeres which would eventually lead to cellular senescence [101]. While these two agents are classical markers of cell line immortalization, a number of other markers are considered important in immortalizing primary cells (as well as in tumor development) including Ras mutations and activation of the PI3K pathway which leads to increased cell proliferation [18, 61, 93, 95, 99, 101].

In our approach to immortalize the endometriotic primary cells, we infected both primary C and primary D cells with retrovirion particles harboring the SV40 Large T Antigen along with a separate batch of cells infected with retrovirion particles harboring hTERT. As a comparison, the immortalization of the normal surface ovarian epithelial cell, T80, previously developed by Dr. Liu (MD Anderson Cancer Center) was performed in a similar fashion [101]. Since T80 and our primary endometriotic cells are both of gynecological origin, we believed a similar approach to immortalization would be successful. Following retroviral infection, the cells were successfully maintained in the absence of ITS (insulin-transferrin-selenite) [101].

Positive cells were selected using the puromycin selective marker. hTERT infection resulted in high levels of toxicity resulting in the inability to maintain the cell line. However,

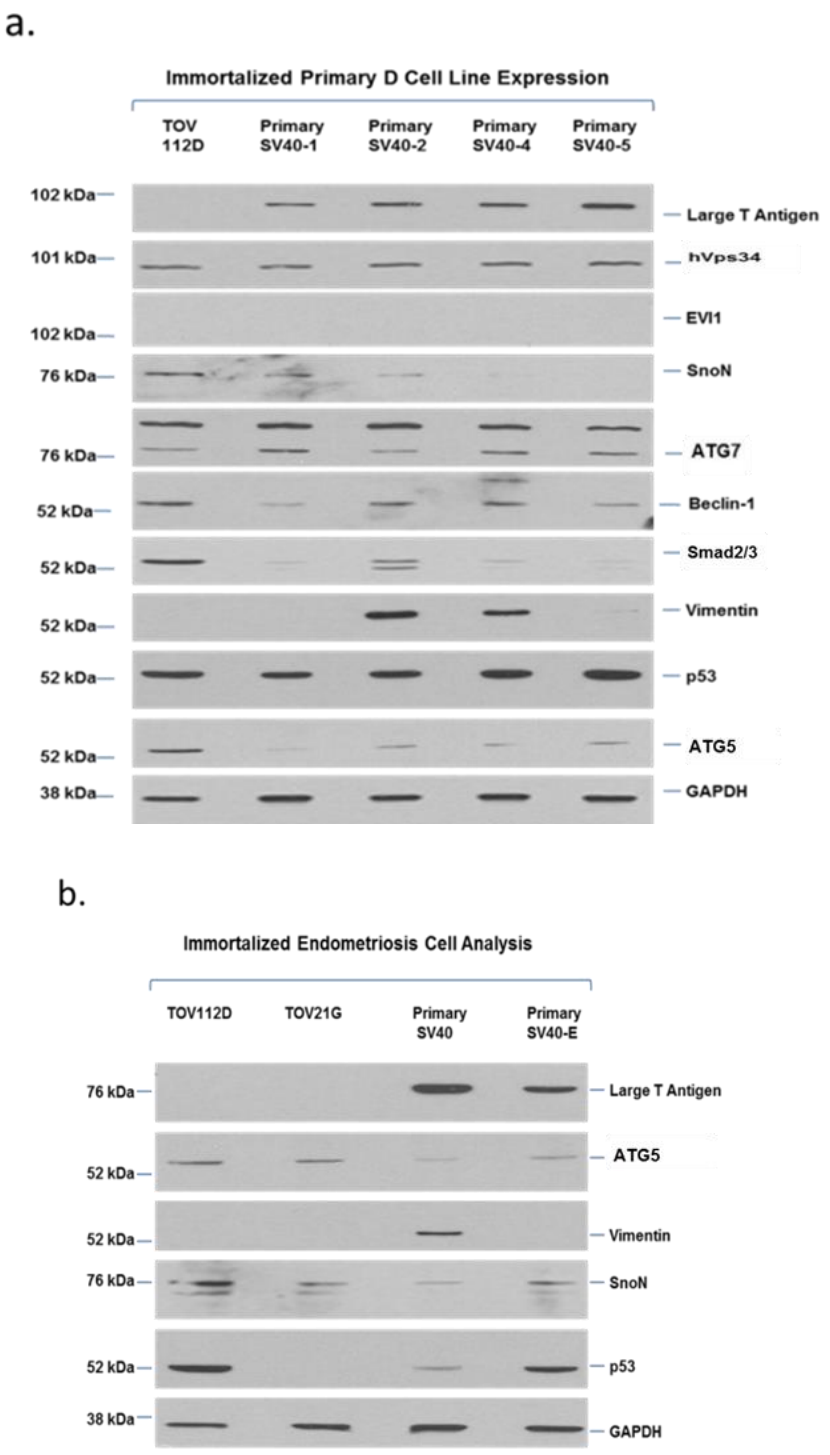

Figure 9: Cell profile of immortalized endometriotic cells.
Continued on following page.

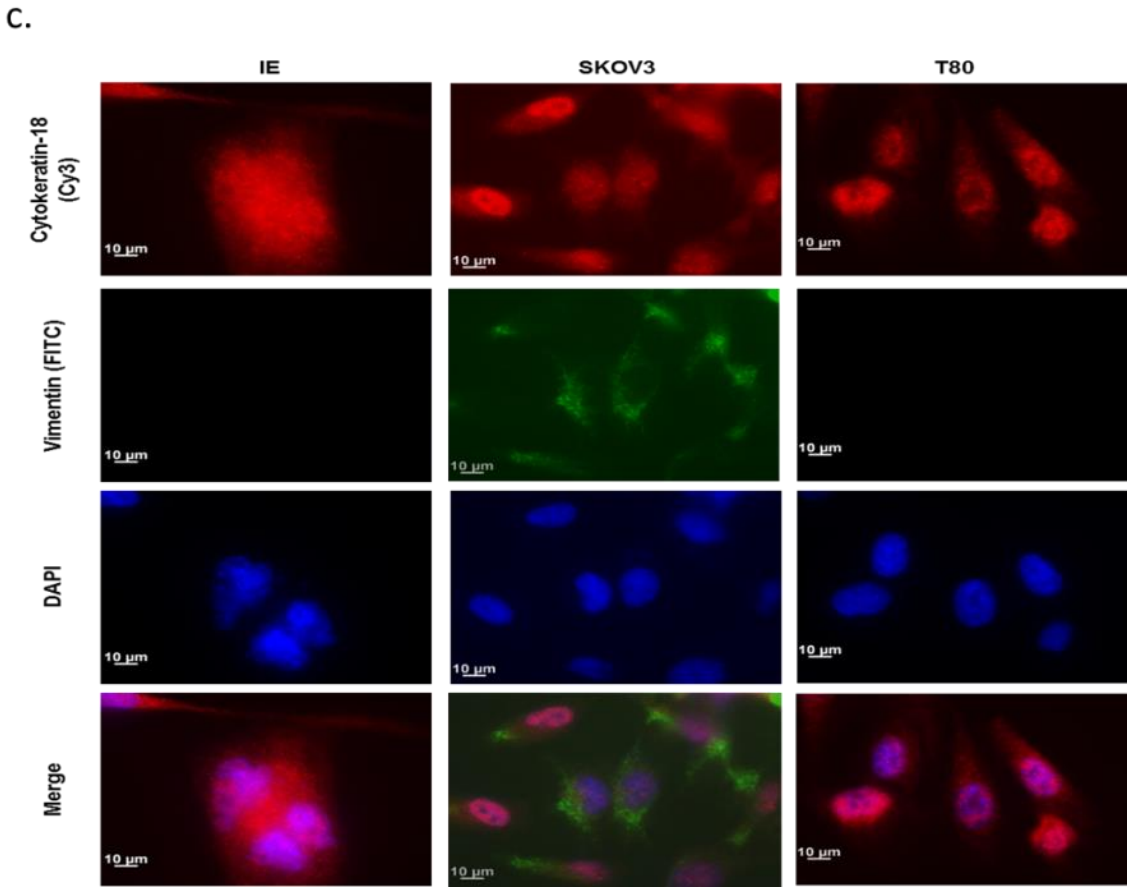

Figure 9: Cell profile of immortalized endometriotic cells
A/B. Primary D endometriotic cells were retrovirally infected with SV40 large T antigen and selected with puromycin. Individual colonies were picked and grown in culture for one month. Lysate was collected from each colony and assessed for expression of large T antigen. Other markers were used to assess change in cell expression due to SV40 large T antigen (EVI1, SnoN, and autophagy markers) as well as confirmation of positive selection of epithelial cells (absence of vimentin). Expression of p53 indicates inactivation via expression of large T antigen. **C**. Confirmation of absence of vimentin and presence of cytokeratin-3 (Cy-3) (epithelial marker) was performed via immunofluorescence. T80 cells serve as a positive control for Cy3 and SKOV3 a positive control for vimentin.

several SV40 large T antigen clonal pools were successfully obtained. Colonies were selected based on the epithelial-like morphology and maintained for a month to ensure stable expression

of large T antigen. Validation of SV40 large T antigen expression in all colonies was performed via western blot analyses (see Figure 9). We observed decreased expression of the stromal marker vimentin (relative to the primary cells), indicating that we successfully selected for the epithelial-like population of endometriotic cells (see Figure 9). To confirm the epithelial nature of the selected populations, we performed immunofluorescence staining for cytokeratin-18 (epithelial marker [102, 103]) and vimentin (mesenchymal marker [104]) (see Figure 9). T80 cells were utilized as a positive control for cytokeratin-18 and a negative control for vimentin while SKOV3 ovarian cancer cell line was utilized as a positive control for vimentin and cytokeratin-18 (see Figure 9) [104, 105]. The results indicate that the endometriotic SV40 large T antigen expressing cells had strong expression of cytokeratin-18 with undetectable expression of vimentin (see Figure 9).

Presently, we have been able to maintain the SV40 large T antigen expressing endometriotic cell lines in culture up to 15 passages. We are still unsure of the effects of long term effects of passaging these cells and are continuing to investigate the behavior of the cell line. Interestingly, we have noted that the cells, after a number of passages, begin to proliferate at a slower rate suggesting that the cells requires the presence of another immortalization marker to become fully immortalized. We attempted to stably express hTERT in the SV40 large T antigen IE cells, but encountered the same high level of toxicity as before. One potential explanation for cell death may be due to hTERTs ability to induce apoptosis in normal human cell lines [106]. Furthermore, transformation via Ras or PI3K modulation may be necessary before the IE cells can tolerate the addition of hTERT.

To confirm that the life-span extended endometriotic cells (IE cells) were not altered by stable expression of SV40 large T antigen, we compared expression of various protein markers

to those expressed in the primary cell lines (endometriotic cells not expressing SV40 Large T antigen) (see Figure 9). Similarly, we detected low levels of tumor promoting signals (EVI1, SnoN), expression of tumor suppressor Smad2/3, and expression of autophagy markers (ATG7/ATG5/beclin-1/hVps34) which were all unchanged relative to the primary cells (see Figure 9). This pattern of expression was also compared to the ovarian cancer cell lines, the clear cell ovarian cancer TOV21G and endometrioid ovarian cancer TOV112D. The morphology of the life-span extended endometriotic cells was indistinguishable from the epithelial endometriotic primary cells. The only striking difference noted, was the increased expression of p53 which could potentially be explained due to the role of large T antigen in inactivating p53 leading to the inability of p53 to turnover (degradation and ubiquitination via MDM2 would be expected to be altered) in normal cellular functions (see Figure 9) [100].

Ras and PIK3CA genomic mutations are lacking in IE cells with a "unique" STR profile

Since Ras and PIK3CA are considered important mediators in the transition from endometriosis to clear cell ovarian cancer, we next assessed the mutational status of the genes in the IE cells. Genomic DNA from IE cells was isolated and primers for PIK3CA (specifically at exons 9 and 20) as well as K-Ras (specific for the GTP binding site) were synthesized and utilized for sequencing. Their sequences were compared to the normal sequence expression derived from T80 parental cells to confirm no mutations were present (data not shown).

In order to ensure that the IE cells lack markers of other potentially contaminating cell types, we isolated genomic DNA from the IE cells and performed a short tandem repeat (STR) profiling analysis (via Genetica Laboratories). STR is the analysis of repeated segments of DNA (roughly 2-6 base pairs) spread through the genome [107]. In brief, Genetica provides a highly

sensitive DNA screen of the cell lines provided and compare them available data bases. The service is useful for both human and mouse cell types and allows for certainty of cross contamination down to 5% of the DNA. The assessment included a survey of a database of cell lines including cells from ATCC. The analysis indicated that the IE cells were unique in origin from any other cell type in the databases available to Genetica (data not shown). We are presently in process of authenticating the cell line using genomic DNA isolated from the patient.

Inhibition of autophagy hinders IE cell survival

Recently, reports have suggested that autophagy is important in the growth and survival of endometriotic cells [8, 28, 78, 81, 108]. In brief, one study showed autophagy was critical in the basic cyclical functions of the endometrium which express high levels of LC3-II in *in vivo* specimens [78, 108]. *In vitro* studies also revealed that inhibition of autophagy led to apoptosis in normal human endometrial Ishikawa cells [78]. To address whether the immortalized endometriotic cells (IE) elicited altered growth survival following inhibition of autophagic flux, we tested the effect of the autophagy inhibitor, chloroquine (CQ). This inhibitor prevents lysosome fusion with the autophagosome, thus inhibiting autophagic turnover [109]. Successful inhibition of autophagy with CQ can be validated via LC3-II accumulation by western analyses. Treatment with CQ at 25μM successfully inhibited autophagic turnover as shown via LC3-II accumulation (see Figure 10). Exposure to CQ led to a significant reduction in cell survival following 96 hour treatment (see Figure 10). These results suggest that IE cells are "addicted" to autophagy which is needed to sustain cell survival.

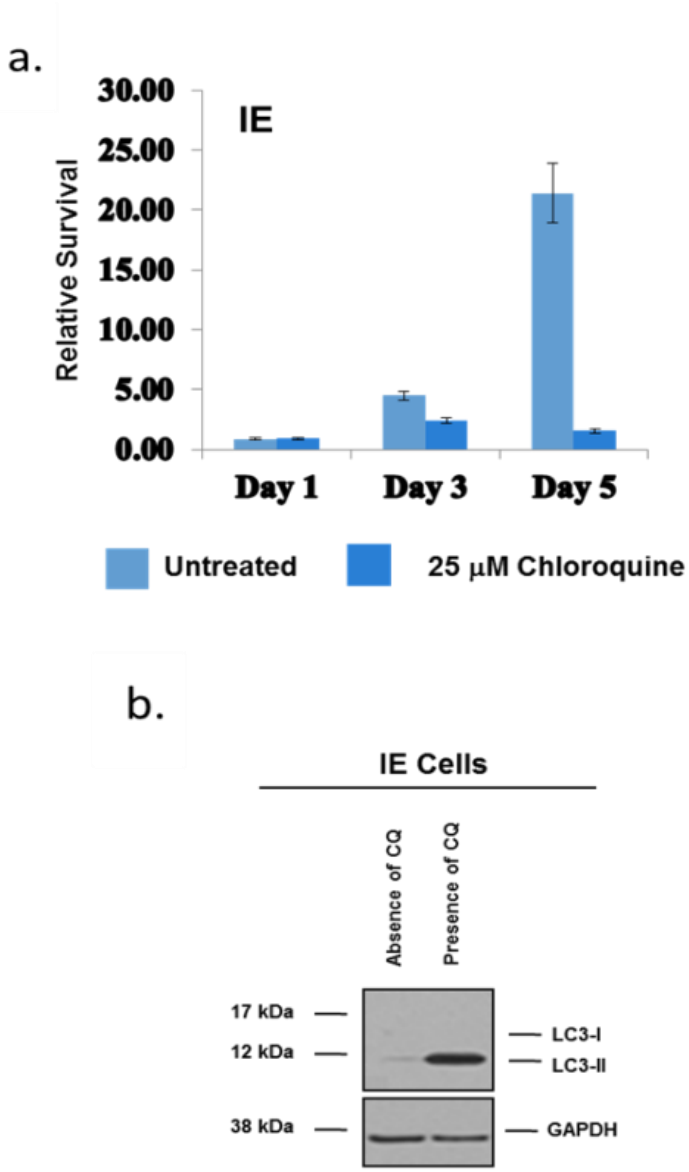

Figure 10: Inhibition of autophagy hinders IE cell growth
A. IE cells were treated with 25 µM chloroquine for up to 96 hours. Cells were stained with crystal violet and measured for overall growth. **B.** Validation of chloroquine inhibition is presented by showing accumulation of LC3-II indicative of inhibited autophagic flux.

Discussion

The field of endometriosis is a rapidly growing research area that has seen significant strides in understanding the origins of endometriosis and improving methods of treatment. However, the investigative tools needed to carry out endometriosis studies have proven very limiting. *In vitro* studies have focused heavily on cell lines that are either not validated, proven to be misidentified, or questionable in cellular origin [4, 5]. We present herein, our attempts to develop a lifespan extended novel endometriotic cell line with epithelial-like characteristics. The development of a validated novel cell line will provide a much needed tool for future *in vitro* based studies in the field of endometriosis and clear cell/endometrioid ovarian cancer research. IE cells are derived from cells obtained from the normal endometriotic tissue of a patient with endometriosis. These cells contained a mixed population of stromal and epithelial-like cells; the latter of which was selected through immortalization with SV40 large T antigen (see Figure 9).

The data presented in this Chapter demonstrates our successful attempts to isolate endometriotic epithelial cells which we confirmed through expression of epithelial marker cytokeratin-18 and the absence of vimentin (see Figure 9). Expression of large T antigen expanded the life span of the cells, but did not fully immortalize the cells. Though we were unable to overexpress hTERT in the cells, the IE cells remain an invaluable resource for further endometriosis research. The extension of the IE cell life span allows for further long term experiments to be performed. Although hTERT immortalization failed with the selected IE clone, we developed six independent IE cell lines expressing SV40 large T antigen. Future attempts to immortalize IE cells will be performed using the other five clones along with other methods for immortalizing the cells (overexpression of Ras or mutation of PTEN). Further, we plan to characterize these cell types to determine if the observations found with IE cells are

reproducible. We have also obtained two other primary endometriotic cell lines (primary A and primary B cells) that we are in the process of characterizing and immortalizing. The development of a panel of normal endometriotic cell lines will be invaluable to demonstrate reproducibility and extend studies.

Future studies would focus on markers important in the transition from endometriotic cells to a more carcinoma-like phenotype. Previous work has demonstrated the ability of normal cells to acquire cancer-like characteristics with the addition of tumor promoting markers such as Ras [105]. We aim to mutate (and overexpress) and silence (knockdown) multiple markers including PI3KCA, ARID1A, Ras, and PTEN. Modulation of the proliferative/survival capacity of the cells will demonstrate the significance of these markers in the transformation of such gynecological cell types.

Autophagy also plays an intriguing role in the survival of endometriotic cells. It has been established that the development and shedding of the endometrial lining during the menstrual cycle is dependent on autophagic turnover [78]. These reported studies provide convincing though limiting insight on the role of autophagy in the endometrial lining. We sought to develop this finding by showing IE cells cease to survive in the presence of the autophagy inhibitor chloroquine (see Figure 10). We have also recently performed a tissue microarray immunohistochemical staining of LC3B of tissue specimens derived from various endometriotic sites (from the fallopian tube and ovary) and normal eutopic endometrial tissue (data not shown). These preliminary studies demonstrated increased LC3 staining in endometriotic lesions in comparison to normal proliferative eutopic endometrial tissue suggesting that the development of endometriosis may be mediated by increased autophagic flux in the epithelial component. Overexpression of autophagic markers such as ULK1 or ATG5 in IE cells may increase the

proliferative capacity which could be assessed *in vitro* as well as *in vivo* mouse xenograft studies. Since treatment with CQ was shown to significantly inhibit cell survival of IE cells, this may suggest that IE cells are dependent on autophagy for basic nutrient and metabolic activity [79]. Indeed, increased autophagic activity may lead to a more robust metabolic response [110, 111]. In contrast, since autophagy is also a mechanism of cell death, overexpression of ULK1 or ATG5 may induce senescence or cell death [73, 79, 80]. As mentioned in Chapter 1, excess production of autophagosomes may be detrimental to vital cell functions thus leading to cell death [73, 79, 80].

Acknowledgments

Data presented in Chapter 3 is a representation of the collaborative work of the Dr. Nanjundan and Dr. Flores laboratories. Primary endometriotic cells were isolated and placed in culture by Dr. Flores and her laboratory. The immortalization and genomic analysis of IE cells were carried out with Dr. Meera Nanjundan's assistance.

Chapter 4

Iron Modulates Cell Survival in a Ras- and MAPK-Dependent Manner in Ovarian Cells

Introduction

Iron is an essential element needed for survival both on a macro (survival of an organism) and a micro level (continued growth of a cell) [25, 26]. This element has a unique role in being both essential and harmful [13, 112]. Its oxidative/redox nature (ability to gain or lose an electron i.e. Fe^{+2} and Fe^{+3} as discussed in chapter 1) allows iron to exist in active (Fe^{+2}) and inactive states (Fe^{+3}) states. In the Fe^{+2} state, iron can be utilized for a variety of functions including metabolism (i.e. citric acid cycle [113]), regulation of DNA synthesis (i.e. DNA helicases with iron sulfur complexes [114]), trafficking of oxygen via heme, and translation of protein from mRNA [13, 112]. The primary means of obtaining iron occurs through consumption of products containing iron or through blood containing iron-rich heme [112]. The presence of such a dynamic element can also elicit many negative effects in the cell. The presence of iron can lead to increased generation of reactive oxygen species which can lead to cellular damage and mutations [13, 70, 112]. These mutations include genomic DNA and mitochondrial DNA damage modulating cell regulatory pathways together with increased inflammation [20, 115-117]. This response can lead to a number of diseases including neurodegeneration, multiple sclerosis, and cancer [20, 115, 117].

Endometriosis (a result of menstrual tissue which retrogrades upward) travels through the fallopian tube and can implant not only in the peritoneal cavity, but also onto the ovaries [53]. The lesions can develop into endometriotic cysts. These cysts are filled with iron rich blood particles [13]. They are classified as "chocolate" cysts due to their dark brown coloration arising from the presence of "old blood" products. This iron exposure causes cell stress which can lead to DNA damage and mutations thus inducing atypical lesions and increased propensity to cancer development [13]. Iron induced ROS has been shown to modulate activator protein 1 (AP-1) and NF-kB [20]. Further, cysts are known to spontaneously burst releasing its content into the microenvironment leading to increased inflammation [32]. Since heme contributes to the cysts' contents, the microenvironment is also exposed to increased iron levels [13, 51, 118].

Interestingly, recent studies have shown a relationship between continual exposure of iron and the transformation of ovarian cell types to a carcinoma like state [34]. One study demonstrated that exposure of ovarian surface epithelial cells to free iron caused the cells to exhibit the behavior of clear cell carcinoma [13, 34]. Another report revealed a correlation between higher levels of iron present in the fallopian tubes with an increased rate of serous carcinoma [31]. While this suggests that iron plays an important role in cellular transformation, the underlying mechanism of this process or positive effect on survival remains elusive in ovarian cancer.

We propose that the exposure of iron to "normal" (immortalized cells) gynecological cell types will lead to transformation to a more carcinoma like nature. To obtain a broad understanding of the effects of iron in gynecological cell types, we obtained a diverse group of cell lines to represent the heterogeneous nature of ovarian carcinoma. As discussed in Chapter 1, autophagy can act as both a cell death mechanism and a cell survival pathway. Due to the ability

of iron to induce ROS, we hypothesized that this may lead to activation of autophagy [29, 79]. Autophagy can serve to remove damaged proteins or organelles allowing for continued cell survival [79]. Interestingly, autophagy may indirectly result in tumor promotion [79]. In order to fully understand the role of autophagy, we performed a panel of assays to assess functional response (cell death, growth, and metabolic changes) to iron. To determine autophagic induction, we identified the formation of autophagosomes as well as its importance in iron response (inhibition of autophagy). We aimed to assess not only how the cell growth is modulated, but if excess iron could modulate cell death pathways.

Treatments were carried out with ferric ammonium citrate (FAC). FAC was selected for the treatments due to its ease of solubility in aqueous solutions. Previous reported studies have shown success utilizing FAC as well [63]. We also attempted iron sulfate but the compound rapidly precipitated upon addition to cell culture media [119]. Not only would this lead to cellular stress but also lead to reduction in total iron intake (lower effective iron dose). A 250 μM dose of FAC was selected based on previous studies [13, 63]. Importantly, 250 μM is the level of iron often found in endometriotic cysts [85]. Herein, we show that iron modulates the autophagy pathway of gynecological cell types. Growth and cell death assays revealed that serous (HEY) and clear cell (TOV21G) carcinoma cell lines are significantly more sensitive to iron treatment relative to non-cancer cell types and endometrioid carcinoma (TOV112D) cell types. HEY and TOV21G contain mutations in Ras which suggests that the Ras pathway may induce iron sensitivity [120, 121]. Use of ovarian surface epithelial cells, T80, with overexpression of Ras confirmed this hypothesis. Interestingly, all of the cell lines expressed similar levels of altered metabolism, cell cycle progression, and wound healing responses

suggesting that iron elicits a global role in modulating the functional properties of gynecological cell types.

Results

Iron inhibits cell growth in Ras overexpressing/mutated cell lines

To investigate changes in cell growth, we performed a crystal violet cell growth assay. The results show differential response to treatment with iron. The normal cell types T80 and IE cells showed no significant change in proliferation (see Figure 11). We also investigated the human endometrial cell line, HES. While it showed similar trends with T80 and IE cells, it was recently reported that HES cells express markers of HeLa cells [4]. Our initial studies were performed before this study was released and we opted to halt further use of HES cells for our investigations. Further, the endometrioid carcinoma cell type (TOV112D) showed only slight decrease in growth as well (see Figure 11). In contrast, serous (HEY) and clear cell carcinoma (TOV21G) cell types showed significant decreases in overall cell growth suggesting these cells are sensitive to excess iron (see Figure 11). Interestingly, both HEY and TOV21G cells contain Ras mutations leading to constitutively active expression. Ras mutations are a common occurrence in ovarian cancer occurring in about 30% of the patient population [18, 61, 105, 122]. To determine if this mutation contributed to reduced cell survival, we obtained T80 cell lines that contained either H-Ras or K-Ras overexpression (see Figure 11) [105]. These cells were treated under the same conditions; strikingly, the cell types showed decreased cell growth upon treatment with FAC. To further understand why cell growth decreased with iron treatment, we performed an apoptosis assay to delineate the mechanism underlying cell growth decreased with iron treatment (see Figure 11). Twenty percent of the HEY cell population were in early

apoptosis and another 20% were in late apoptosis (necrosis) (see Figure 11). Since a large percentage of HEY cells were in late apoptosis and had a distinct necrotic appearance, we next performed an LDH assay to determine the percentage of necrotic cells following iron treatment. The LDH assay showed a dramatic increase in cytotoxicity supporting earlier evidence that FAC induces necrosis in HEY cells (see Figure 11). Interestingly, the TOV21G clear cell line showed no significant changes in PI or Annexin V staining. This suggests the mechanism of cell death may vary between cell lines and another mechanism of cell death/reduced cellular viability may be occurring in TOV21G cells following treatment with iron.

Iron modulates multiple cellular functions in gynecological cell types

Treatment with iron after 18 hours leads to distinct morphological change in the gynecological cell types tested. The morphology of multiple cell types could be described as

a.

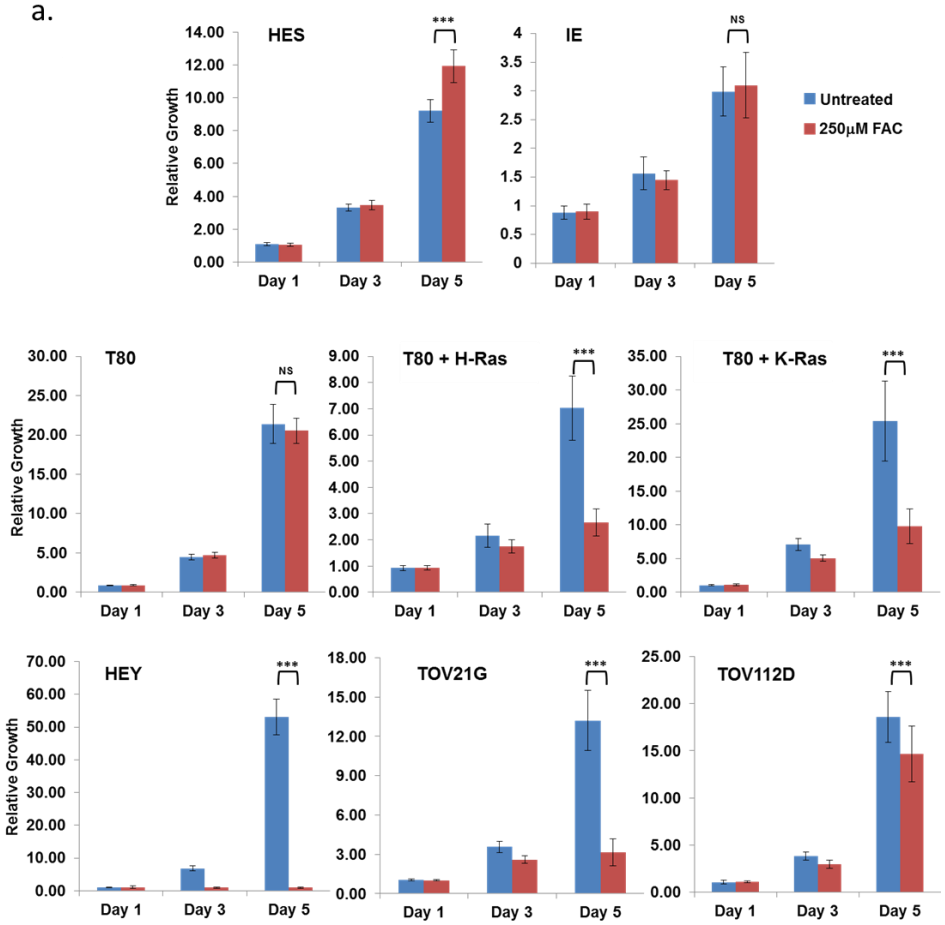

b.

Cell Lines	Description	Ras Overexpression/ Mutation status	250μM FAC % Growth Reduction
HES	Human Endometrial Epithelial Cells	-	-29.52±10.90
IE	Immortalized (LTAg) Endometriotic Cells	-	-3.75±19.15
T80	Immortalized (LTAg/hTERT) Normal Ovarian Surface Epithelial Cells	-	4.01±7.52
T80 + H-Ras	T80 Cells with H-Ras Overexpression	H-Ras	62.09±7.24
T80 + K-Ras	T80 Cells with K-Ras Overexpression	K-Ras	61.49±10.14
HEY	Serous Epithelial Ovarian Carcinoma	K-Ras Cys12Val/Gly13Ser	98.12±0.36
TOV21G	Clear Cell Epithelial Ovarian Carcinoma	K-Ras Gly13Cys	76.05±7.83
TOV112D	Endometrioid Epithelial Ovarian Carcinoma	-	21.1±15.90

Figure 11: Iron inhibits cell growth in Ras overexpressing/mutated cell lines.

Continued on following page

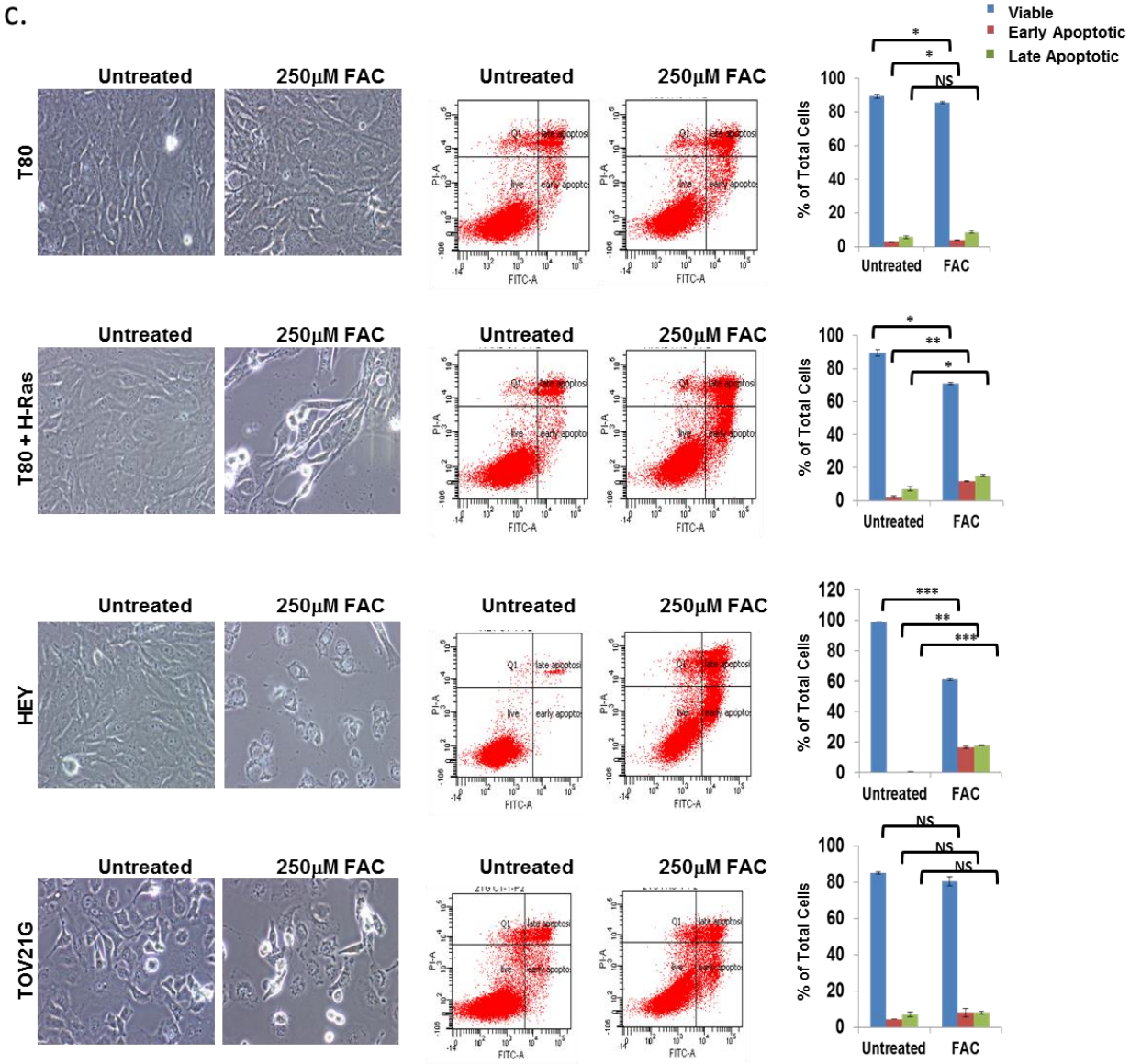

Figure 11: Iron inhibits cell growth in Ras overexpressing/mutated cell lines.

Continued on following page

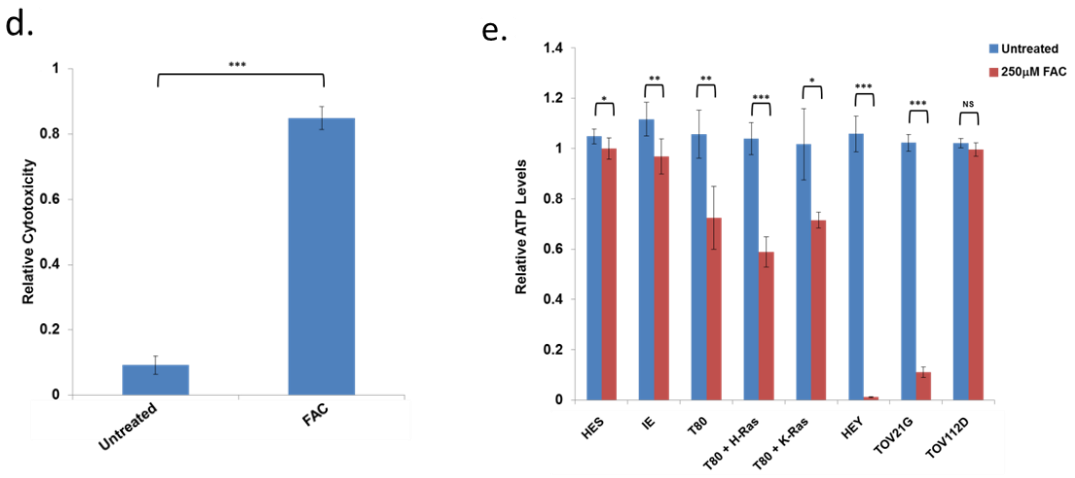

Figure 11: Iron inhibits cell growth in Ras overexpressing/mutated cell lines.
A. Crystal violet growth assays were carried out over a 96 hours period of time on T80, T80 + H-Ras, T80 + K-Ras, IE, HES, TOV112D, HEY, and TOV21G cell lines. Cells were treated with 250 µM FAC. **B.** The percent change in growth was documented for each cell type relative to its untreated control. **C.** T80, T80 + H-Ras, HEY, and TOV21G cells were treated with 250 µM FAC for 72 hours. Adherent and floating cells were collected and treated with Annexin V and Propidium Iodide (PI). They were then assessed via flow cytometry. Light microscopy images show images before collection and the graph represents changes in alive, early, and late apoptotic cells. **D.** LDH cytotoxicity assay was performed on HEY cells treated with FAC for 72 hours. **E.** All cells lines assessed via growth assay were also screened for ATP levels after 72 hours of FAC treatment.

spindle-like together with a decrease in cell size. We carried out an ATP viability assay to determine metabolic changes due to excess iron. ATP levels decreased in combination of FAC suggesting that iron-induced cellular arrest occurred as a result of diminished ATP levels. HEY and TOV21G cells showed greatest reduction of ATP levels after iron treatment (see Figure 11). This is likely due to the overall decreased number of cells and decreased growth observed.

Since FAC decreased metabolic activity, we were interested if this would result in other changes in cellular development. We performed a wound healing assay to see if iron would

reduce the ability of gynecological cells to migrate. Treatment with FAC reduced the ability of gynecological cells to fill-in the wounded area in comparison to untreated cells (see Figure 12). Untreated cells covered the wound after 30 hours of treatment while the iron treated cell types showed marked inhibition. Further, iron showed a slight but significant change in the cell cycle progression (see Figure 12). Iron halted gynecological cell progression (T80, HEY, TOV21G, TOV112D) in G1 by 5% and reduced the cell number present in S phase by 3% (data not shown). These percentages varied with each cell type with a small but significant increase of cells in G1 phase.

Iron treatment induces autophagy

We observed distinct formation of vacuoles upon treatment of iron with all gynecological cell types. Vacuoles are considered potential markers for autophagic activation which provided motivation to investigate further additional markers of autophagic activation [123]. These vacuoles were first detected in robust levels in T80 cells and we initially carried out our investigation with these cells as a model (see Figure 13). Vacuole formation, however, could be indicative of multiple cell phenomena including accumulation of lipids and aggregates. Thus, validation with tested markers of autophagy is required before confirmation of autophagy activation [123]. Treatment with FAC up to 30 hours shows increase in LC3-II which is suggestive of the formation of autophagosomes (see Figure 13). To confirm autophagosome formation with other gynecological cell types, we performed another western blot analysis of LC3-II looking at 18 hours of treatment (see Figure 13). The panel of cell lines all show increase in LC3-II suggesting autophagy was induced in all gynecological cell types tested (see Figure 13). We also investigated changes in p62 but observed variable response. Although p62 is

traditionally thought to decrease during autophagic activation, there are additional functions reported for p62 which thus explains this variability

a.

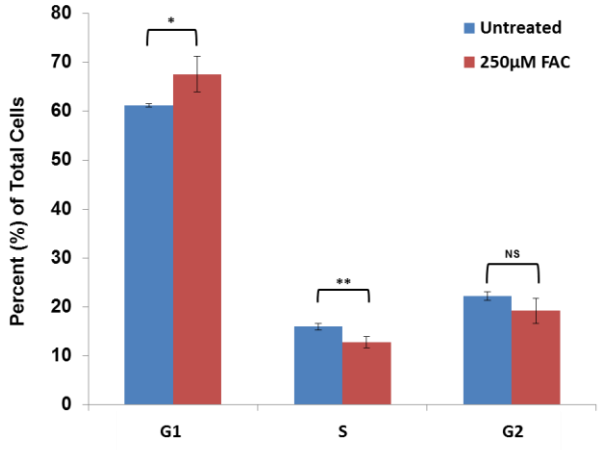

Cell Treatments	% G1	% S	% G2
Untreated	61.21±0.37	15.99±0.64	22.23±0.82
250μM FAC	67.60±3.68	12.81±1.12	19.21±2.53

b.

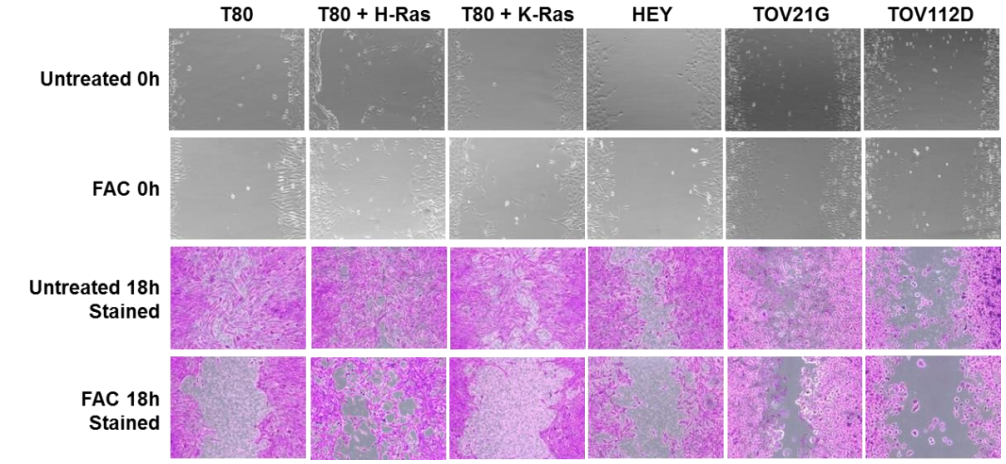

Figure 12: Iron modulates cellular functions in gynecological cell lines. **A.** Cell cycle analysis was performed on T80 cells treated with FAC for 30 hours. Slight but significant increase in G1 and decrease in S phase were reported. Similar trends were seen in HEY, TOV21G, and TOV112D cells (data not shown). **B.** Wounds were developed in confluent plate followed by treatment with and without FAC for 18 hours. Cells were imaged via light microscopy.

(data not shown) [124, 125]. Since autophagic response was similar across multiple cell lines, we decided to utilize the T80 cells to elucidate the mechanism for autophagy induction.

An N-terminal EGFP-LC3 plasmid was transfected into T80 cells followed by 18 hour treatment of FAC (see Figure 13). Cells were viewed via direct immunofluorescence viewing for the presence of LC3 punctae (see Figure 13). If autophagy is occurring in the cell, the EGFP-LC3 would change from a diffuse green, to punctate formation suggestive of conversion from LC3-I to the lipidated LC3-II form (see Figure 13). Two hundred cells per experimental replicate were analyzed for distribution of LC3-II, specifically diffuse versus punctate localization. We set a minimum of 20 punctae per cell as a requirement to confirm the presence of autophagosomes [98, 123]. Treatment with FAC showed more than a 3-fold increase in cells undergoing autophagic flux, supporting the LC3 results obtained via western analysis.

Since increase of LC3-II is only an indication of increased autophagosomes and not increased autophagic flux which involves turnover (fusion of autophagosome with the lysosome), further studies were required. To address this question, we utilized the autophagy inhibitor chloroquine (CQ) to determine if FAC increased autophagic flux. CQ inhibits the fusion of lysosomes with autophagosomes leading to an increased accumulation of LC3-II (interpreted through western analysis) (see Figure 13). If the level of LC3-II is higher in combination of chloroquine with FAC in comparison to chloroquine alone, this indicates that autophagic turnover is occurring via FAC treatment. In all cell lines, we found that 250μM FAC leads to increased LC3-II in combination with CQ in comparison to cells treated with CQ alone (see Figure 13). Interestingly, iron treatment at 5mM levels prevented autophagic turnover suggesting that extremely high levels of iron can block autophagic flux. Along with CQ, we utilized a free GFP-LC3 assay to examine autophagic activity [126]. In this assay, the plasmid

has a C-terminal tagged GFP to LC3. The C-terminus is cleaved upon conversion of LC3-I to LC3-II which liberates the GFP portion into the cytosol. Increase of untagged GFP would be an indication of increased autophagic flux. We performed this study with HEY cells and found increase of GFP in tandem with increased LC3-II with FAC treatment (see Figure 13). Further, the increased presence of autophagosomes was visualized via transmission electron microscopy (see Figure 13). T80 cells, treated with FAC after 18 hours, were identified to contain distinct double bound membrane structures indicative of the presence of autophagosomes (see Figure 13) [123].

We were also interested in understanding the mechanism of autophagic activation via iron treatment. We carried out siRNA transfections for ATG5, ATG7, hVps34, and beclin-1, all of which are classic regulators of autophagy (see Chapter 1, Figure 3). Knockdown of ATG5 and ATG7 successfully reversed the LC3-II induced by treatment with FAC (see Figure 14). However, knockdown of beclin-1 and hVps34 did not inhibit induction of LC3-II; thus leading to the inference that FAC-induced activation of autophagy is beclin-1/hVps34 independent (see Figure 14). We validated this by treating with the autophagy inhibitor 3-MA (3-methyladenine) which inhibits the PI3K/hVps34/beclin-1 autophagic pathway (see Figure 14). No changes were observed in LC3-II levels with the addition of this inhibitor suggesting that beclin-1/hVps34 does not play a role in iron-induced autophagy. We were also interested to see if autophagy activation was beneficial to iron treated cells. Thus, we investigated the changes in cellular response to iron upon knockdown of ATG5 and ATG7. We carried out growth and ATP viability assays to determine if any change would occur in HEY cells (see Figure 14). There was only a slight but significant change suggesting autophagy plays at most a minimal role in

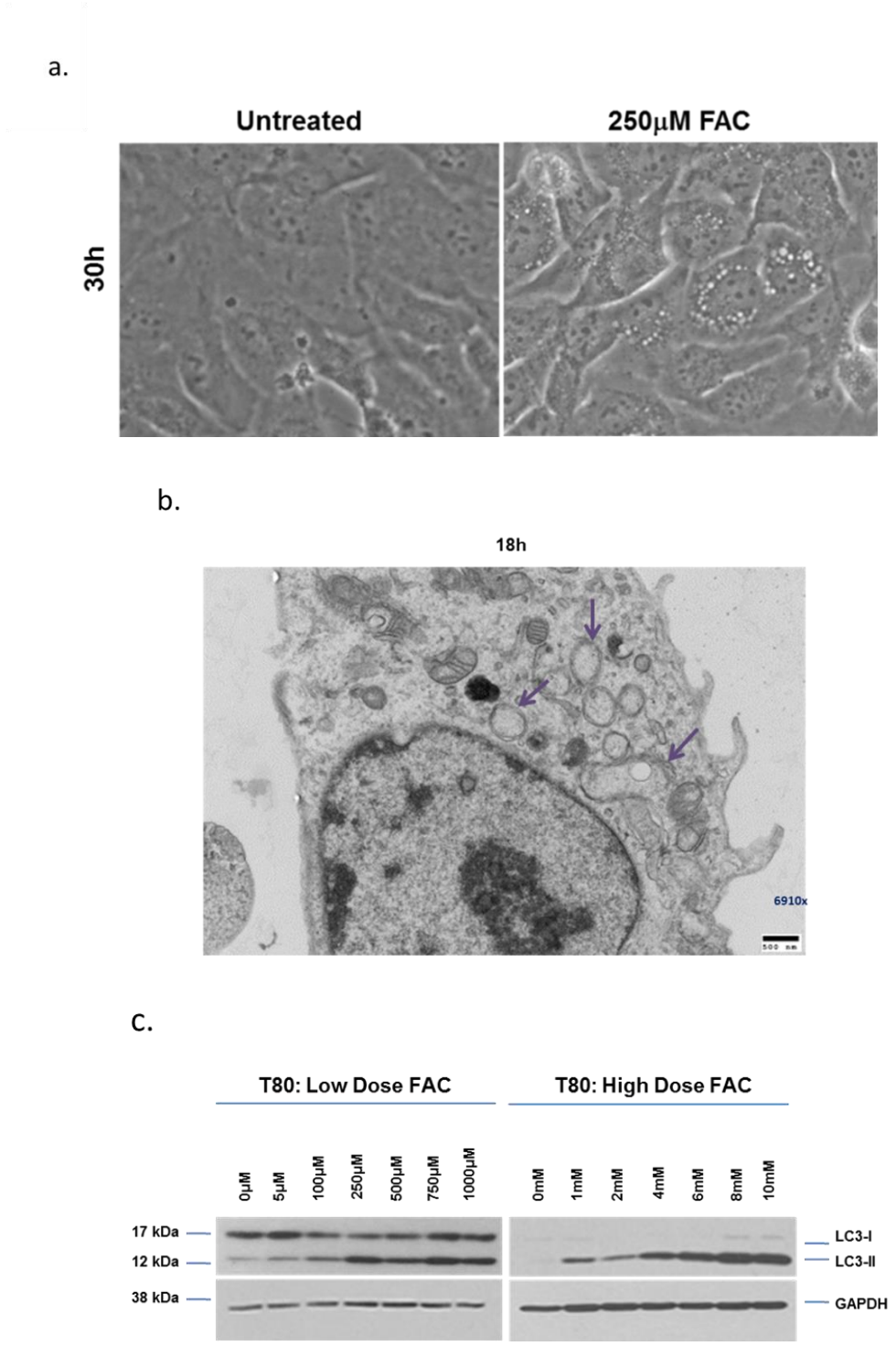

Figure 13: Iron treatment induces autophagy.
Continued on following page.

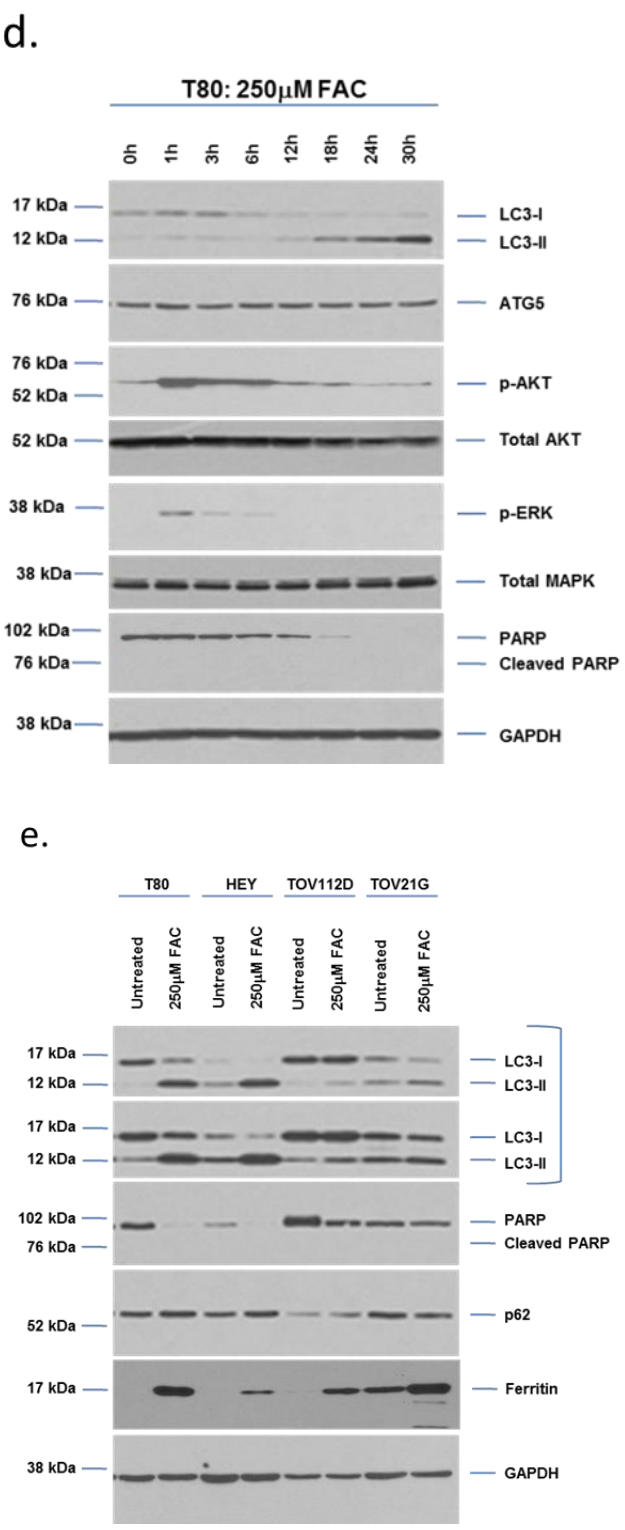

Figure 13: Iron treatment induces autophagy.
Continued on following page.

f.

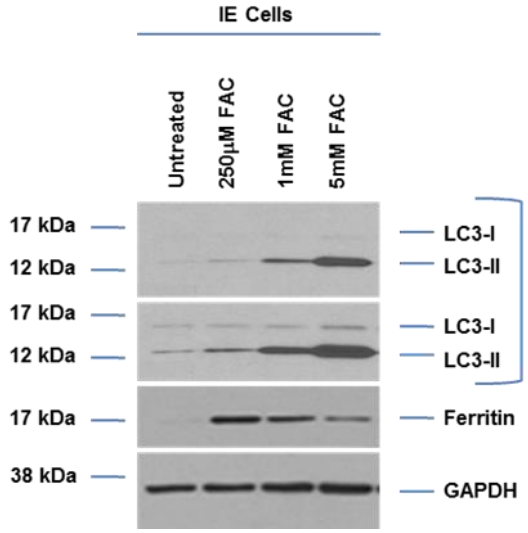

g.

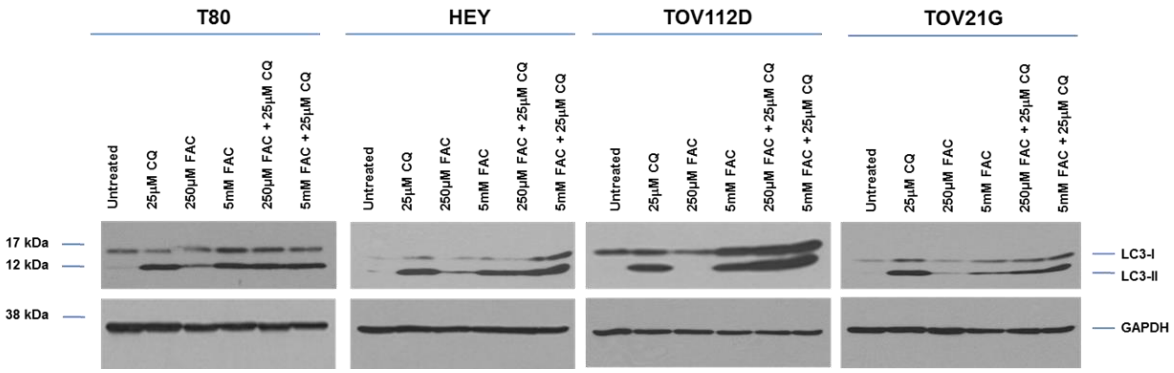

Figure 13: Iron treatment induces autophagy.
Continued on following page.

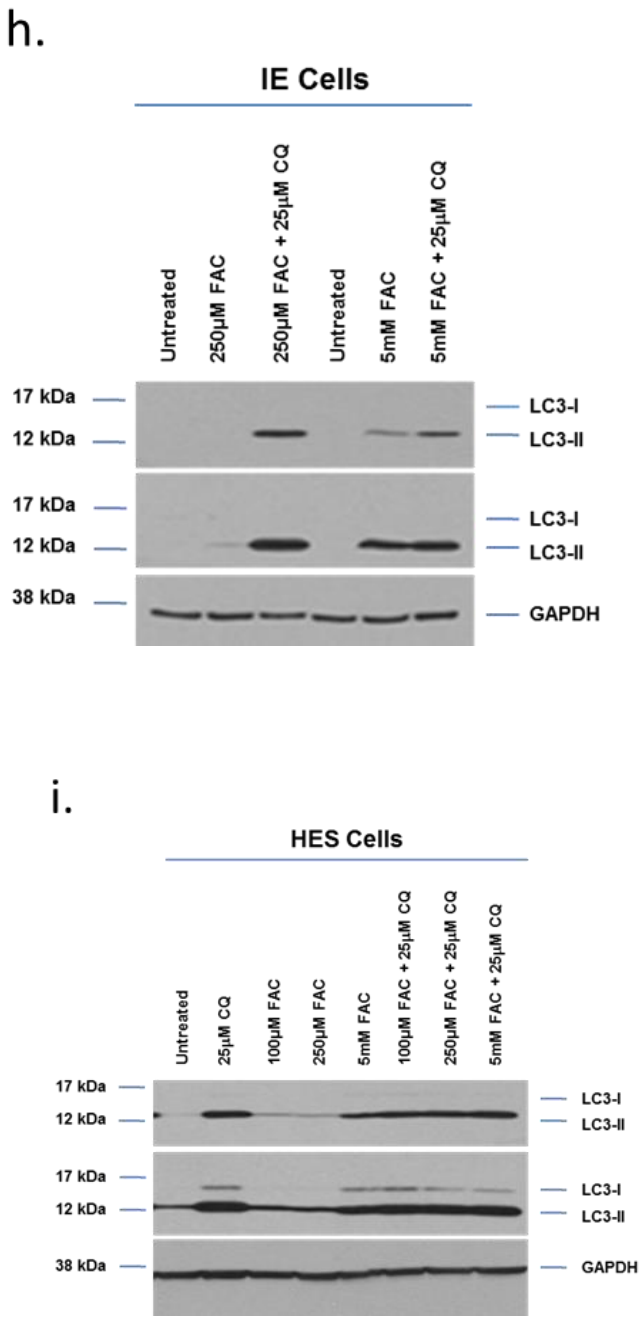

Figure 13: Iron treatment induces autophagy.
Continued on following page.

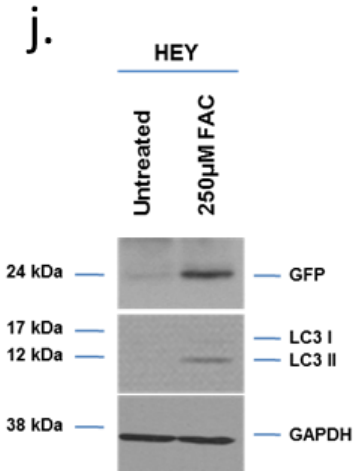

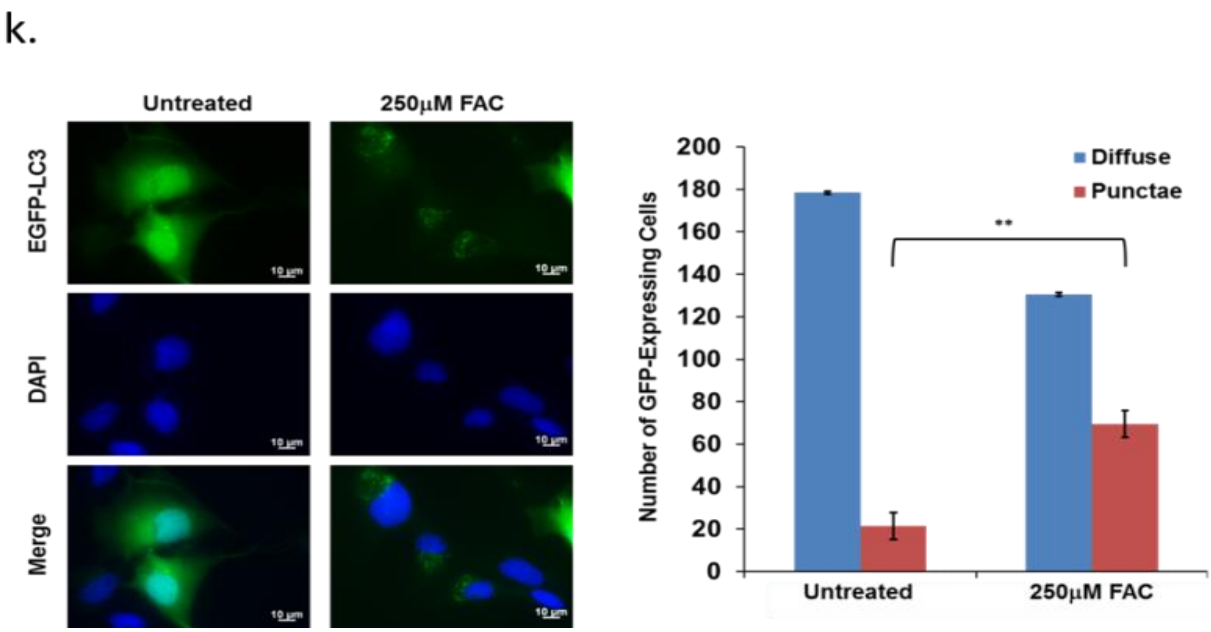

Figure 13: Iron treatment induces autophagy.
Continued on following page.

Figure 13: Iron treatment induces autophagy.
A. Light microscopy (40x) image of T80 cells treated with 250 μM FAC for 30 hours. **B.** T80 cells treated with iron for 18 hours were analyzed via TEMs. Arrows indicate double bounded membrane autophagosomes. **C.** Lysate of iron treated T80 cells was assessed for LC3-II levels at increasing doses of FAC (5 μM to 10 mM). **D.** T80 cells treated with 250 μM FAC over multiple time points (0 h to 30 h). **E.** 18 hour 250 μM FAC profile of T80, HEY, TOV112D, and TOV21G cell lines. **F.** IE cells treated with increasing doses of FAC (250 μM to 5 mM) over 18 hours. **G.** T80, HEY, TOV21G, and TOV112D cells treated with 250 μM FAC, 5 mM FAC, 25 μM CQ, or a combination of FAC and CQ were assessed after 18 hours of treatment. **H.** IE cells were treated with 250 μM FAC, 5 mM FAC, 25 μM CQ, or a combination of FAC and CQ and lysate was collected and analyzed. **I.** HES cells were treated with 100 μM FAC, 250 μM FAC, 5 mM FAC, 25 μM CQ, or a combination of FAC and CQ. **J**. HEY cells were transfected with GFP-LC3 and then treated with 250 μM FAC and then assessed. **K.** T80 cells were transfected with EGFP-LC3 and then treated with FAC at 250 μM. An inverted fluorescence microscope was used to assess samples. Cells with greater than 20 punctae were classified as autophagy positive cells.

iron induced cell death. We also performed these studies with T80 cells and found no significant modulation in T80 cell growth with and without iron treatment in the presence of ATG5/7 siRNA (data not shown).

Treatment with iron leads to increased lysosomes in a Ras-independent manner

Along with an increased presence of autophagosomes, the TEM studies revealed an increased number of lysosomes after 24 hours of treatment in T80 cells (see Figure 15). The large lysosome structures (around 1.2 μm ranging on the high end of lysosome size) could potentially be late stage autophagolysosomes [123]. These structures are the end product of autophagy, where the inner membrane is broken down and the contents are degraded.

Interestingly, we also observed the presence of iron particles inside of the lysosomes. This was validated using iron dissolved in liquid media (see Figure 15). The iron particles were determined to be 2-3nm in size. These particles were detected in clusters inside the lysosomes following 24 hours FAC treatment (see Figure 15). To validate the changes in lysosomes observed by TEM, we carried out a lysotracker analysis of T80 as well as other cell lines investigated in this study.

Lysotracker is highly selective for acidic organelles, specifically lysosomes.. We also were interested in confirming the presence of iron inside the lysosomes. To achieve this, we stained with Calcein-AM which is a cell permeable chemical that is classically used to assess cell viability (see Figure 15) [127]. Calcein-AM, however, fluoresces in the presence of iron and thus is a useful tool for detection of localization of the element as well [128]. We treated T80 cells for 24 hours and stained with Lysotracker Red and Calcein-AM and found an increase of both lysosomes and iron in the cells (see Figure 15). We also found co-localization of the two stains supporting the TEM findings of iron being present within the lysosome (see Figure 15). Interestingly, HEY cells showed no increase of lysosome number after 24 hours of FAC treatment together with a diffuse Calcein-AM staining (see Figure 15). This suggests HEY cells may undergo lysosomal permeabilization when exposed to iron leading potentially to cell death. However, this observation was not seen in T80 + H-Ras cells where there was no significant difference in lysosome numbers compared to T80 parental cells (see Figure 15). This suggests iron-induction of lysosomes occurs independently of Ras modulation. We quantified the Lysotracker Red

a.

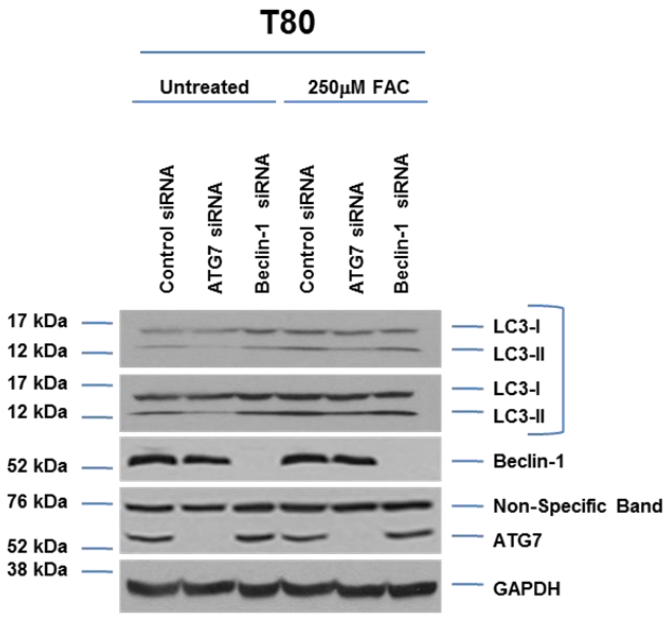

b.

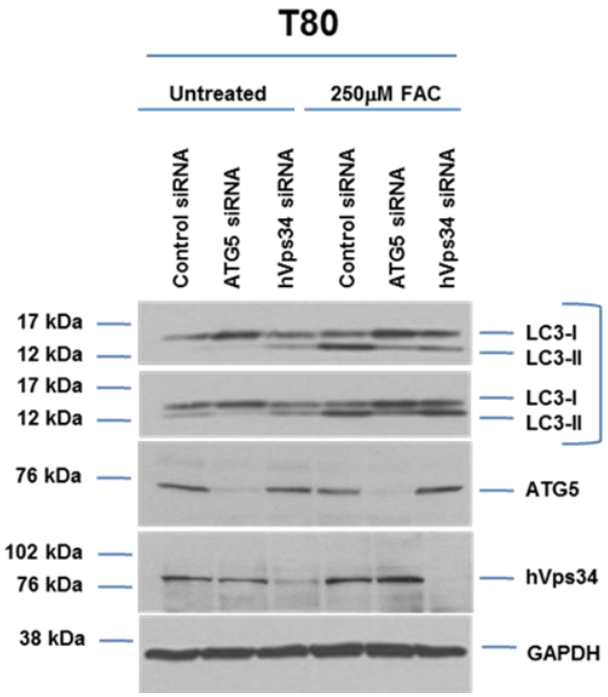

Figure 14: Iron induced autophagy is ATG5/7 dependent and beclin-1/hVps34 independent

Continued on following page.

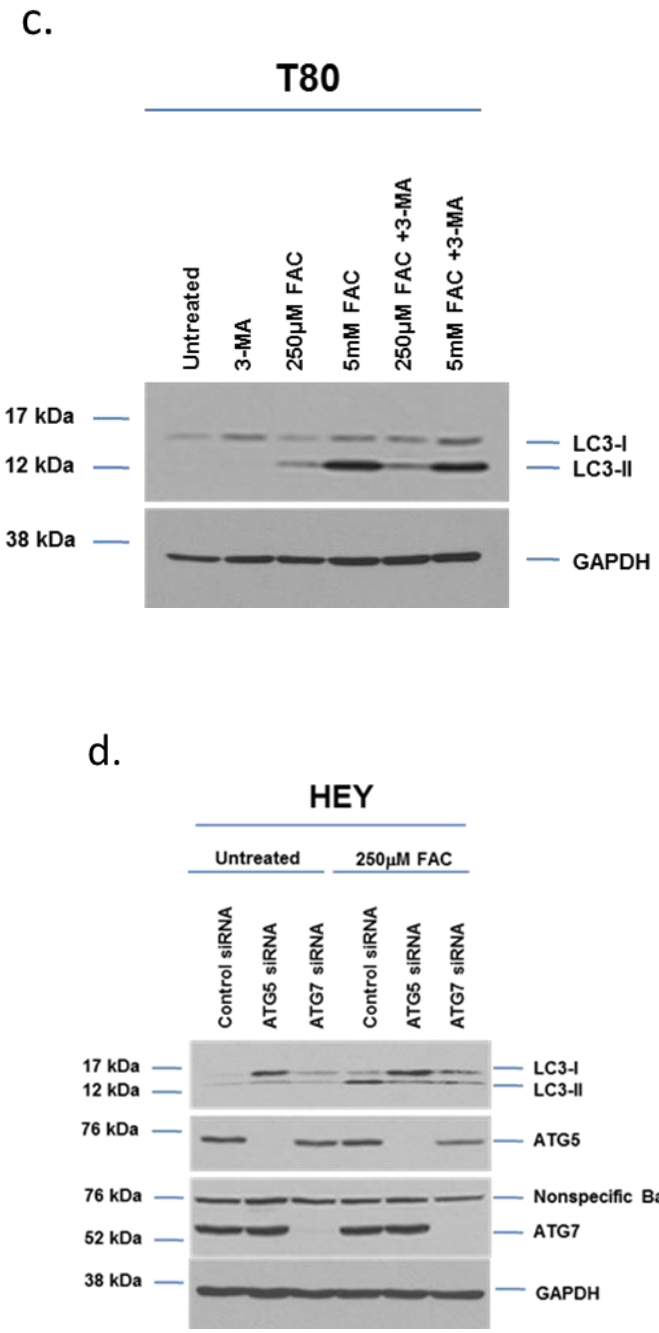

Figure 14: Iron induced autophagy is ATG5/7 dependent and beclin-1/hVps34 independent

Continued on following page.

e.

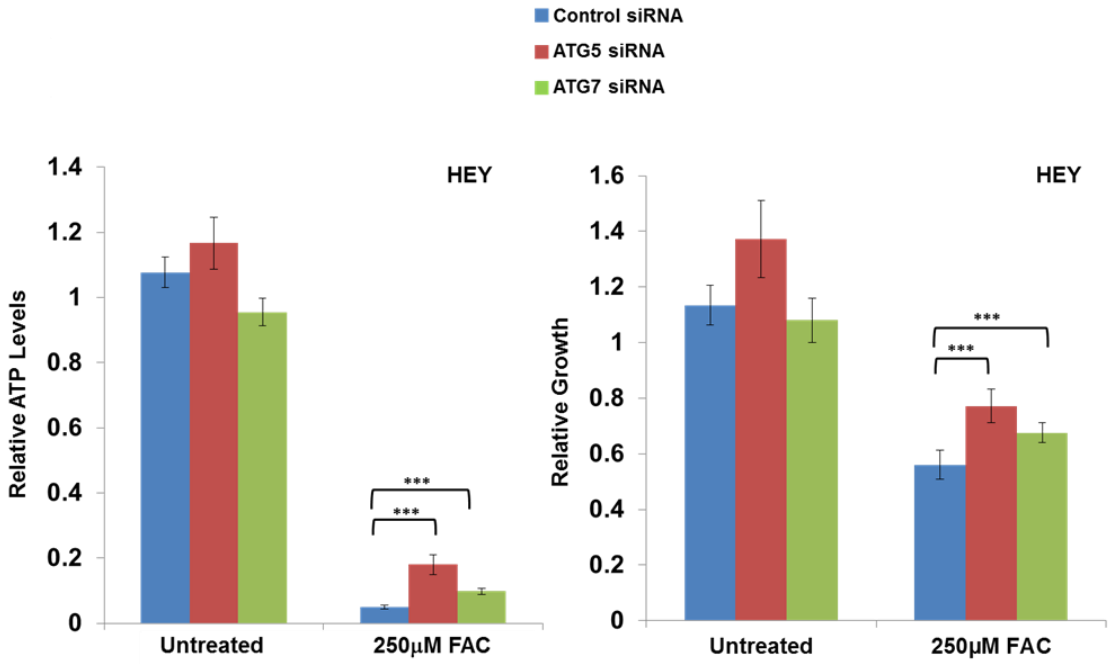

Figure 14: Iron induced autophagy is ATG5/7 dependent and beclin-1/hVps34 independent

A. T80 cells were transfected with ATG7 and beclin-1 siRNA followed by treatment with 250 μM FAC. Cell lysate was assed for proteins as indicated. **B.** T80 cells were transfected with ATG5 and hVps34 siRNA followed by treatment with 250 μM FAC. Cell lysate was assed for proteins as indicated. **C.** T80 cells were treated with either 250 μM FAC, 5 mM FAC, 2 mM 3-MA, 250 μM and 2 mM 3-MA, or 5 mM FAC and 2 mM 3-MA or left untreated. **D.** HEY cells were transfected with ATG5 and 7 siRNA followed by treatment with 250 μM FAC and then assessed for protein expression via western analysis. **E.** HEY cells transfected with ATG5 or ATG7 siRNA were treated with 250 μM FAC for 72 hours then assessed via ATP viability and growth (crystal violet staining).

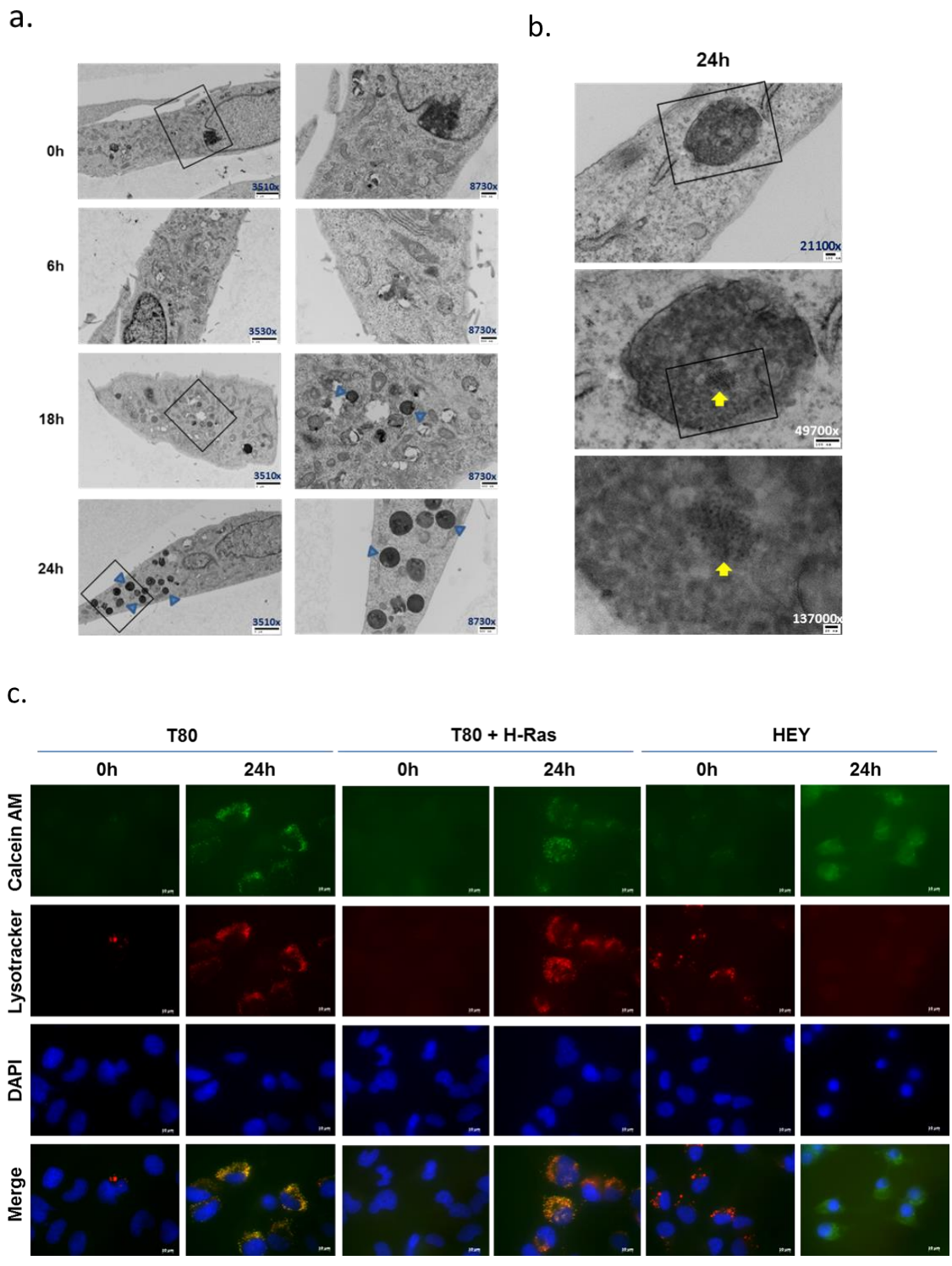

Figure 15: Treatment with iron leads to increased lysosomes in a Ras independent manner.

Continued on following page.

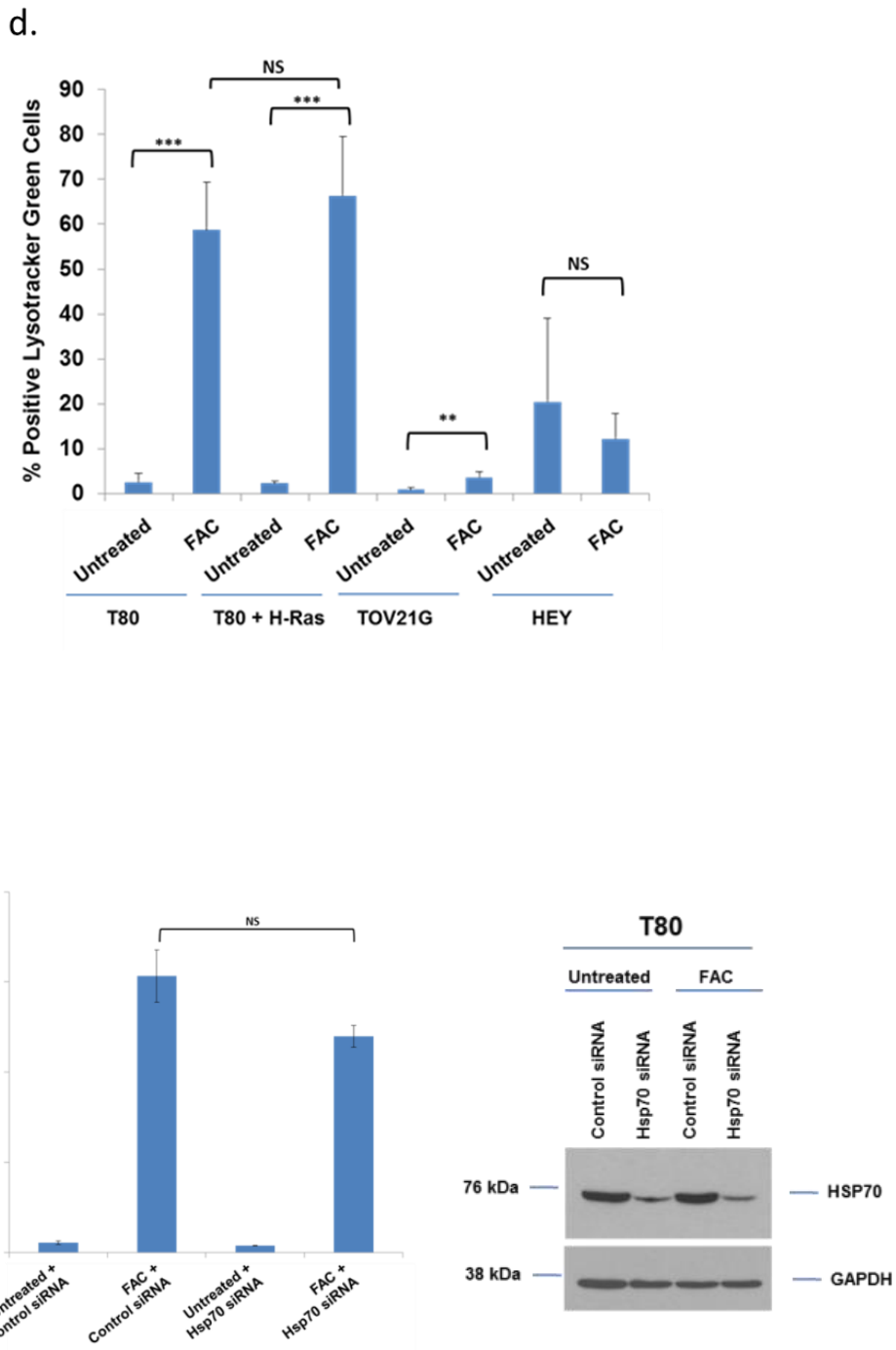

Figure 15: Treatment with iron leads to increased lysosomes in a Ras independent manner.

Continued on following page.

f.

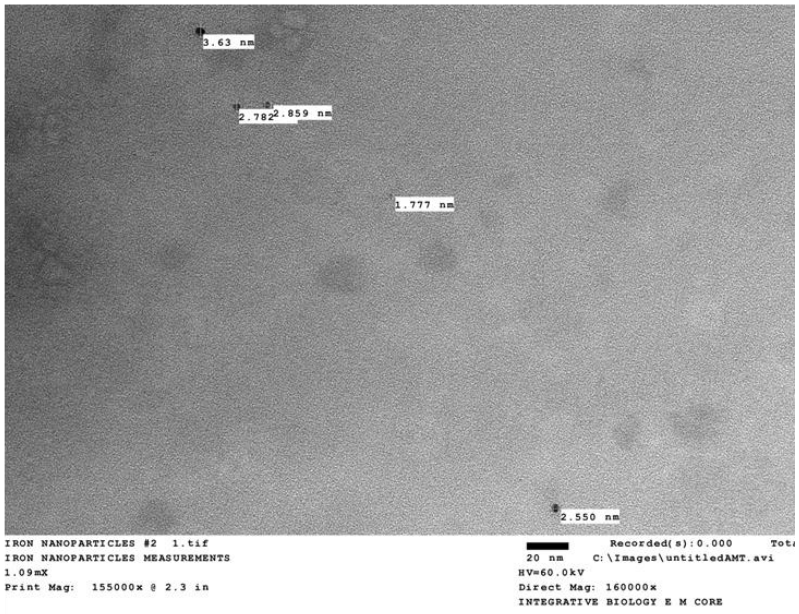

Figure 15: Treatment with iron leads to increased lysosomes in a Ras independent manner

A. T80 cells treated with 250 µM FAC for 24 hours were analyzed via TEM at x3530 and x8730 magnification. Lysosomes are indicated by blue arrows **B.** TEM images of T80 cells were assessed for presence of iron inside the lysosomes indicated by yellow arrows. **C.** T80, T80 + H-Ras, and HEY cells were treated with Calcein-AM followed by treatment of 250 µM FAC. After 24 hours of treatment, media was removed and replaced with media treated with Lysotracker Red. Cells were images via inverted fluorescents microscopy. **D.** T80, T80 + H-Ras, and HEY cells were treated with Lysotracker Green following treatment with 250 µM FAC after 24 hours. Cells were collected and analyzed via flow cytometry. **E.** T80 cells were transfected with HSP70 siRNA then treated with 250 µM FAC for 24 hours. Cells were treated with Lysotracker Green and analyzed via flow cytomertry or assessed via western analysis. **F.** Liquid media treated with FAC analyzed under TEM at x8730 magnification. Iron particles were determined to be about 3 nanometers in size.

findings by flow cytometry with Lysotracker Green and found a similar significant increase of lysosomes after 24 hours of iron treatment in T80, T80 + H-Ras, and a lack of lysosomes in HEY cells.

We were interested to see if lysosome stability contributed to iron-induced cell death of HEY cells. Since HSP70 has been shown to stabilize lysosomes and prevent permeabilization [129], we knocked down HSP70 expression using siRNA in T80 cells (see Figure 15). Loss of HSP70 did not lead to a marked modulation in cell survival in the presence of iron (see Figure 15). This suggests HSP70 does not influence lysosomal response to iron treatment.

FAC activates the MAPK pathway to modulate autophagy, lysosome numbers, and cell death response.

The treatment of ovarian cell lines with iron leads to activation of p-AKT and p-ERK, starting as early as 30 minutes (see Figure 16). Expression of these phosphorylated proteins were slightly increased and occurred earlier in the Ras modulated cell types in comparison to the T80 parental type. To determine if activation of p-AKT and p-ERK led to increased LC3-II and autophagy activation, we utilized inhibitors of each pathway (U0126 for MAPK and LY294002 for PI3K) (see Figure 16). Both inhibitors led to a significant decrease in LC3-II levels via western analysis and via EGFP-LC3 immunofluorescence studies (see Figure 16). Similar modulation of LC3-II activity was also observed in HEY cells with the U0126 inhibitor (see Figure 16).

Since HEY cells showed a lack of lysosomes in the presence of iron (24 hour treatment), we were interested if the MAPK inhibitor U0126 would modulate lysosome numbers (see Figure 16). Strikingly, treatments with U0126 in combination with FAC led to increased lysosome

numbers seen via confocal microscopy and flow cytometric analysis (see Figure 16). Further, Calcein-AM tagged iron to be co-localized within the lysosomes present in the U0126/FAC treated samples. This suggests the presence of lysosomes is critical for survival of iron treated HEY cells.

We next tested if the PI3K and MAPK inhibitors would result in reversal of cell death in Ras mutated and overexpressed cell types. The PI3K inhibitor, LY49002, did not reverse cell death in Ras mutated cell types suggesting that activation of this pathway did not correlate with survival (see Figure 16). However, the MAPK inhibitor, U0126, showed significant and near complete reversal of cell death in all Ras mutated and overexpressing cell types. Further, the necrosis response observed with HEY cells upon FAC treatment could also reversed with U0126, as determined via an LDH assay (see Figure 16).

Ras expression leads to HO-1 induction in response to iron treatment.

HO-1 serves as a rate limiting enzyme in the breakdown of heme into iron, biliverdin, and carbon monoxide [9, 10]. We investigated whether this regulator of iron was modulated during iron treatment. We treated T80 and T80 + H-Ras cells with iron at 48 and 72 hours and found increased protein expression of HO-1 protein and mRNA (see Figure 17). Interestingly, the overall level of HO-1 was higher in the Ras overexpressing T80 cells via protein expression. This was confirmed via mRNA levels showing significantly higher HO-1 levels in H-Ras cells. To determine the mechanism of HO-1 induction, we knocked down NRF2 which serves as a regulator of antioxidant activity and HO-1 transcription [10]. We used siRNA to reduce expression of NRF-2 in T80 cells and treated with FAC (see Figure 17). We found no modulation in HO-1 mRNA expression suggesting that HO-1 induction is NRF-2 independent.

a.

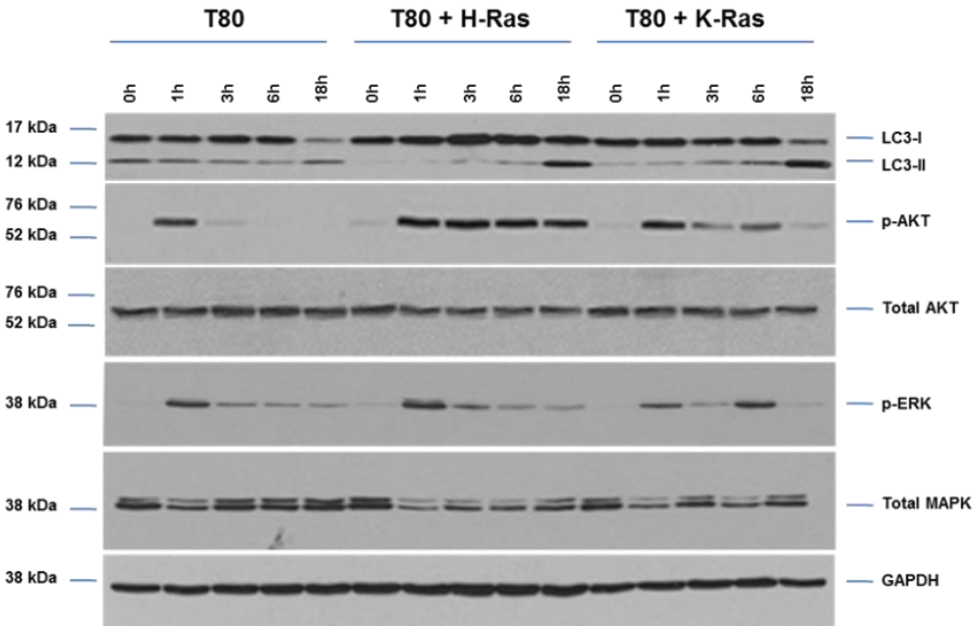

b.

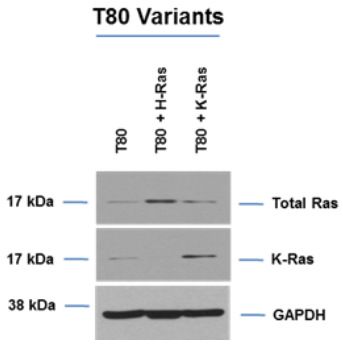

Figure 16: FAC activates the MAPK pathway to modulate autophagy, lysosome numbers, and cell death response.

Continued on following page.

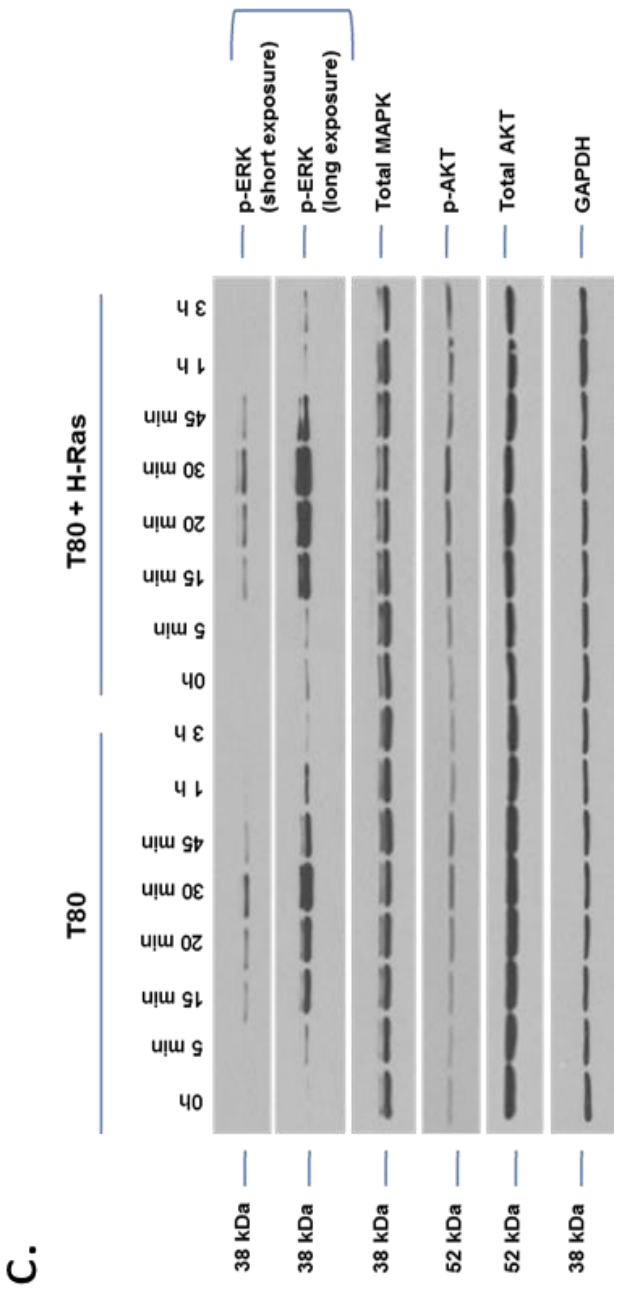

,

Figure 16: FAC activates the MAPK pathway to modulate autophagy, lysosome numbers, and cell death response.

Continued on following page.

d.

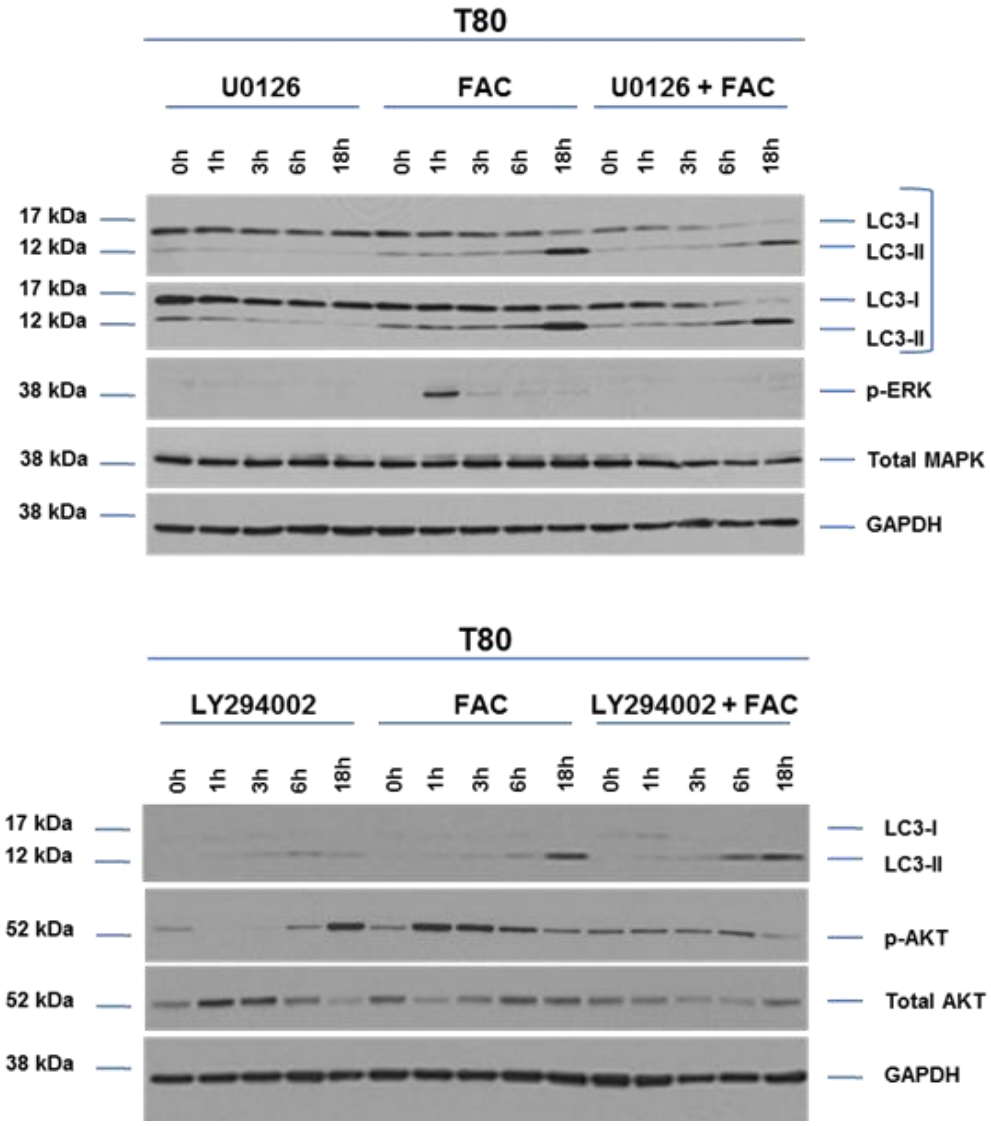

Figure 16: FAC activates the MAPK pathway to modulate autophagy, lysosome numbers, and cell death response.
Continued on following page.

e.

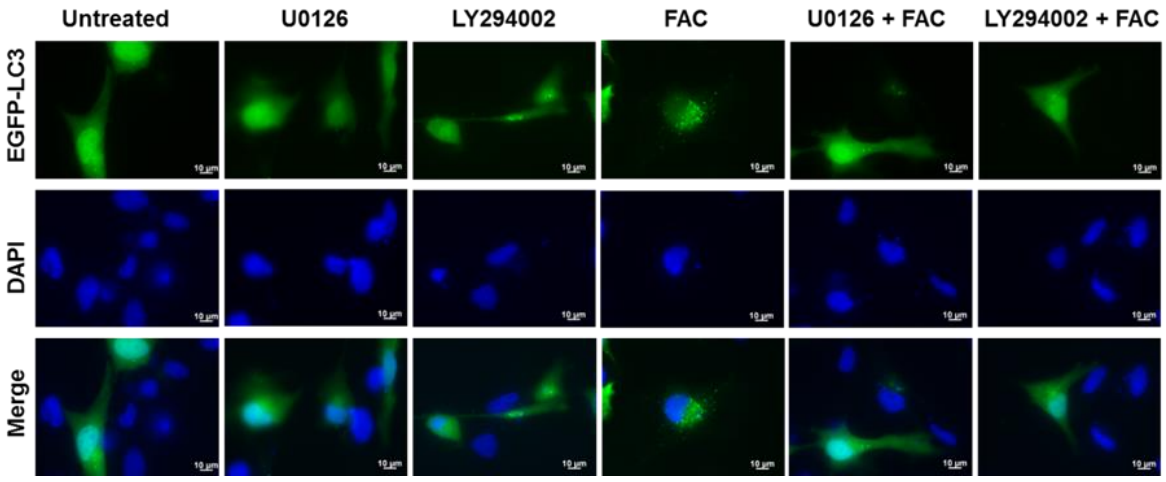

f.

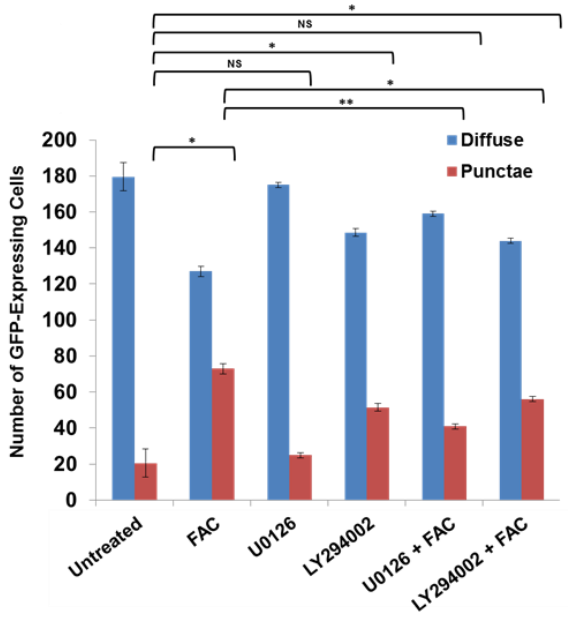

Figure 16: FAC activates the MAPK pathway to modulate autophagy, lysosome numbers, and cell death response.

Continued on following page.

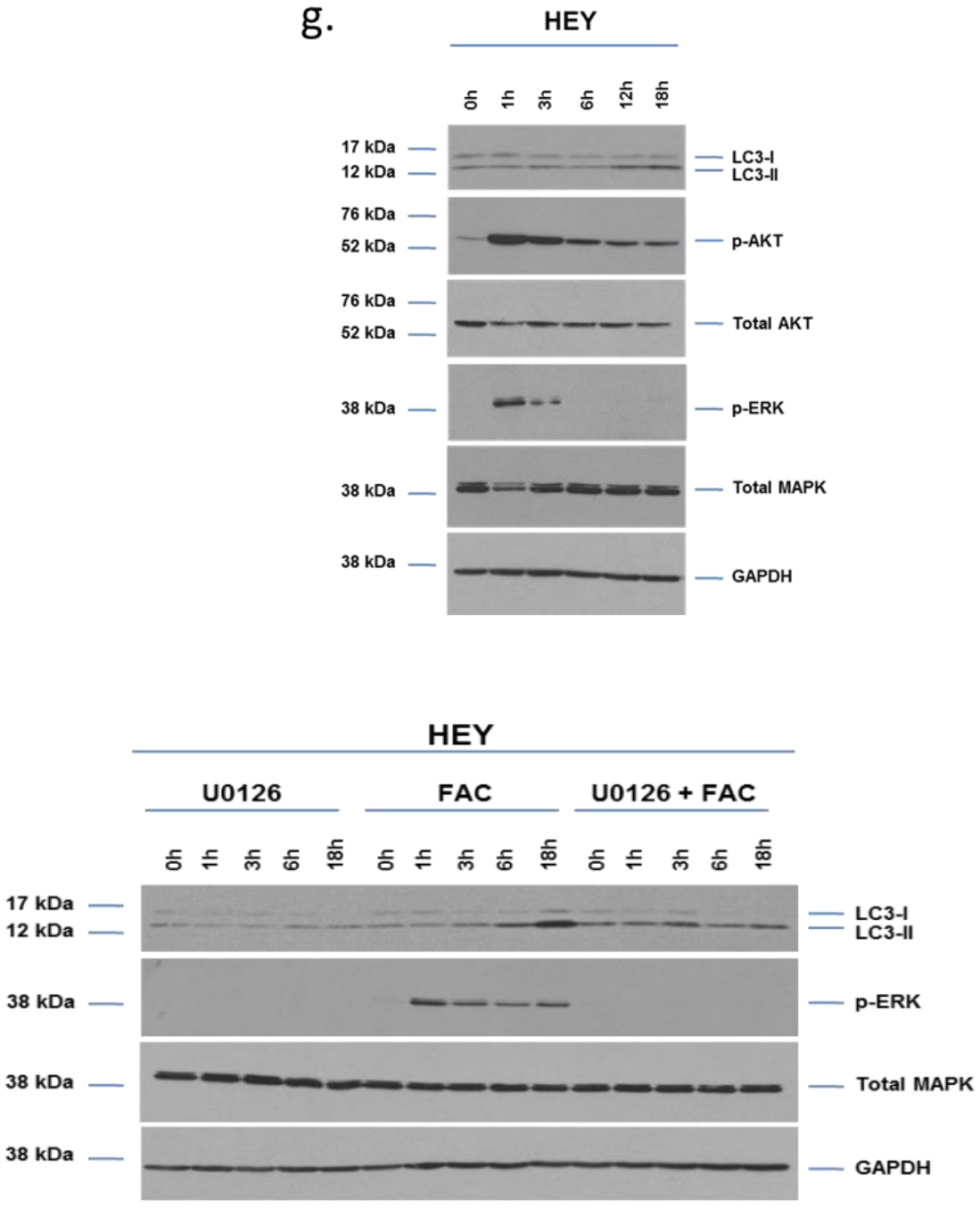

Figure 16: FAC activates the MAPK pathway to modulate autophagy, lysosome numbers, and cell death response.
Continued on following page.

h.

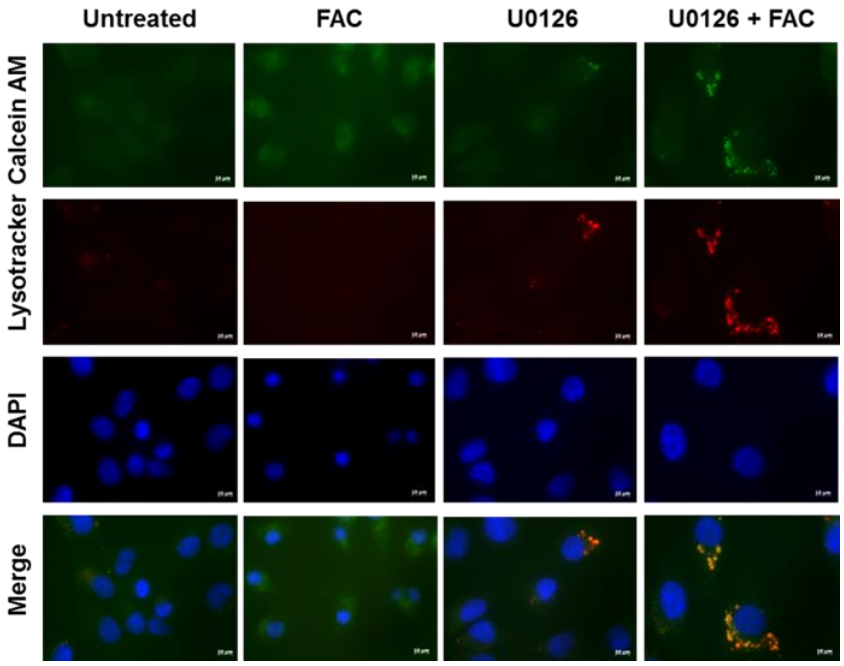

i.

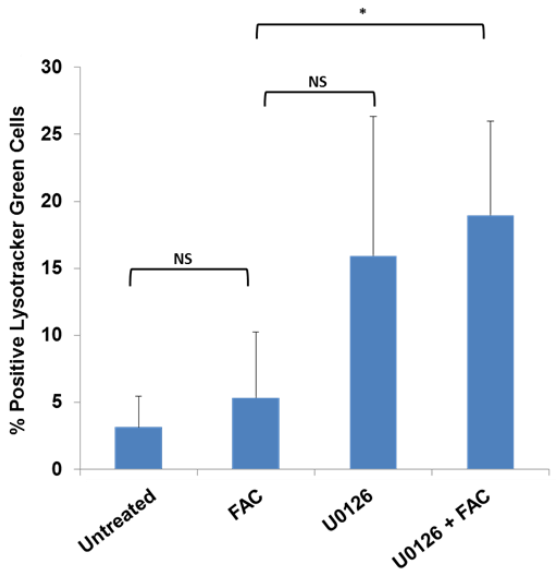

Figure 16: FAC activates the MAPK pathway to modulate autophagy, lysosome numbers, and cell death response.

Continued on following page.

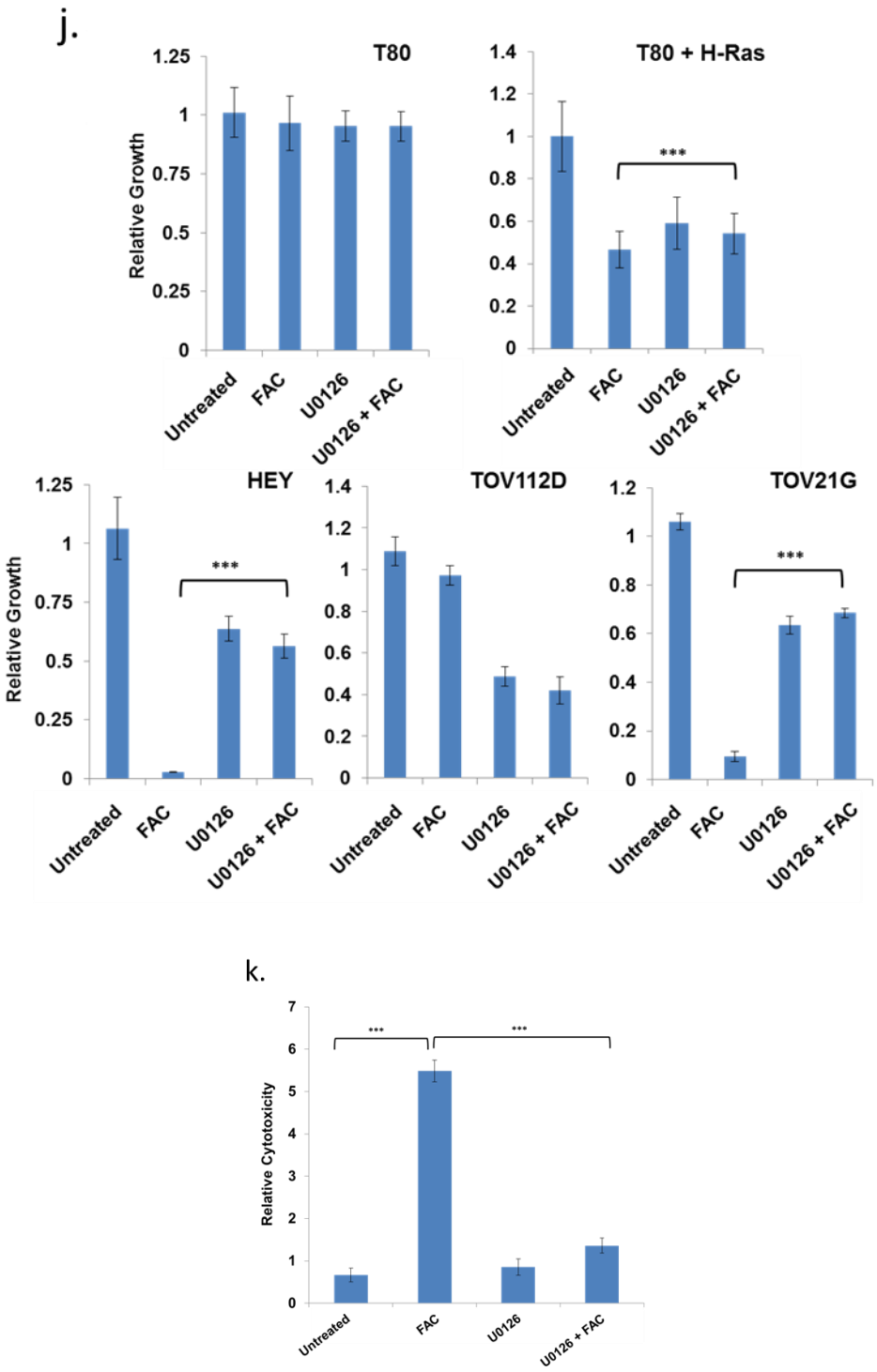

Figure 16: FAC activates the MAPK pathway to modulate autophagy, lysosome numbers, and cell death response.

Continued on following page.

Figure 16: FAC activates the MAPK pathway to modulate autophagy, lysosome numbers, and cell death response.

A. T80, T80 + H-Ras, and T80 + K-Ras cells were treated with 250 µM FAC between 1 h to 18 hours. Lysate was collected and analyzed via western analysis. **B.** T80, T80 + H-Ras, and T80 + K-Ras cell lysate was collected and assessed via western. **C.** T80 and T80 + H-Ras cells were treated with 250 µM FAC between 5 mins and 3 hours and assessed via western. **D.** T80 cells were treated with 10 µM U0126, 250 µM FAC, or 10 µM U0126 and 250 µM FAC for 18 hours in the first western blot and treated with 25 µM LY294002, 250 µM FAC , or 25 µM LY294002 and 250 µM FAC for 18 hours in the second. **E.** T80 cells were transfected with EGFP-LC3 followed by treatment of 10 µM U0126, 250 µM FAC, 10 µM U0126 and 250 µM FAC, 25 µM LY294002, or 25 µM LY294002 and 250 µM FAC for 18 hours. Cells were imaged via inverted fluorescents microscopy. **F.** Quantifiable data from E. was assembled. Cells with greater than 20 punctae were classified as autophagy positive cells. **G.** HEY cells were treated with 250 µM FAC between 1 hour and 18 hours. Lysate was collected and assessed via western. The second study treated HEY cells with either 10 µM U0126, 250 µM FAC, or 10 µM U0126 and 250 µM FAC for 18 hours. **H.** HEY cells were treated with Calcein-AM followed by treatment of 10 µM U0126, 250 µM FAC, or 10 µM U0126 and 250 µM FAC. After 24 hours of treatment, media was removed and replaced with media treated with Lysotracker Red. Cells were images via inverted fluorescents microscopy. **I.** HEY cells were treated with Lysotracker Green following treatment with 10 µM U0126, 250 µM FAC, or 10 µM U0126 and 250 µM FAC after 24 hours. Cells were collected and analyzed via flow cytometry. **J.** T80, T80 + H-Ras, HEY, TOV112D, and TOV21G cells were treated with 10 µM U0126, 250 µM FAC, 10 µM U0126 and 250 µM FAC, or DMSO. Cells were stained with crystal violet after 96 hours of treatment. **K.** HEY cells were treated with 10 µM U0126, 250 µM FAC, 10 µM U0126 and 250 µM FAC, or DMSO for 72 hours and then assessed for LDH activity.

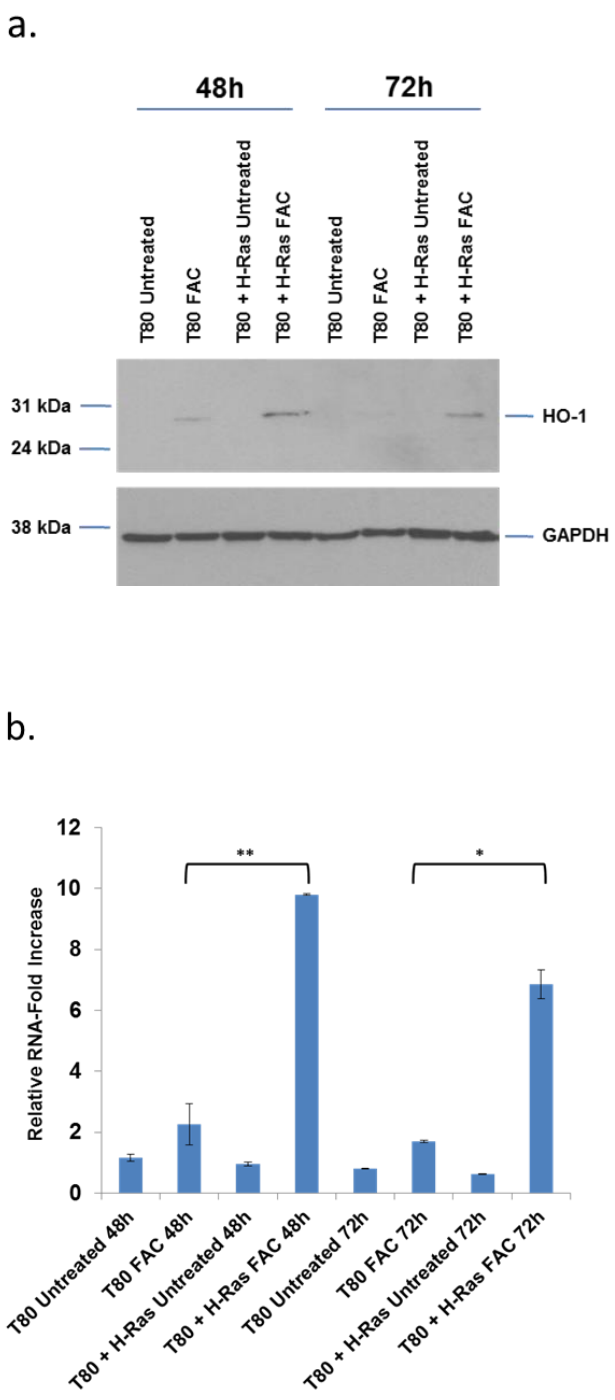

Figure 17: Elevated Ras expression induces increased HO-1 induction in response to iron treatment.

Continued on following page.

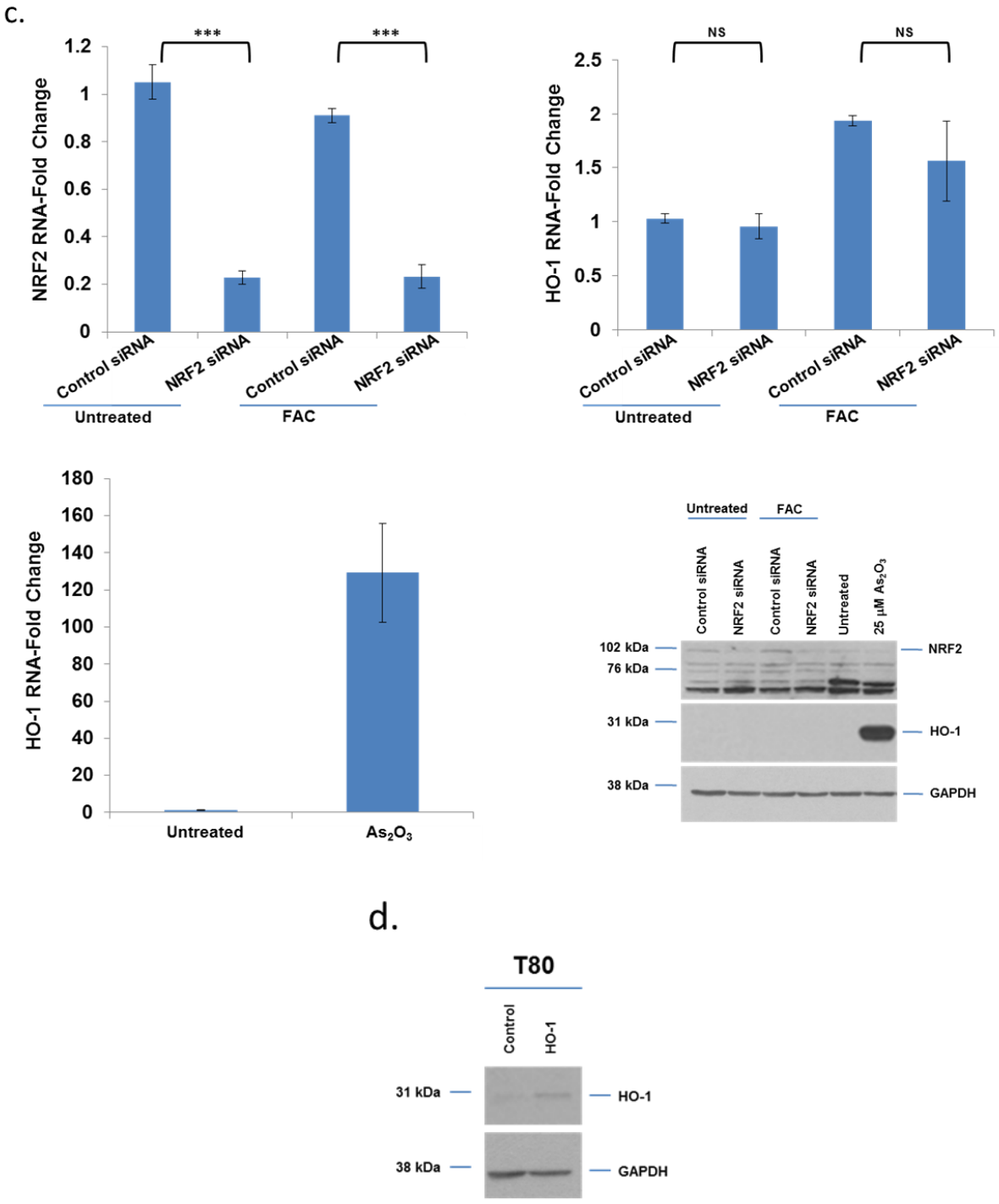

Figure 17: Elevated Ras expression induces increased HO-1 induction in response to iron treatment.

Continued on following page.

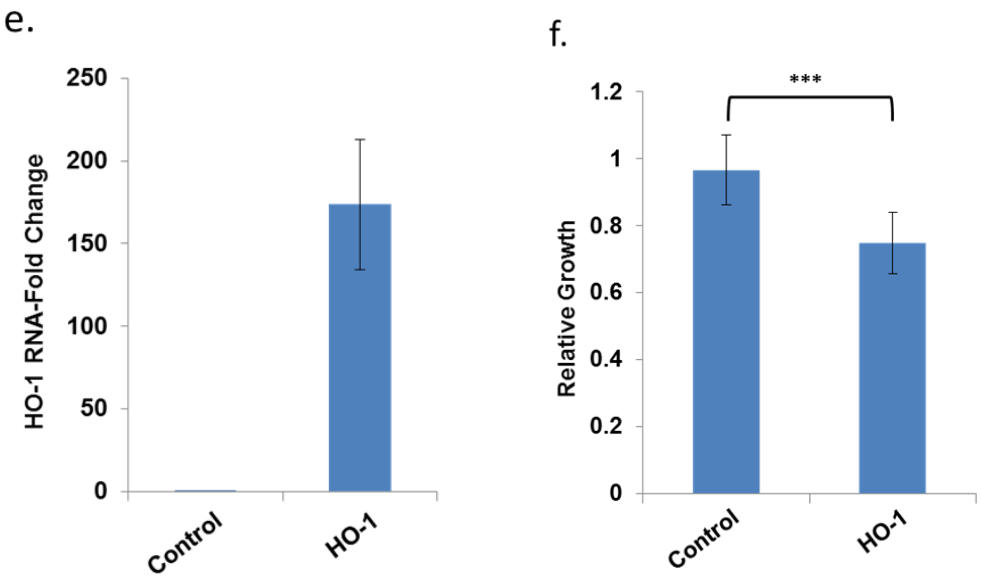

Figure 17: Elevated Ras expression induces HO-1 in response to iron treatment

A. T80 and T80 + H-Ras cells were seeded and immediately treated with 250 µM FAC for 48 and 72 hours and assessed via western analysis. **B.** T80 and T80 + H-Ras cells were seeded and immediately treated with 250 µM FAC for 72 hours. RNA was extracted from the samples and real time PCR analysis was performed on HO-1 expression. **C.** T80 cells were transfected with NRF2 siRNA and then re-seeded and immediately treated with 250 µM FAC for 72 hours. RNA was extracted and used to analyze HO-1 and NRF2 levels via real time PCR. T80 cells treated with As_2O_3 were also assessed for HO-1 mRNA levels to serve as a positive control. NRF2 knockdown was confirmed via western analysis as well. **D/E.** T80 cells with HO-1 retroviral stable overexpression were generated and assessed via protein level (western analysis) and RNA level via RT-PCR. **F.** A growth assay of T80 and T80 HO-1 cells was performed over 96 hours to assess relative change in growth due to HO-1 overexpression.

To determine the role of HO-1 in iron treatment, HO-1 retroviral stable T80 cells were created (see Figure 17). Increased expression lead to decreased cell growth suggesting HO-1 serves to hinder cell growth. We attempted to develop stable HO-1 overexpressing T80 + H-Ras cells. Unfortunately, the cells already express resistance to puromycin selection marker associated with the HO-1 plasmid construct.

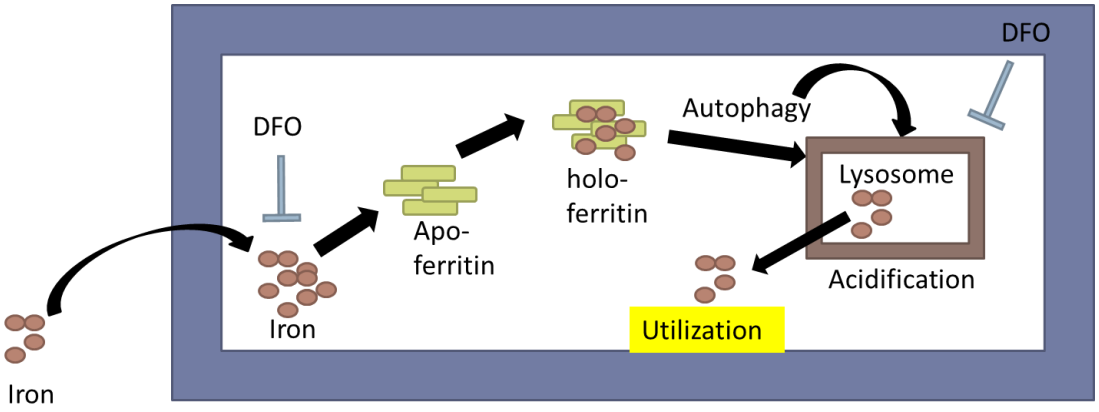

Figure 18: Model of DFO interaction with intercellular iron.
DFO is cell membrane permeable allowing for DFO to easily enter the cell. DFO actively binds to iron and upon association prevents iron from being utilized for cellular functions [11]. *Model created by Kyle Bauckman.

Iron chelator, desferrioxamine (DFO), induces cell death in gynecological cell types

Iron chelators are able to interact with iron by removing it from the cell. The exact cellular mechanism for iron chelators is not fully understood, but some studies suggest that degradation of ferritin occurs reducing the ability to utilize iron [11]. We utilized desferrioxamine (DFO), a chelator that is FDA approved to treat patients for iron overdose [11]. DFO removes both intracellular and extracellular iron from the environment (see Figure 18). We initially utilized DFO with treatment with FAC to see if activation of autophagy was reversible

upon inhibition of iron. We found that DFO was able to inhibit the autophagic effects of iron at a 1:1 ratio of treatment (250 μM each) (see Figure 19). We confirmed this via LC3 western analysis and EGFP-LC3 immunofluorescence (see Figure 19). Surprisingly, we found DFO treatment alone led to an increase of cell death and shrunken cell morphology. Since the cells were confirmed to not be undergoing autophagy and the membrane integrity was not lost (necrosis), we investigated the possibility of apoptosis occurring in DFO treated cells (see Figure 19). We detected an increase in cleaved PARP after 18 hours of DFO treatment in T80 cells. Interestingly, the addition of iron at a 1:1 ratio led to a decrease of cleaved PARP suggesting the presence of increased iron helps bring equilibrium to the cell (see Figure 19). To test this, we performed growth assays on T80, HEY, and TOV21G cells to see if combination of FAC and DFO would reverse loss of cell growth. The combination at 1:1 led to a slight but significant increase in cell growth in all cell lines tested. Since the gynecological cell lines we tested were sensitive to DFO at a level considered to be a normal dose, we performed a kill curve growth assay (see Figure 19). We found that all gynecological cell types we tested were sensitive to DFO treatment down to 1 μM levels.

Iron does not modulate adhesion

To observe effects of iron on cell adhesion, TOV21G cells were seeded into 96 well plates and treated with or without iron. The plates were pre-treated with either laminin, fibronectin, or left untreated. Cells were allowed to attach for one hour and then plates were stained with crystal violet. Treatment with iron did not appear to modulate cell adhesion under any of the conditions tested suggesting iron does not lead to altered adhesion abilities (see Figure 20).

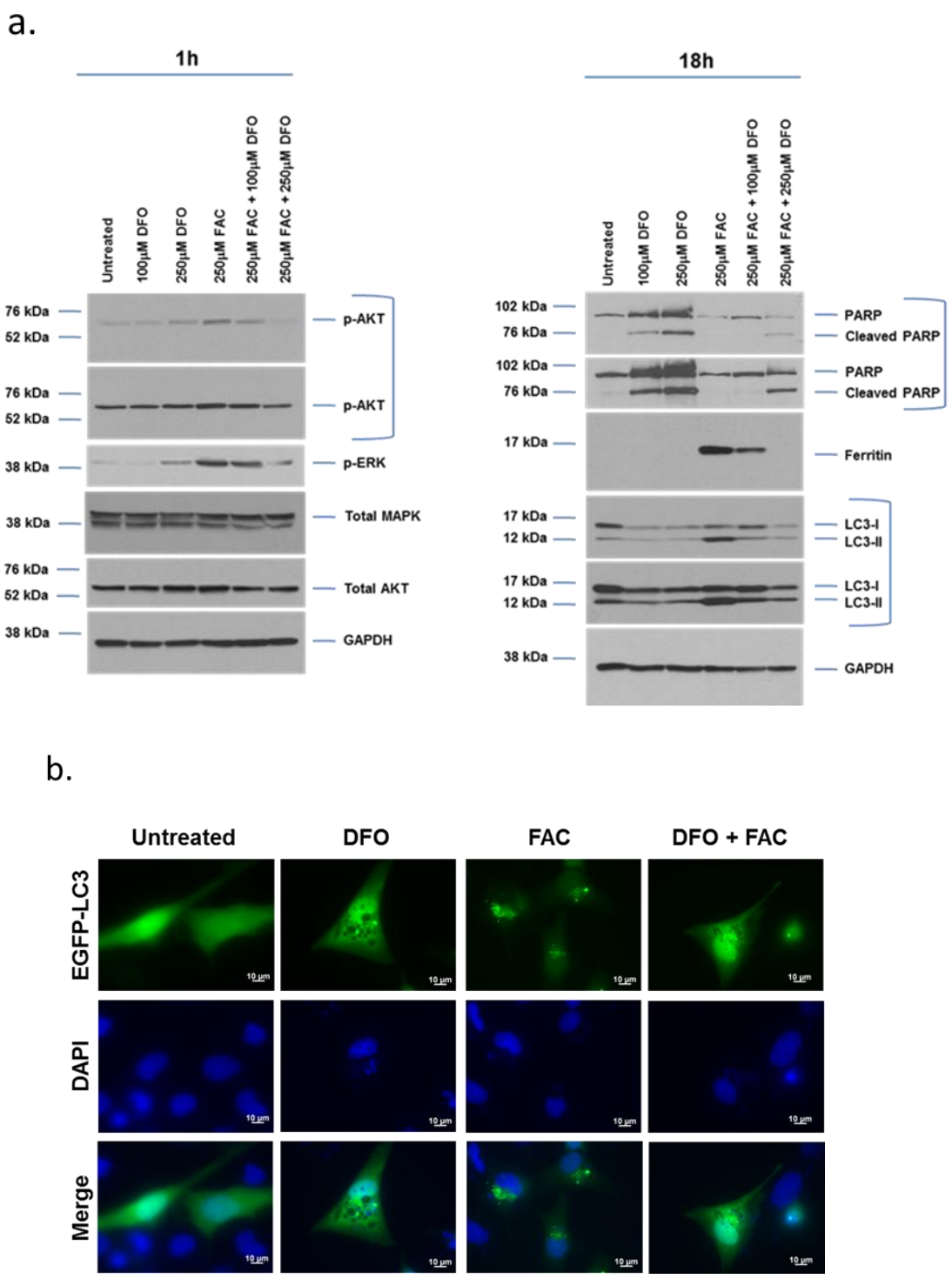

Figure 19: Iron chelator, DFO, induces cell death in gynecological cell types

Continued on following page.

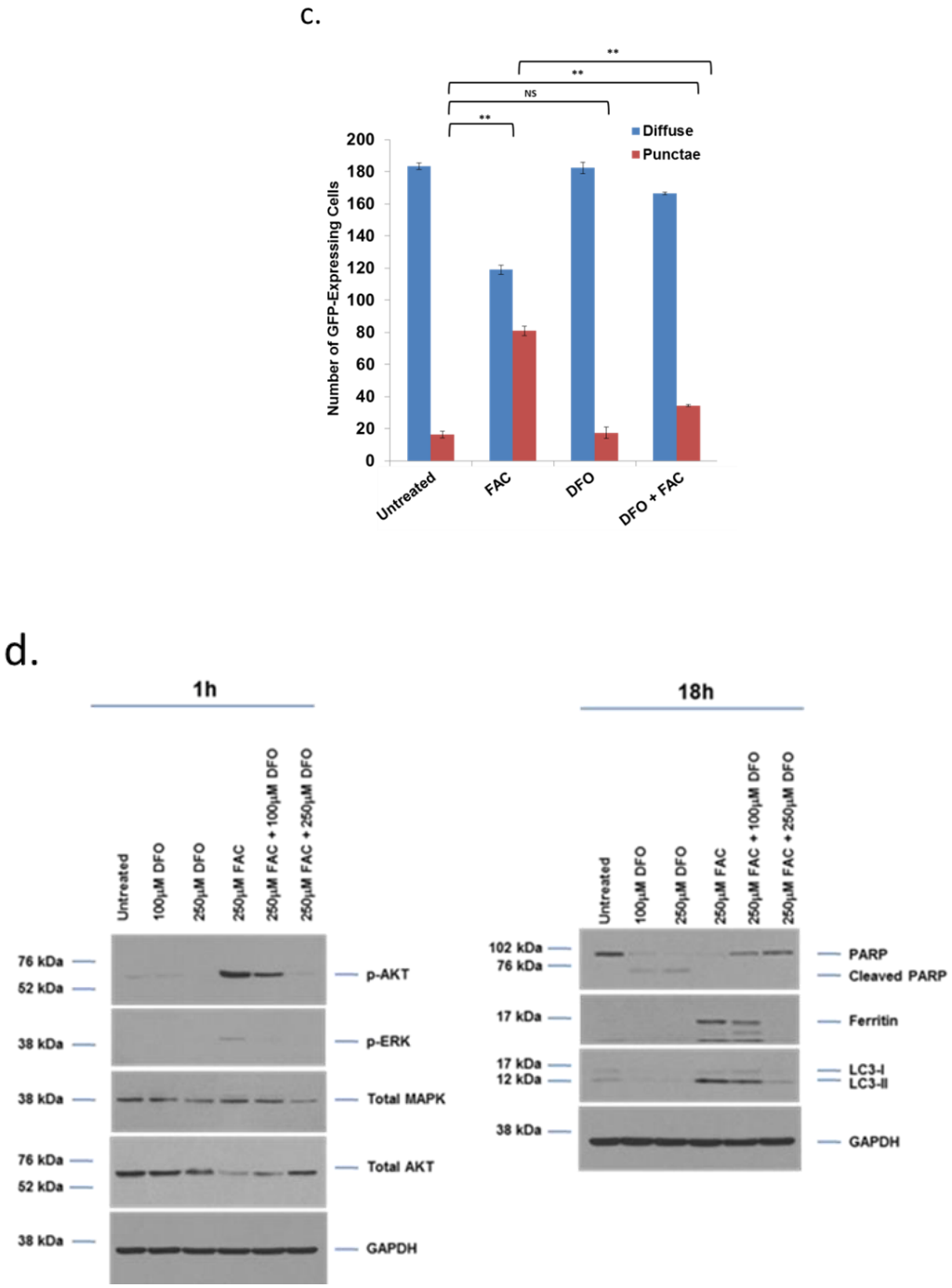

Figure 19: Iron chelator, DFO, induces cell death in gynecological cell types

Continued on following page.

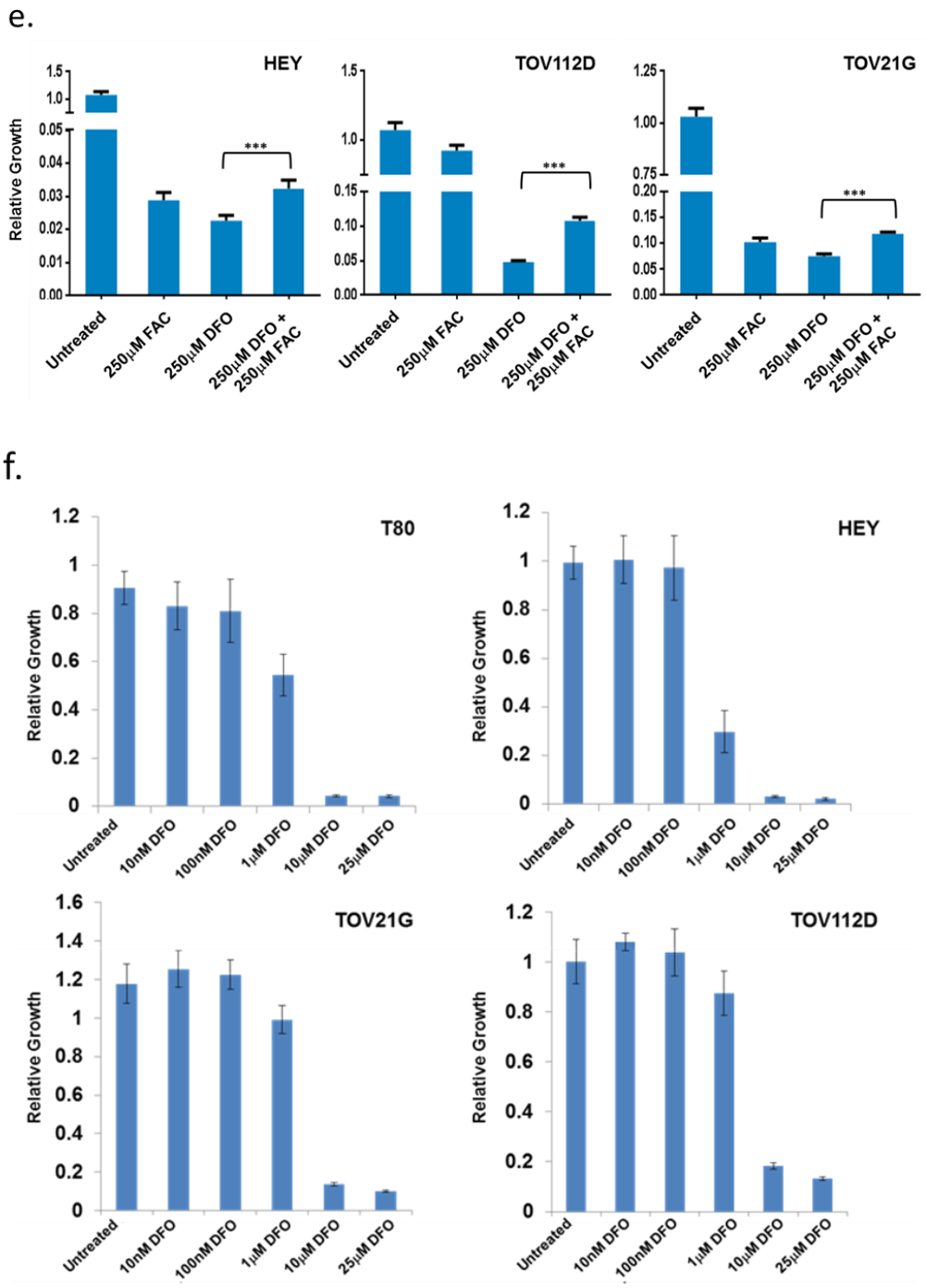

Figure 19: Iron chelator, DFO, induces cell death in gynecological cell types

Continued on following page.

g.

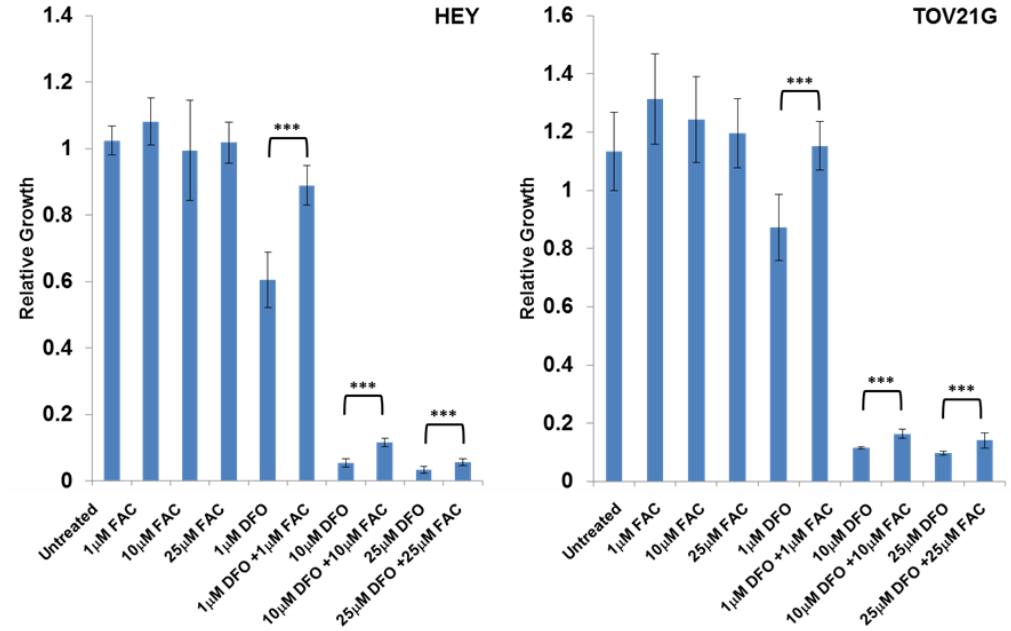

Figure 19: Iron chelator, DFO, induces cell death in gynecological cell types

A. T80 cells were treated with 100 µM DFO, 250 µM DFO, 250 µM FAC, 100 µM DFO and 250 µM FAC, 250 µM DFO and 250 µM FAC, or left untreated for 1 hour and 18 hours. **B/C.** T80 cells were transfected with EGFP-LC3 followed by treatment of 250 µM DFO, 250 µM FAC, 250 µM DFO and 250 µM FAC, or left untreated for 18 hours. Samples were imaged via inverted fluorescence microscopy. Cells with greater than 20 punctae were classified as autophagy positive cells. **D.** HEY cells were treated with 100 µM DFO, 250 µM DFO, 250 µM FAC, 100 µM DFO and 250 µM FAC, 250 µM DFO and 250 µM FAC, or left untreated for 1hour and 18 hours. **E.** HEY, TOV21G, and TOV112D cells were treated with 250 µM DFO, 250 µM FAC, 250 µM DFO and 250 µM FAC, or left untreated for 96 hours and then stained with crystal violet to assess growth. **F.** T80, HEY, TOV21G, and TOV112D cells were treated with DFO from 100 nM to 25 µM and assessed for growth changes. **G.** HEY and TOV21G cells were treated with DFO and FAC from 1 to 25 µM in dose and in combination to assess for growth changes.

Long term iron exposure modulates LC3-II expression and morphology of normal ovarian surface epithelial cells (T80)

Previous investigations have shown that continued exposure to iron leads to altered cellular morphology, specifically a clear cell appearance [34]. This would suggest iron has

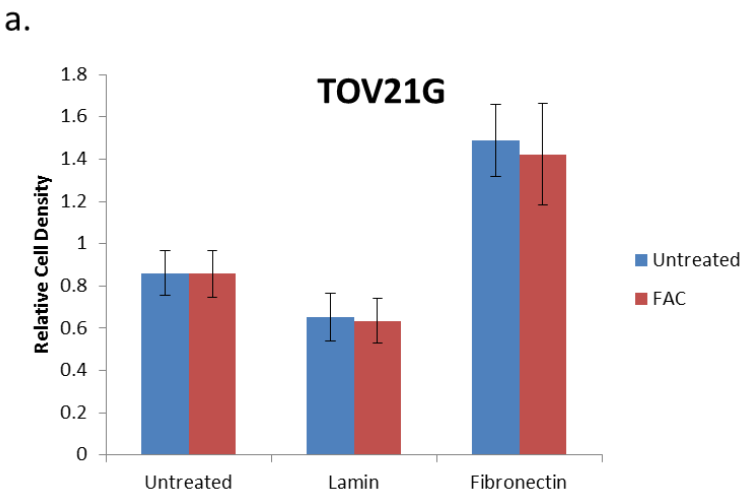

Figure 20: Iron does not modulate adhesion
A. TOV21G cells were seeded on 96 wells plates treated with fibronectin, lamin, or nothing and allowed to adhere for 1 hour. Cells were treated with or without FAC. After 1 hour media was removed and cells were stained with crystal violet. Treatment with FAC did not increase the ability of cells to adhere to wells.

transformative effects on "normal" gynecological cell types. We wanted to induce this response in T80 cells with continued exposure of FAC to observe the long term autophagic response. We treated T80 cells weekly with 250 µM iron changing the media and adding fresh iron each time. Cells were passaged once confluent and then continued to be treated with FAC once re-seeded. After one month of exposure to FAC, T80 cells went through an initial period of cell death followed by the formation of small colonies. The growth of these colonies slowed dramatically but remained viable. After a week of observing this phenomenon we decided to remove the

colonies and grow them in individual plates without iron. Interestingly, once the iron was removed, the colonies resumed cell growth. Continued treatment of iron followed similar response with initial loss of cells, followed by the continued presence of small colonies. We harvested these cells and compared them to normal T80 cells untreated and treated with iron and observed altered LC3-II levels (see Figure 21). However, the change in LC3-II expression was quite variable with some samples showing distinct changes in LC3-II relative to the parental T80 population and others showing no distinct changes (see Figure 21). These observations led to difficulty in drawing a definitive conclusion. Further investigations should utilize parental T80 cells treated with and without FAC to compare change in LC3-II expression.

Treatment with FAC in HEY cells led to a rapid and robust level of cell death. While iron reduced HEY cell numbers significantly in all survival assays performed, there were always a few cells remaining. These cells though altered in morphology (compared to controls), were surviving. We were interested in the ability of these remaining cells to continue growing and developing. A single 35mm dish of HEY cells was treated with 250 μM iron for long term observation. To ensure cell growth was due to resistance to iron induced cell death and not iron depletion, we changed the media with fresh iron treated media daily. After continual exposure with iron, colonies grew and developed into a resistant iron cell type (data not shown). This suggests that iron may have a dual role in ovarian cells. Though iron leads to robust cell death in Ras mutated/overexpressing cell types, this may be a means of rapidly selecting more robust and potentially more aggressive cells. Further studies are required to fully investigate the cellular mechanisms underlying FAC mediated resistance. Future studies will utilize these cells in comparison to parental HEY cells to observe functional and cell signaling pathway alterations.

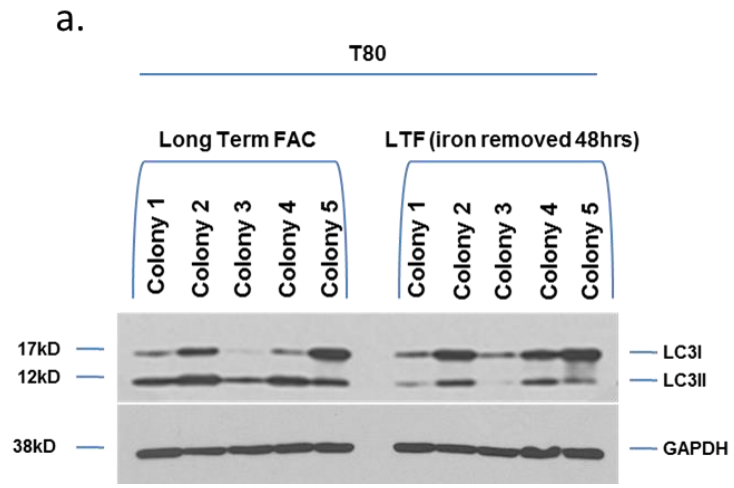

Figure 21: Long term iron exposure modulates LC3-II expression and morphology of normal ovarian surface epithelial cells (T80)
A. T80 cells were treated with continuous treatments of iron (Long term FAC or LTF). Fresh iron was added every other day. Colonies were selected after weeks of continuous treatment. These colonies were treated further. Samples of colonies were taken for western analysis that were treated continuously with FAC or had iron removed for 48 hours.

Discussion

The initial assessment of the functional response of iron was carried out via a cell growth assay. We were interested in observing the potential benefits or modulation of cell types upon exposure to iron. Surprisingly, we observed minimal changes in all of the selected cell types with the exception of HEY and TOV21G cells (see Figure 11). Interestingly, these cells both have a K-Ras mutation, a pathway that a recent publication has shown to be connected with a novel iron induced cell death pathway known as ferroptosis [3]. We were particularly interested in this discovery of a novel cell death pathway due to its similarities to our studies. Both our findings and the Dixon [3] group have identified that iron induced cell death mediated by the Ras

pathway leads to loss of plasma membrane integrity. Further, the ferroptosis paper [3] reports altered mitochondrial morphology which we address in Chapter 6. Interestingly, another group also reported ferroptosis with the added observation of autophagy. Similar to our studies, autophagy did not contribute significantly to cell death. Though trends are evident between Dixon's work and the data presented here, we do not believe it is appropriate to classify our observations as ferroptosis. The mechanism has not fully been established and the characteristics of ferroptosis are still not well-defined. Our primary concern is that ferroptosis closely resembles necrosis. This is a point that is addressed by Dixon and colleagues but remains unclear [3]. We propose that ferroptosis may simply be a form of necroptosis.

We continued our investigation into the Ras-dependent cell death effects of iron in the following chapter (6). Confirmation of cell death was determined via an apoptosis assay that revealed increased apoptosis and necrosis in HEY cells (see Figure 11). Interestingly, no change in early or late stage apoptosis was detected in TOV21G cells. This implies other means of cell death for TOV21G. We performed a β-galactosidase senescence assay but the results appeared negative (data not shown).

Since we observed formation of vacuoles with iron treatment, we hypothesized autophagy may play a role in iron induced cell death. Treatment with iron induced autophagic activation in the entire gynecological cell selection tested. Iron exposure led to a gradual increase in LC3-II up to 18 hours along with increased lysosome numbers detected at 24 hours (see Figure 13 and 15). The presence of iron inside of lysosomes at 24 hours suggests that this process is important for processing iron. Indeed, previous studies have shown lysosomes to be important in transporting free iron into the cytosol for utilization and further storage [21, 130]. The lack of lysosomes present in HEY cells infers that lysosomes are critical for ovarian cell

types to survive exposure to extracellular iron Further, the inhibition of autophagy via ATG5/7 knockdown led to significant reversal, though modest, of decreased cell growth presented in HEY cells (see Figure 14). Since this change was only slight, it may imply that autophagy plays only a minor role in the death of HEY cells. However, since 24 hour exposure of iron showed the absences of lysosomes, it is possible that iron leads to lysosomal permeabilization and thus, dysfunctional autophagy after long term FAC exposure (post 24 hours).

Exposure to iron induced physical change in the treated cells resulting in spindle-like cell formation. Metabolic activity, detected via ATP, was reduced in all cell types due to exposure to iron (see Figure 11). The HEY and TOV21G cell types showed the greatest change in ATP levels, but this decrease might reflect the decrease in cell growth (hence decreased cell number) and not metabolism alone. Similar changes in cell cycle and migration imply the exposure of excess iron leads to halt in normal cell functions (see Figure 12). Since continued exposure to iron does not lead to significant changes in growth or cell death in the gynecological cells (with the exception of HEY and TOV21G) these changes may be a normal response of excess iron. The cells' decrease in ATP levels and wound healing ability may be a temporary response to focus on storage and removal of iron. Time points beyond 96 hours could be assessed to see if the cells return to normal metabolic function.

Exposure to iron did not lead to a dramatic change in functional responses in the normal T80 cells. Previous investigations suggested exposure of normal cells to continuous levels of increased iron would lead to a more clear cell-like cell type [13]. Treatment with iron in T80 cells lead to altered cell morphology as well as increased induction of LC3-II (see Figure 21). However, once iron was removed, the cells gradually returned to a normal morphology and LC3-II levels returned to original levels. This suggests that iron exposure can modulate signaling

pathways in normal cells and potentially make them more aggressive, but this can only be achieved via continued iron exposure. The presence of a specific mutation may also be required to elicit stable expression of cancer like characteristics. Further, treatment with iron did not increase the cells' adhesive ability (see Figure 22). However, our studies focused only on the ability of cells to adhere in the presence of iron. We propose that future studies could examine the ability of cells pre-treated with iron to adhere.

Finally, we were interested in why ovarian cancer cells with Ras expression would respond so dramatically to iron treatment (see Figure 22). Iron is a naturally occurring element in the body and has been shown to lead to the development of clear cell ovarian carcinoma [13, 34]. Why an element so essential to growth and development would be so damaging to cancer growth is a conundrum. We hypothesized that large levels of stress induced by iron may serve

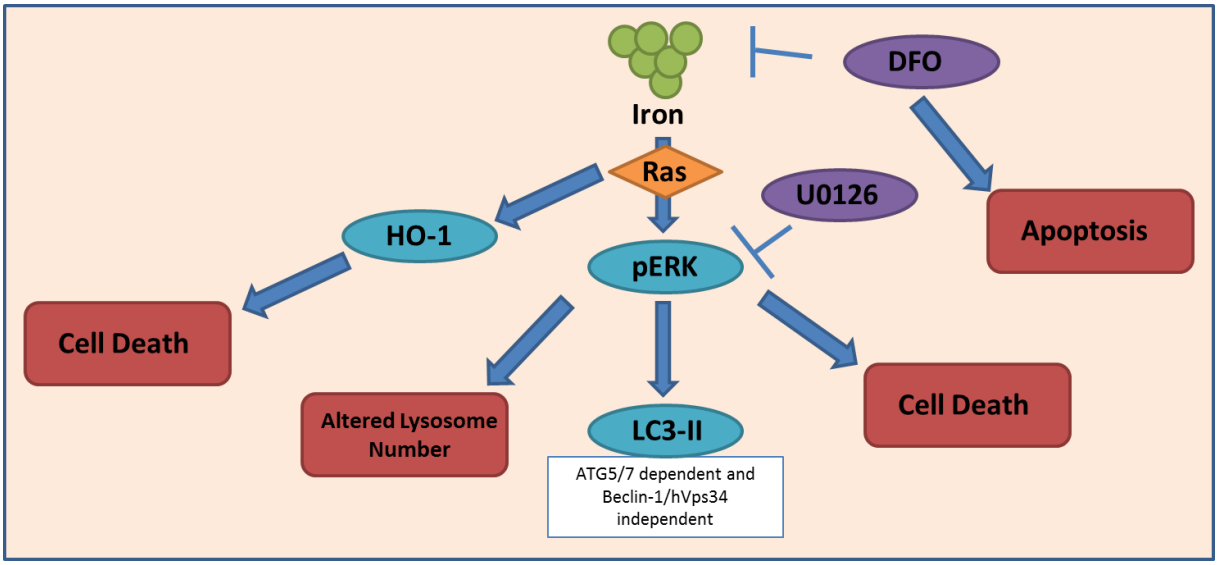

Figure 22: Model of the cellular responses of iron in gynecological cell types. *Model created by Kyle Bauckman.

as a means of survival. Thus, this leads to selection of cells that can grow advantageously in an iron-rich environment. Interestingly, we found that a small population of HEY cells treated with iron continually survived after 96 hours. We continued treatment of these cells with iron and found that they eventually recovered and become tolerant to iron exposure. This rapid change in cell growth response suggests that high iron levels may lead to a more aggressive ovarian cancer type. Future work should focus on the role of iron in long term progression of ovarian cancer. These studies should focus on both the ability of iron to induce cell death as well as its ability to increase survival long term.

Acknowledgments

Transmission electron microscopy (TEM) slides and images were generated by Edward Haller in the Department of Integrative Biology, College of Arts and Sciences at the University of South Florida. HO-1 cloning was carried out in part by Stephanie Rockfield and Dr. Meera Nanjundan. Flow cytometry was performed with the assistance of Dr. Karoly Szekeres in the College of Medicine, University of South Florida [1].

[1] Request for reproduction of article for thesis: The paper titled "Iron modulates cell survival in a Ras- and MAPk- dependent manner in ovarian cells" is represented in Chapter 4 of the thesis presented herein [28].

Chapter 5

Iron Alters Autophagic and Anoikis Response in Gynecological Cell Lines Under Anchorage-Independent Conditions

Introduction

Anoikis is a cell death phenomenon that occurs due to the loss of adhesion to the extracellular matrix (ECM) [75-77]. This loss of interaction with the ECM leads to an apoptotic form of cell death [73, 75, 77]. Interestingly, a critical step in a cells' transition to cancer is acquired resistance to anoikis [73, 75, 77]. The ability of a cancer cell to detach from the ECM, survive, and proliferate is a hallmark of metastasis [75]. The transition from an anoikis sensitive to resistant state occurs through a number of mechanisms including increased expression of integrins and exposure to reactive oxygen species (ROS) [74]. The effects of ROS have been reported to be bifunctional [74, 79, 117]. In one aspect, ROS is capable of generating pro-survival expression patterns leading to a cell type more tolerable to external stress such as chemotherapeutic agents [74]. For example, ROS activates mediators in specific signaling pathways including Src tyrosine kinase and EGFR, thus hindering apoptosis [131]. Other studies have shown that cellular properties critical for cellular adherence at distance metastatic sites is dependent on activation of the Ras/MAPK and PI3K pathways [132, 133]. Mutations acquired

via exposure to ROS may lead to inactivation of specific genes that sensitize cells to anoikis including loss of Rb and p66-Shc [133, 134].

Endometriosis may elicit similar characteristics to invasive tumor cells. In this regard, we propose that anoikis-resistant endometrial cells travel from their originating location (uterine endometrium) to ectopic sites (peritoneal cavity, surface of the ovary, and other sites) via the fallopian tube via the process of retrograde menstruation. These endometrial cells maintain the ability to survive and proliferate [37, 38]. The ability of endometrial cells to travel to a distant site suggests that these cells have acquired resistance to anoikis. Further, one study has implicated increased expression of tyrosine receptor kinase B (TrkB) in eutopic endometrium from endometriosis patients (compared to eutopic endometrium from patients without endometriosis) leading to anoikis resistance [135]. Previous studies have suggested that autophagy is important in the regulation and survival of endometrial cells [78]. Interestingly, autophagy has also been found to contribute to anoikis resistance in cancer cells [73, 79].

As previously described in Chapter 1, recent evidence indicates that iron may play a role in the transition from endometriotic lesions (particularly those described as "chocolate" cysts) to clear cell-like ovarian cancer characteristics [13, 136]. This transition is considered to occur through continued exposure to ROS generated by iron exposure [13]. We hypothesize that iron promotes this transition by allowing survival of cells grown under anchorage-independent conditions. Additionally, we propose that autophagy may be a key regulator in the acquired anoikis resistance. Using a simulated three-dimensional *in vitro* growth assay, we tested whether the anoikis (and autophagic) response was altered following iron treatment. The use of tissue culture sterile plates coated with poly-HEMA (a hydrogel polymer) has been previously

described [134]. This hydrophobic coating prevents cells from adhering to the plate causing them to grow in suspension with spheroid morphology (see Figure 23).

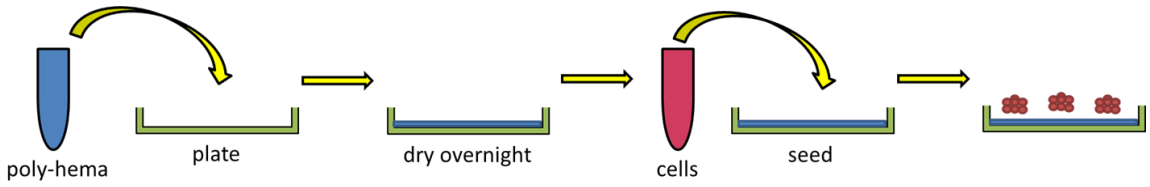

Figure 23: Model of 3D poly-HEMA plate formation.
Poly-HEMA is placed on cell plates and left to dry. Two rounds of poly-HEMA are placed on the plate to ensure full coverage. Once the plate is ready, cells can be seeded into the wells. The cells are unable to attach to the plate leading to the formation of floating colonies. *Model created by Kyle Bauckman.

Result

Iron and autophagy reduces the apoptotic response in ovarian cell lines grown under anchorage-independent conditions

In order to determine whether iron influences cell survival of ovarian cells grown under three-dimensional conditions, we utilized poly-HEMA coated plates and treated our panel of cells with 250 µM FAC. This was followed by western analyses of markers of apoptosis (cleaved PARP) and autophagic response (LC3-II) (see Figure 24). Since we previously observed that iron induces autophagy via increased LC3-II expression (Chapter 4, Figure 13), we thus documented how cells grown in this three-dimensional environment would elicit changes in these cell death/survival responses. Interestingly, we identified increases in cleaved PARP in the "normal" ovarian cell type (T80) relative to the untreated adherent cells (see Figure 24). We also looked at HES cells and their response to anoikis conditions (data not shown).

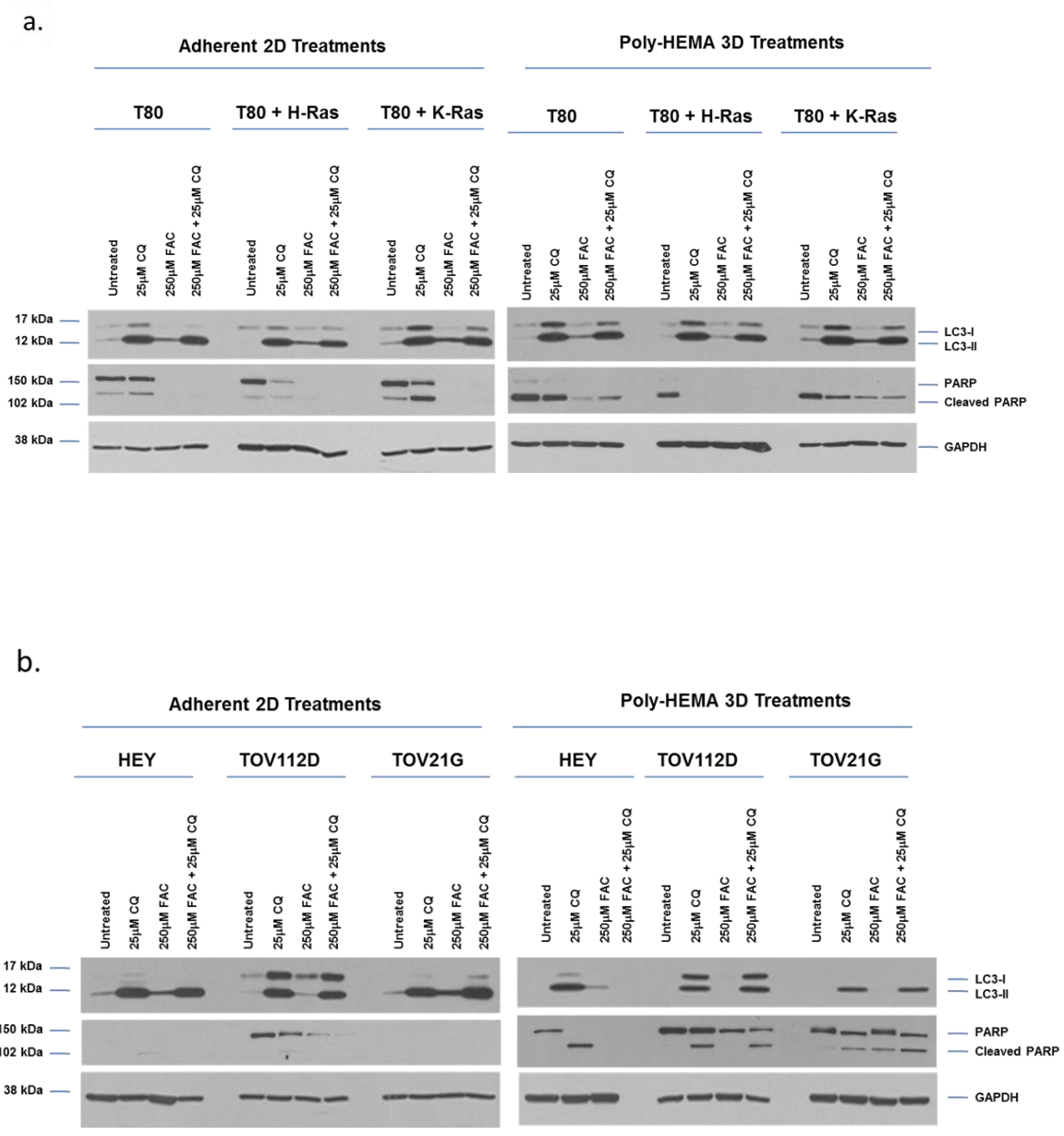

Figure 24: Iron and autophagy reduce apoptosis in ovarian cell lines under anchorage-independent conditions

Continued on following page.

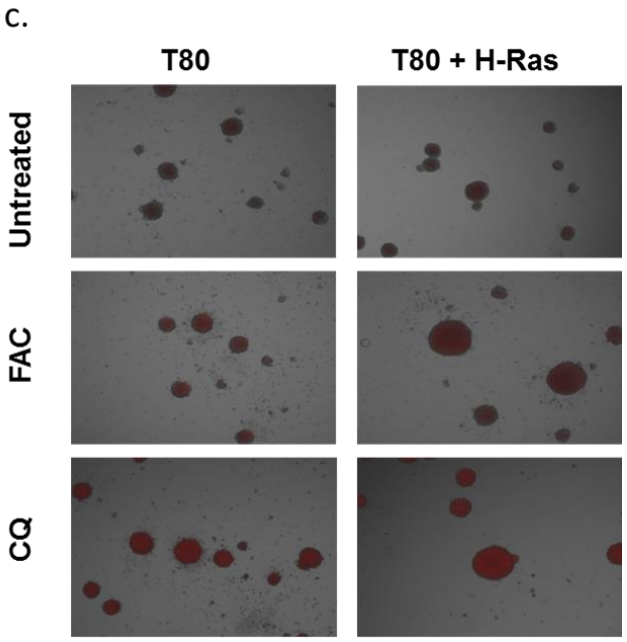

Figure 24: Iron and autophagy reduce apoptosis in ovarian cell lines under anchorage-independent conditions
Plates were pretreated with and without poly-HEMA and left to dry overnight. Cells were seeded into wells and treated with 250 µM FAC, 25 µM CQ, both, or left untreated. **A.** T80, T80 + H-Ras, and T80 + K-Ras cells were assessed for changes in LC3-II and cleaved PARP after 72 hours of treatment. 2D represents cells that adhered to the plate and 3D represents poly-HEMA coated plates. **B.** Assessed response of anoikis in ovarian cancer cell lines HEY, TOV112D, and TOV21G. **C.** T80 and T80 + H-Ras cells were seeded in poly-HEMA treated plates for 72 hours and then treated with ethidium bromide. Images were viewed via an immunofluorescence microscope.

These studies were carried out before we became aware that HES cells were HeLa cell contaminated [4]. Thus, we limit our interpretations of "normal" gynecological response to T80 cells. In contrast, the ovarian carcinoma cell lines (HEY, TOV21G, and TOV112D) did not show noticeable changes in cleaved PARP (see Figure 24). This was an expected outcome as the ability of cancer cells to survive anoikis-like conditions are a key characteristic of tumorigenesis [137-139].

Next, we investigated whether autophagy could influence the anoikis response of ovarian cells lines grown under anchorage-independent conditions. We treated cells with the autophagy inhibitor chloroquine (CQ) to determine whether this could alter the apoptotic response following autophagy inhibition (see Figure 24). Treatment with the autophagy inhibitor is well established to prevent turnover of autophagy, thus hindering the ability of FAC to activate the pathway. We hypothesized that activation of autophagy induced by FAC would alter cell survival in cell maintained under anchorage-independent conditions. Interestingly, the reduction in autophagic flux decreased cleaved PARP in the T80 cells (see Figure 24). In contrast, inhibition of autophagic flux via CQ in cancer cell lines dramatically increased cleaved PARP (see Figure 24). These results suggest that autophagic flux appears to be essential in modulating the anoikis response. In cancer cell lines, autophagic flux antagonizes apoptosis whereas in normal T80 cells, autophagic flux contributes to apoptosis. Thus, a dual role for autophagy is noted where it serves to promote anoikis in normal cell types and to oppose anoikis in cancer cell types. Further studies are needed to determine if the cleaved PARP is indicative of increased apoptosis. An apoptosis assay (involving Annexin V/PI staining) will be utilized to validate this cleaved PARP response. We also will investigate if cell death is decreased with reduced cleaved PARP. Loss of cleaved PARP may lead to altered cell death events (to necrosis or autophagy) instead of completely reversing the process [140].

In addition, we assessed the ability of iron to modulate survival of cells grown under these above-described anchorage-independent conditions. Thus, we treated cells with 250 μM FAC. Since we previously demonstrated that FAC was able to induce autophagy (Chapter 4, Figure 13), we treated cells with FAC in absence/presence of CQ in order to determine whether the FAC cell death response was dependent on autophagic flux. Our results indicate that iron did

not alter cleaved PARP response of the ovarian cancer cell lines we tested. Only minor changes in LC3-II were observed in the TOV21G cells. In contrast, iron treatment of T80, T80 + H-Ras, and T80 + K-Ras cell lines decreased cleaved PARP levels suggesting that iron may play a role in modulating normal ovarian cell anoikis response. To further assess the effect of iron and CQ on cell survival in the T80 cell lines, we performed a cell viability assay utilizing ethidium bromide. Cells treated with CQ or FAC elicited increased ethidium bromide staining compared to the untreated cells (see Figure 24). Further, the T80 + H-Ras cell line appeared to have denser spheroids when treated with FAC or CQ relative to their untreated counterparts.

Discussion

Anoikis is a cell death phenomenon that occurs due to loss of adhesion to the ECM [75, 77, 135]. The ability to survive this detachment promotes cancer cell invasion and metastasis. The ability of cancer cells to lose its ability to adhere to the ECM promotes increased propensity to metastasize to distant regions of the body [75]. Interestingly, one of the multifactorial elements required for development of ectopic endometriotic lesions is the ability of endometrial cells (which normally undergo apoptosis following detachment) to travel in a retrograde motion from the uterine cavity through the fallopian tube and onto the ovaries as well as other locations in the peritoneal cavity [53, 141, 142]. Although the association between anoikis and endometriosis is poorly understood, one study has demonstrated increased tyrosine receptor kinase B (TrkB) expression which occurs in the eutopic endometrium of patients diagnosed with endometriosis (relative to eutopic endometrium from patients with no endometriosis) which could potentially contribute to acquired resistance of these endometrial cells to apoptosis/anoikis [135].

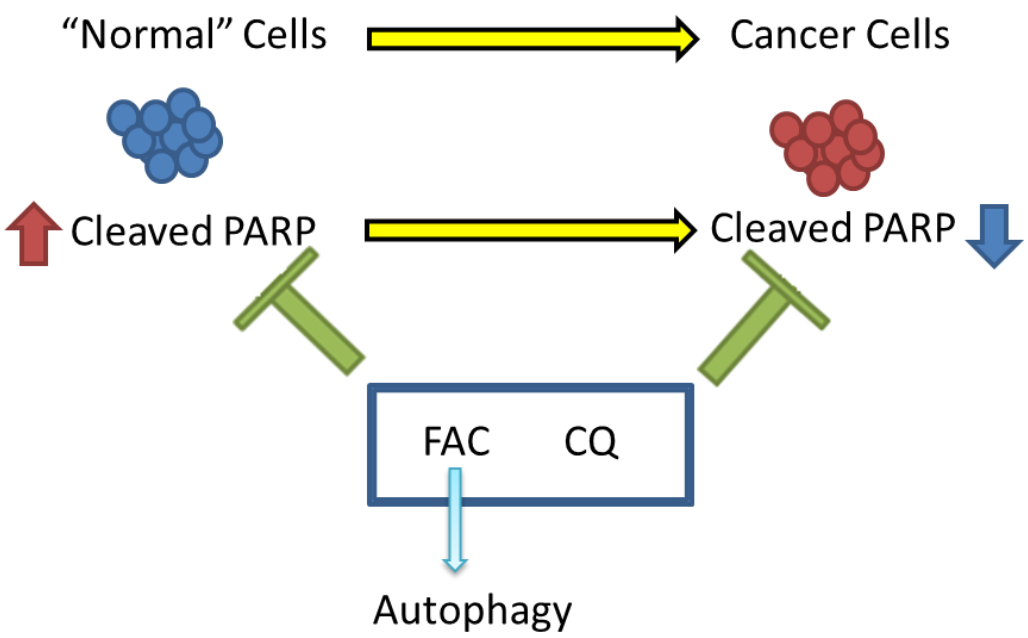

Figure 25: Model of gynecological cell response to anoikis.
"Normal" cell types will undergo apoptosis shown via increased cleaved PARP. Cancer cells, however, do not undergo PARP cleavage suggesting that they are resistant to anoikis. Treatment with FAC or chloroquine (CQ) leads to reduced cleaved PARP and cell death in "normal" cell types. In contrast, these compounds induce cleaved PARP in cancer cells. *Model created by Kyle Bauckman.

Treatment with iron could promote the transition to a clear cell like ovarian cancer phenotype in endometrial/endometriotic cell [34]. We wanted to observe iron response in a 3D environment to approximate an *in vivo* response. Interestingly, we show that iron leads to reduction in apoptosis via modulation in cleaved PARP in normal ovarian cell types (see Figure 25). This was supported by the increase of ethidium bromide staining in the T80 and T80 + H-Ras cell types. We plan to continue these studies by investigating cell death responses via apoptosis assays. This would help to elucidate other mechanisms of cell death (i.e. necrosis, apoptosis, etc). Further, determination of the mechanism of apoptotic death (i.e. intrinsic or extrinsic apoptosis) is also critical. These results indicate that iron may assist in preventing

anoikis, allowing for continued survival and an opportunity to transform into a more aggressive cell type (see Figure 25). While no change in apoptosis was observed in the cancer cell types, suggests that there is increased benefit to the cells. We previously demonstrated that iron induced non-apoptotic cell death in cell types with altered Ras mutation/overexpression. Further studies are necessary to validate that these cells are not undergoing cell death.

There was also a marked increase in autophagic protein, LC3-II, in both normal cell types as well as ovarian cancer cell lines. Treatment with CQ (inhibition of autophagic turnover via hindering lysosomal fusion with autophagosomes) reduced cleaved PARP levels in normal cells while enhancing cleaved PARP in cancer cell types (see Figure 24). This phenomenon has been well documented in various autophagy studies [29, 79, 80, 109, 125]. Often, autophagy will switch from inducing cell death to inducing cellular survival [79]. The stress induced by an anchorage-independent environment leads to apoptotic cell death. This stress can be reduced by activation of autophagy allowing for continued survival (see Figure 25). In contrast, the loss of autophagy may lead to excess cell stress and apoptotic death in the cancer cell types [143-145]. The T80 cell types showed a reduction of cleaved PARP in the presence of CQ. A previous report demonstrated not only cross talk between autophagy and apoptosis but potentially influence each other [146]. Since the anoikis data demonstrated distinct responses in cell survival with iron treatment as well as a dependence on autophagy, future studies should focus on *in vivo* models. In this regard, we plan to study the survival and proliferative capacity of normal cells in a mouse endometriosis model. This model was developed specifically to assess the effect of drugs and other agents on the development of endometriotic cysts [147]. Briefly, the uterine horn tissue of an estrogen-treated donor mouse is removed and injected into a recipient mouse. This recipient tissue will develop into endometriotic cysts in the peritoneal

cavity, similar to development of human endometriosis [147]. Iron treatments can be performed on these mice to determine the ability of iron to modulate cyst number and size.

Acknowledgments

Anoikis protocols were designed with the guidance of Dr. Meera Nanjundan.

Chapter 6

Mechanisms Underlying Iron-induced Responses Downstream of the Ras/MAPK Signaling Pathway

Introduction

As described in Chapter 4, we determined that the Ras/MAPK pathway increases sensitivity to iron (presented as ferric ammonium citrate, FAC). This was directly supported by the T80 +/- H-Ras studies and MAPK inhibitor trials presented in Chapter 4. In cell lines with Ras mutations or overexpression, exposure to iron markedly decreased cell survival with a particularly significant necrotic response noted in the HEY serous epithelial ovarian carcinoma cell line (Chapter 4) [28]. However, the identity of the downstream mechanism following Ras/MAPK activation to this iron-induced response remained elusive. In our efforts to identify these mechanisms, we engaged three independent means of investigation.

Our initial approach focused on identifying signaling pathways that were modulated downstream of the Ras/MAPK cascade. The translational control pathway was of particular interest: (a) identified to be altered from a high-throughput proteomics approach (RPPA, reverse phase protein array) and (b) reported cross-talk activity with the AKT pathway [1, 2, 148]. As presented in Chapter 4, we identified AKT to be activated following 1 hour FAC treatment together with the MAPK pathway [28]. The AKT and MAPK pathways have shown to

simultaneously induce translational activation through mTORC1 regulation (see Figure 26) [148]. Activation of this pathway appears to promote cell survival, invasion, migration, and proliferation [1, 2, 148].

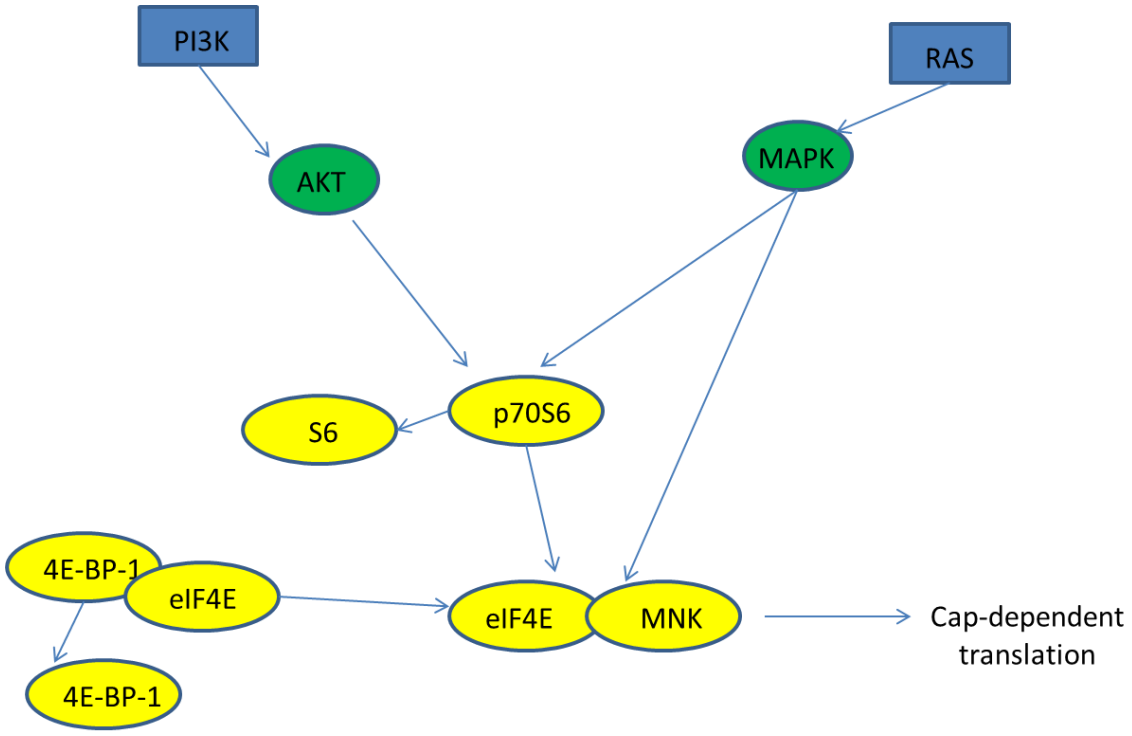

Figure 26: Model of translational control activation [1, 2]. *Model created by Kyle Bauckman.

Activation of the translational control pathway leads to phosphorylation of the S6 and p70S6 kinases thus leading to recruitment of eukaryotic initiating factors (i.e. eIFs) [1]. The formation

a.

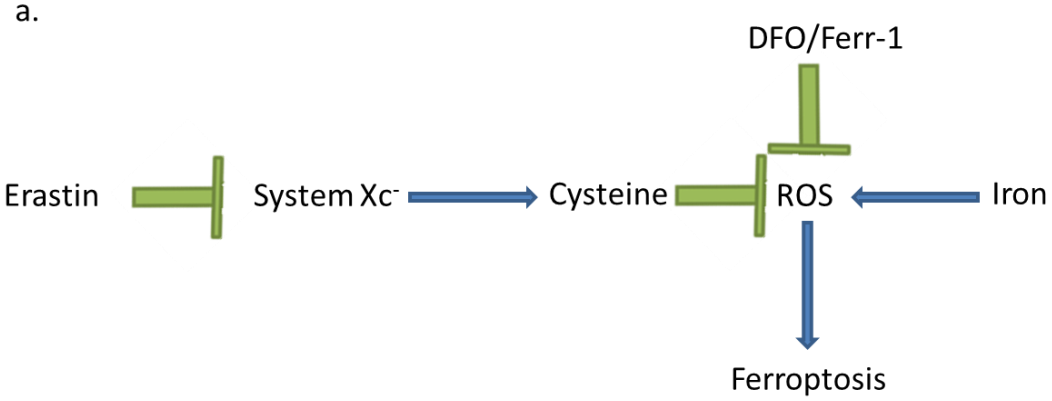

b.

Classifications for Ferroptosis
Shrunken Mitochondria
No chromatin condensation
No organelle swelling
No formation of double bounded membranes *
*Double bounded membranes can be present if shown to not directly lead to drug induced cell death
ERK/ RAS associated cell death (recovery via MAPK inhibitors)
Iron Chelators inhibit ferroptosis
Increased ROS presences
RPL8 and IREB2 inhibition lead to inhibition of cell death
Autophagy inhibitors do not reverse cell death
Pan caspase inhibitors do not reverse cell death

Figure 27: Model of the ferroptosis pathway
A. The pathway was described in Dixon and colleagues paper [3]. The small molecule inhibitor erastin inhibits cysteine channel Xc leading to reduced levels of cysteine. This leads to an increase of ROS inducing ferroptosis. Iron chelators DFO and inhibitor Ferrostatin-1 (Ferr-1) can reverse this response. It is speculated that iron may contribute to ROS production, but its exact mechanism is yet unknown. **B.** A list of traits classifying ferroptosis is provided. *Data is conflicting on the involvement of autophagy. *Model created by Kyle Bauckman.

of eIF complexes is particularly limited by eIF4E which is found at low levels relative to other eIFs. eIF4E thus becomes the rate limiting step for translational activation [1]. The eIF complex

forms a cap on the 5' untranslated region of a given mRNA [1]. This cap assists in the translation of the mRNA to protein. This cap formation can be inactivated by 4E-BP1. This protein binds to eIF4E preventing it from forming a 5' cap [149]. Phosphorylation of 4E-BP1 releases eIF4E allowing translational activation to ensue [149]. While Ras-induced translational activation is considered a tumor promoting mechanism, modulation of this pathway can also lead to expression of pro-death mediators [148, 150]. As presented herein, since we observed that the translational control pathway could be altered by iron exposure, we also assessed the contribution of this pathway to the iron-induced cell death response in HEY cells using inhibitors (i.e. MNK inhibitor) which are known to regulate this pathway.

In the second approach, we investigated whether signaling events activated by ferroptosis, a recently reported novel iron-regulated cell death pathway, occurred following Ras/MAPK activation under our conditions [3]. The similarities in ferroptosis to the cell death response we observed were intriguing and merited further investigation (see Figure 27). The initial study on ferroptosis was reported during publication of our studies presented in Chapter 4. Presently, only two groups have published work relating to this pathway [3, 84]. Ferroptosis is mediated by the Ras pathway and can be induced by a small-molecule inhibitor of Ras called erastin [3]. Further, a novel inhibitor called Ferrostatin-1 was also developed that appears to be capable of reversing the iron-induced cell death response [3]. Ferroptosis closely resembles a necrotic form of cell death in which loss of membrane integrity occurs. However, they conclude that ferroptosis is simply a novel form of necrotic response. Since we observed that iron treatment in the HEY ovarian cancer cell line exhibited loss of plasma membrane integrity (indicative of necrosis), we then sought to determine whether iron induced a ferroptosis response in this cell line.

Our third approach involved investigating whether the iron pathways regulated by IRP1/2 (iron regulatory protein 1 or 2) could be altered as a result of Ras mutation or overexpression. As described in Chapter 1 and Figure 5, the IRP1/2 proteins are critical for regulating expression of molecules in iron uptake (CD71, transferrin receptor and DMT1, divalent metal transporter), preprocessing (ISCs), iron utilization (FTH, ferritin), and export (ferroportin and hepcidin) in the cell [25]. Intercellular uptake of iron occurs through the transferring receptor which becomes internalized into endosomes [25]. Here, iron is converted from Fe^{+3} to Fe^{+2} via ferroreductases such as STEAP proteins and is then exported into the cytosol via DMT-1 [25]. This bioactive iron (as Fe^{+2}) is redox-active and can bind to IRP1 to regulate its RNA-binding activity [19]. Under conditions of excess iron, it may be stored by binding to ferritin or exported out of the cell by ferroportin [25]. Ferroportin, itself, is regulated by a small peptide hormone called hepcidin. Hepcidin is produced and regulated by the liver. Cell exposure to hepcidin leads to degradation and internalization of ferroportin [25]. Interestingly, high levels of hepcidin have been observed in breast cancer patients [69]. Similarly, breast cancer patient tissue and cancer cells express low levels of ferroportin promoting iron retention [69]. In addition, iron is needed for production of iron-sulfur clusters which regulate proteins critically involved in transcription, translation, and cellular respiration (i.e. aconitase, electron transport chain, citric acid cycle [21]), amongst many others [22, 25, 29, 68, 70]. Iron-sulfur clusters are generated in the mitochondria and thus iron needs to be imported into this organelle via as yet unknown transporters [21, 22, 63, 64, 68, 113, 116]. Intriguingly, frataxin (FTX), a mediator of mitochondrial iron-sulfur cluster biogenesis, harbors a critical mutation in Friedreich's Ataxia [21] which leads to FTX downregulation in this disease [68]. This neurological disorder leads to the degradation of nerve tissue and the spinal

cord [21]. Of interest to cancer research is that FTX elicits tumor suppressive activity and is downregulated in liver cancer and neuroblastoma [22, 64, 151].

Result

Iron activates the translational control pathway downstream of Ras/MAPK activation

The translational control pathway is commonly activated by the Ras/MAPK pathway [1, 2]. Recently, it has been shown that dual activation of the PI3K and Ras pathway may be required to induce the translational control pathway [148]. Based on a Reverse Phase Protein Array (RPPA) high-throughput proteomics approach (data not presented), we identified "hits" in the translational control pathway. We validated these hits via western analysis using cell lines (T80, T80 + H-Ras, TOV21G, and HEY cells) we previously reported in Chapter 4. Once again these cells were treated with FAC at the 1 hour and 18 hour time points (see Figure 28). We determined that iron exposure leads to activation of the following translational control markers including S6, p70S6K, and eIF4E in cell lines that elicited the most marked iron-induced reduction in cell survival responses. Specifically, the T80 cell types showed relatively modest expression of translational control markers compared to HEY, TOV21G, and T80 + H-Ras cell types (see Figure 28).

Since treatment of iron activated the translational control pathway, we next assessed whether inhibition of this pathway could modulate iron-induced sensitivity to reduced cell survival response. We inhibited activation of the translational control pathway using cycloheximide (a general translational inhibitor) and found no change in cell growth with or without iron treatment (data not shown). We then selected a specific inhibitor targeting the MNK pathway [152]. The MNK protein is involved in recruiting eIFs to the 5' UTR region of mRNAs

allowing for translation. Inhibition of MNK reverses translational activation in the presence of elevated eIF4E levels [1, 2, 152]. The inhibitor only elicited modest yet significant reversal of cell death in HEY cells (see Figure 28). This indicates that the translational control pathway only plays a minor role in the Ras/MAPK-dependent iron induced reduction in cell survival response. In support, we performed siRNA studies targeting p70S6K, S6, and 4E-BP1 but we did not observe marked changes in cell survival in the absence or presence of FAC (data not shown).

Inhibition of ferroptosis does not reverse iron induced cell survival reduction in HEY and TOV21G cell lines

Recently, a new form of cell death coined ferroptosis was described [3]. As the name suggests, this cell death mechanism is iron-dependent and was found to be distinct from apoptosis, autophagy, and necrosis. Since the exact type of cell death remained elusive in Chapter 4, we were interested to determine whether iron-induced death we observed resembled ferroptosis. The cellular characteristics of ferroptosis are not fully delineated. To improve our understanding of ferroptosis, we summarize the so far described changes induced under this unique mechanism of cell death in tabular format (see Figure 27) from which we concluded that ferroptosis appears to be an essentially a form of programmed necrosis or "necroptosis" [3, 71, 84]. To determine if iron treatment of cell lines with Ras mutation or overexpression led to induction of ferroptosis, we assessed the effect of Ferrostatin which was developed by Dixon and colleagues [3]. Co-treatment of Ferrostatin with iron led to a reduction in p-ERK, p-AKT, as well as autophagic response (see Figure 29). However, Ferrostatin did not reverse the reduced

viability of iron sensitive cells, HEY and TOV21G (up to an equimolar level of Ferrostatin to iron).

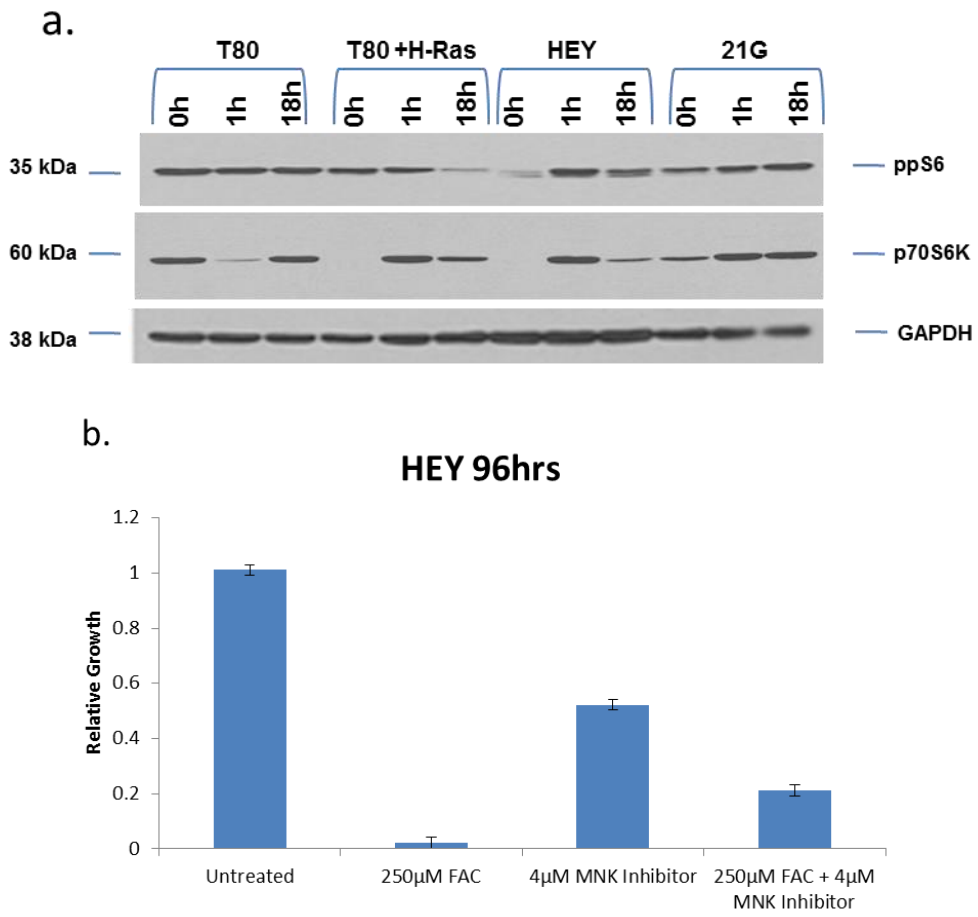

Figure 28: Iron modulation of the Ras/MAPK pathway activates the translational control pathway

A. T80, T80 + H-Ras, HEY, and TOV21G cells were treated with FAC for 1 and 18 hour time points. Phosphorylation of translational control regulators, S6 and p70S6K were elevated in HEY, T80 + H-Ras, and TOV21G cell lines. **B.** Use of a MNK inhibitor hinders activation of the translational control pathway. Treatment with the inhibitor in combination of FAC slightly reversed cell death in HEY cells after 96 hours of treatment.

a.

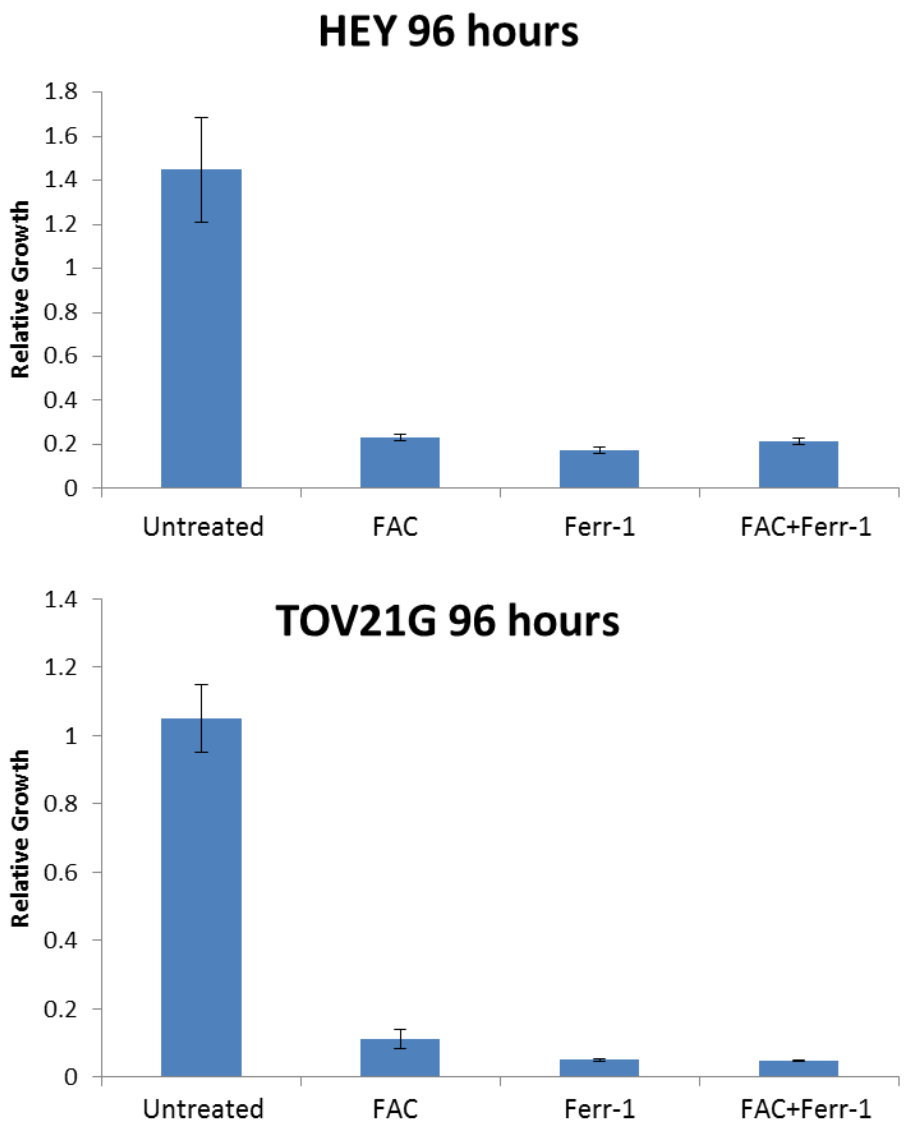

Figure 29: Inhibition of ferroptosis does not reverse iron cell death
A. HEY and TOV21G cells were treated with ferroptosis inhibitor, Ferrostatin-1 (Ferr-1), at 250 µM concentration. Cells were treated with and without ferrostatin and in combination of FAC (250 µM). Ferrostatin-1 did not reverse iron induced cell death and instead also caused reduction in cell growth.

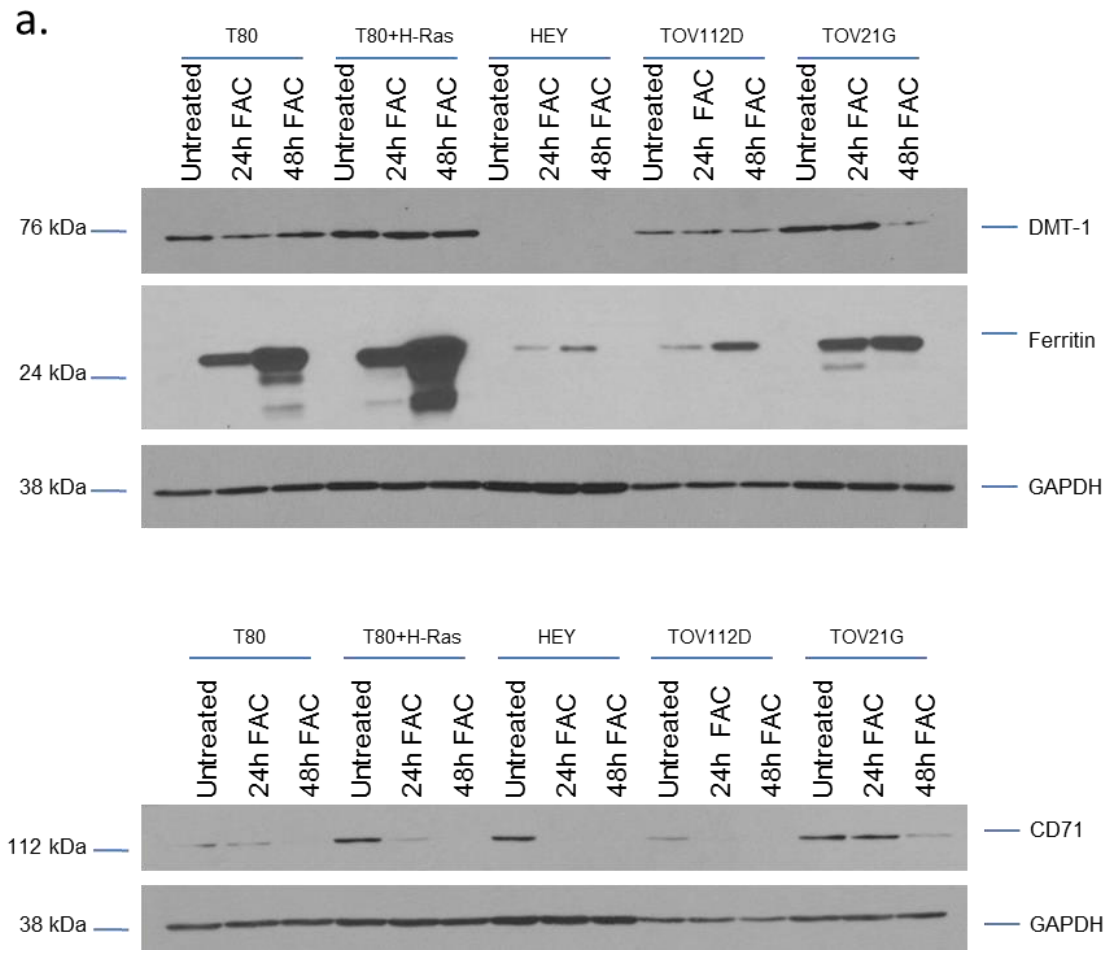

Figure 30: Iron regulation in ovarian cell types
A. FAC cell profiles of gynecological cells T80, T80 + H-Ras, HEY, TOV112D, and TOV21G do not show a trend with iron regulatory proteins (DMT-1, Ferritin, and CD71). Ras mutation or overexpression does not alter response to iron. Top panel is a 10% gel and the bottom is 8%.

FAC modulates iron regulating signals in ovarian cell lines

Previously (in Chapter 4), Figure 19 we assessed the expression of ferritin in iron treatment. However, the pattern did not identify any association. Nevertheless, dysregulated expression of molecules involved in iron regulation has previously been demonstrated in cancer cells leading to increased iron uptake and intracellular iron retention [25, 69]. Therefore a more

comprehensive western analyses of these and other classical iron regulators were performed to identify any notable patterns. We assessed CD71, FTH, DMT-1, as well as ferroportin (see Figure 30). Our data did not reveal any correlations in expression with and without FAC treatment across the panel of gynecological cells we assessed. Since hepcidin (involved in internalization and degradation of ferroportin) levels increases in breast cancer, we thus assessed its transcript levels relative to HepG2 cells (a hepatocellular carcinoma cell line) [69, 153]. Due to the unavailability of hepcidin antibodies, we assessed expressing via real time PCR. However, hepcidin mRNA levels was undetectable by real-time PCR methods across all of the ovarian cell types investigated while detectable levels in HepG2 cells was detected (data not shown). These results suggest that at the intercellular level, hepcidin is unlikely to influence iron retention in cell lines with Ras mutation or overexpression.

We also investigated the protein expression of IRP1/2 and did not find a distinct trend for these molecules across the cell lines tested (T80, T80 + H-Ras, HEY, TOV21G, and TOV112D) (data not shown). Treatment with iron did not alter total IRP1 and IRP2 protein levels. Since we were also interested in determining whether expression of iron regulatory proteins (IRP1 and IRP2) could modulate the ovarian cell response to FAC, we performed knockdown of IRP1, IRP2, as well as both IRP1/2 (see Figure 31). We observed that the combined IRP1 and IRP2 knockdown via siRNA, led to >90% reduction of the corresponding protein; however, knockdown of both IRP1/2 was needed to decreased expression of ferritin. This finding was similar to treatment with U0126 where we observed downregulation of FTH following treatment (see Figure 31). These results suggest that the MAPK pathway is involved in the translation of iron regulating proteins, including FTH and CD71. However, since combined knockdown of

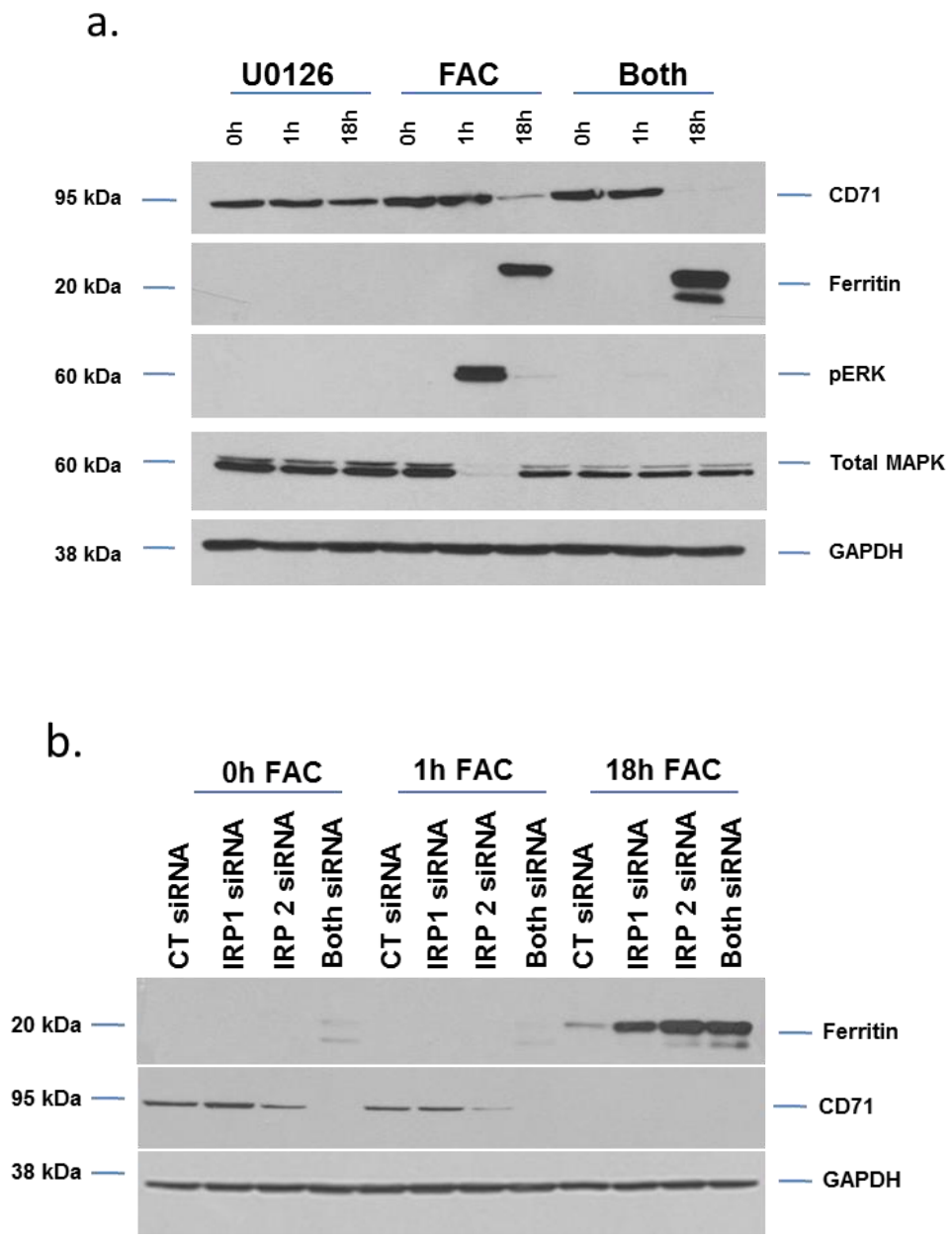

Figure 31: IRP1/2 influence on FAC response.
A. HEY cells were treated with and without FAC and U0126 for 1 hour and 18 hour time points. **B.** HEY cells were transfected with IRP1, IRP2, or both siRNA. Following 2x transfection, cells were treated with FAC at 1 hour and 18 hour time points.

IRP1/2 did not lead to inhibition of iron induced cell death in HEY cells, other mechanisms must account for this reduction in cell survival (data not shown).

Iron hinders mitochondrial functions to modulate cell survival in a Ras/MAPK dependent manner

In Chapter 4, we reported that 24 hour iron treatment of T80 cells led to increased numbers of lysosomes. In contrast, HEY cells treated with iron resulted in a marked reduction in lysosome numbers (assessed via Lysotracker Red immunofluorescence staining) (Chapter 4, Figure 15). Interestingly, it was reported that such loss of lysosome integrity may lead to a shift of iron localization from the lysosome to the mitochondria [130]. In this respect, we next investigated whether iron treatment modulated specific functions of mitochondria differentially in the Ras mutated/overexpressing cell lines. Intriguingly, we noted a marked decrease of TOM20 and TOM40, outer mitochondrial membrane transporter proteins, in HEY, TOV21G, and T80 + H-Ras cell lines treated with iron for 72 hours (see Figure 32). In contrast, the T80 and TOV112D cell types showed no reduction in these TOM proteins during the same time frame (see Figure 32). These results suggest that mitochondrial permeabilization may be occurring in with a Ras dependent manner in iron treatment. To determine if mitochondrial stress was induced by iron, we initially utilized a mitotracker ROS assay. The immunofluorescence assay stains for mitochondria and its fluorescent intensity increases in the presence of ROS (see Figure 32). High fluorescent intensity relative to untreated samples would indicate an increase of mitochondrial based ROS. We found increased mitochondrial staining with T80, T80 + H-Ras, TOV21G, TOV112D, and HEY cells suggesting increased ROS activity (see Figure 32). Interestingly, we determined that iron treatment promoted fragmentation of the mitochondria

from a filamentous-like mitochondrial network in all cell types. This result suggests that mitochondrial morphology and its behavior are altered in response to iron exposure. Next, in order to assess whether iron exposure was leading to increased mitochondrial stress, we assessed glutathione (GSH) levels in all of the ovarian cell types. Although there was variability in the GSH assay, the results indicated decreased GSH levels with iron treated HEY cells (data not shown). This was further supported with a ROS detection assay showing increased levels of ROS in all of the gynecological cell types upon treatment with FAC (see Figure 32).

Previous reports implicate shuttling of iron into the mitochondria via the calcium uniporter channel [62, 63, 130]. In order to assess whether inhibition of this channel could modulate iron-induced cell survival responses, we treated cells with Ru360 (an inhibitor of this channel) in combination with/without FAC treatment in HEY cells (see Figure 32). We determined that inhibition of this unipoter channel dramatically reversal in cell death (assessed using a cell viability assay) (see Figure 32). This suggests Ras modulated cell types are sensitive to iron overload due to import of iron into the mitochondria. Even more striking, Ru360 in combination of FAC reversed the induction of LC3-II (see Figure 32). This suggests FAC induction of autophagy is downstream of iron-induced mitochondrial stress. Furthermore, this preliminary data hints that autophagy activation may specifically be mitophagy (degradation of mitochondria via autophagosomes) [24].

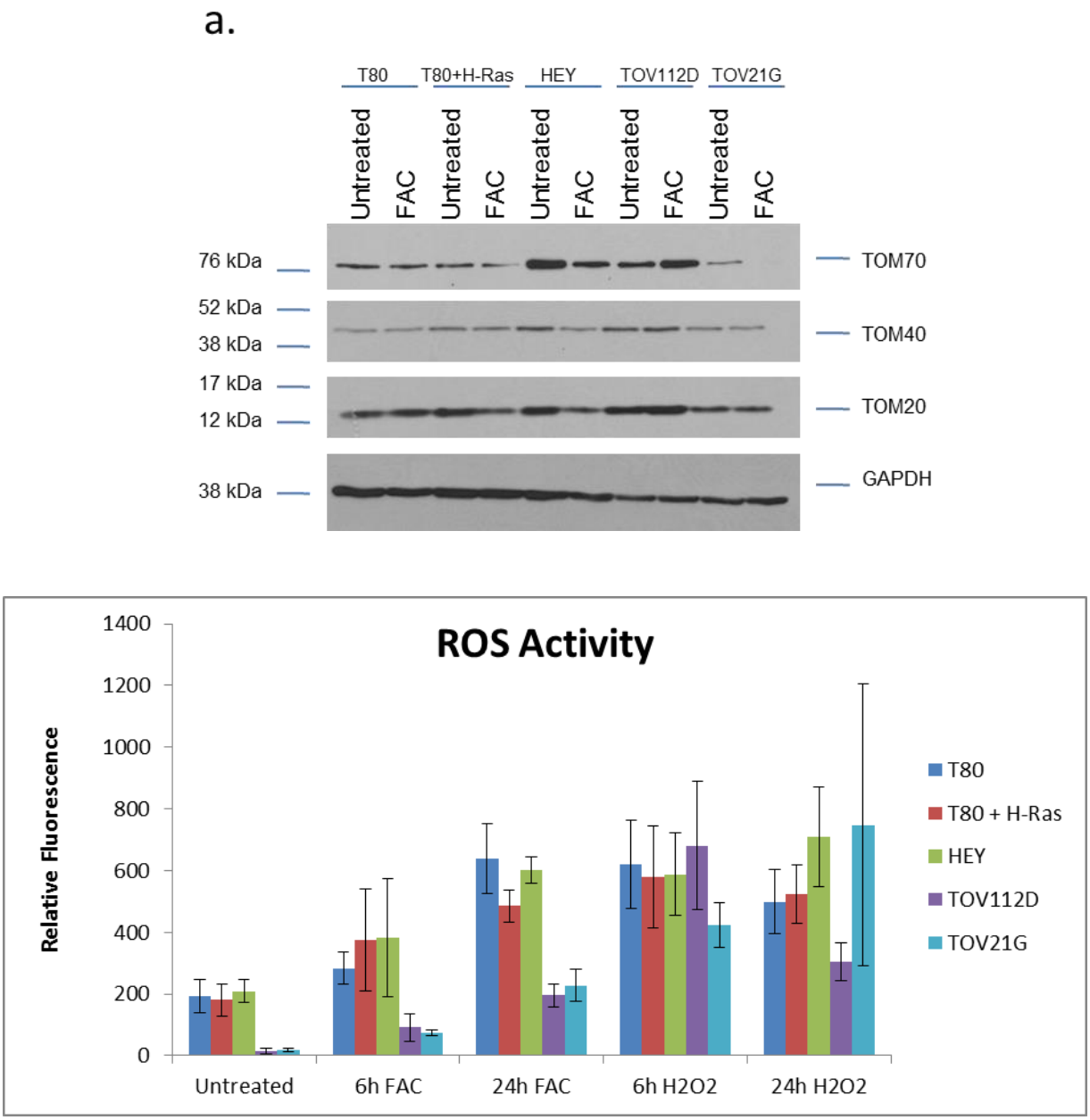

Figure 32: Iron modulates mitochondrial functions and leads to cell death in Ras modulated cell types

Continued on following page.

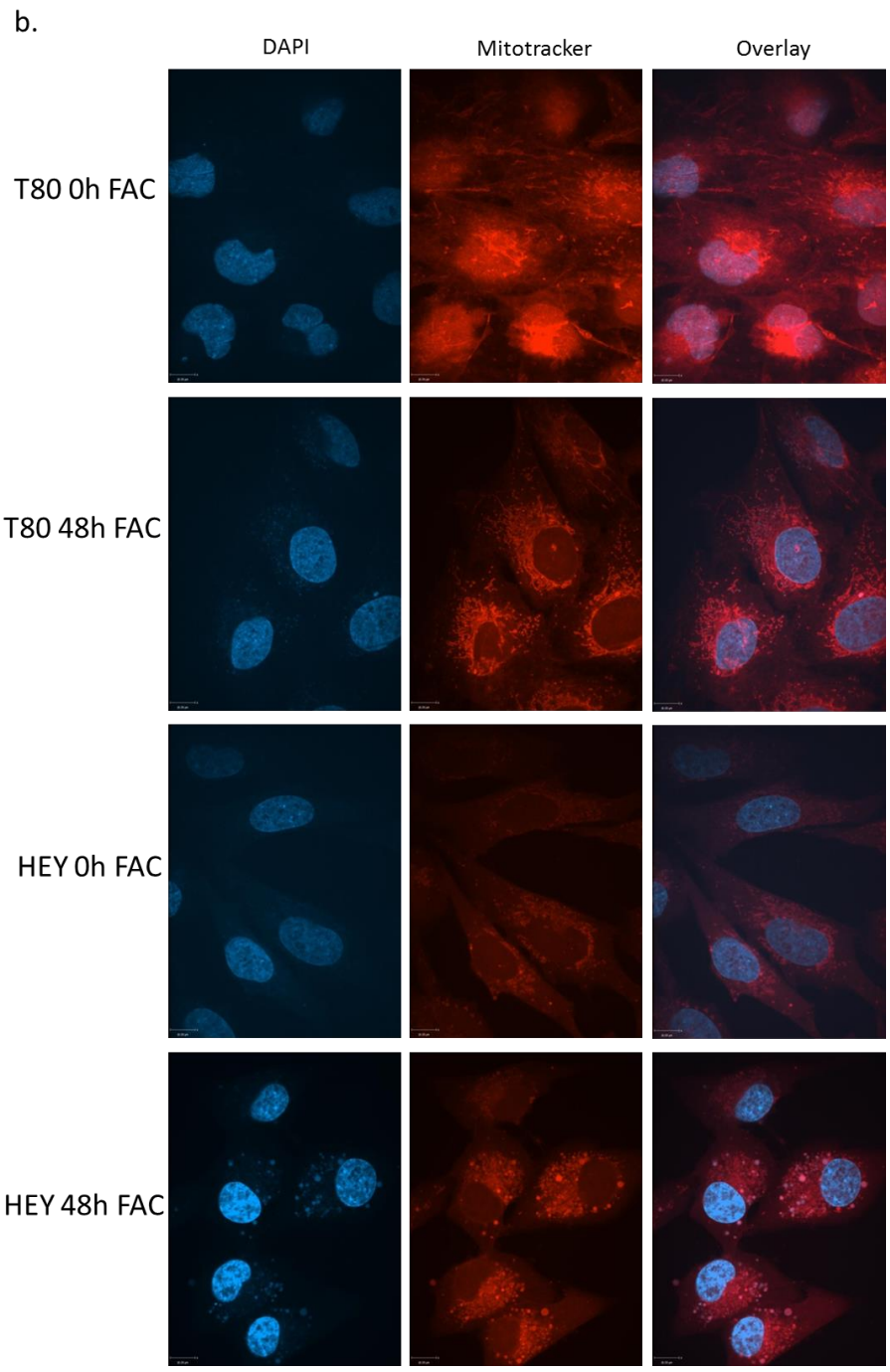

Figure 32: Iron modulates mitochondrial functions and leads to cell death in Ras modulated cell types

Continued on following page.

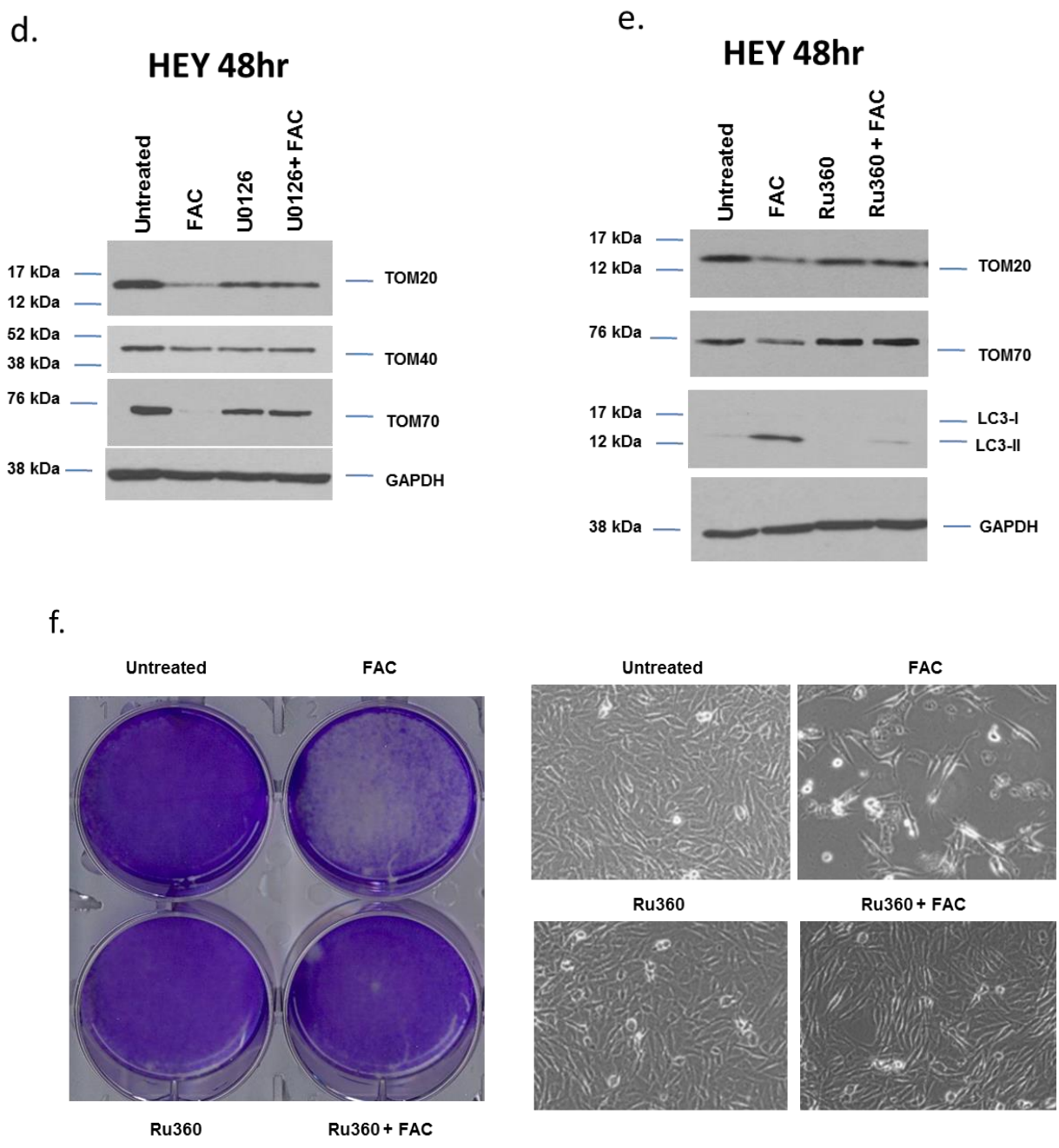

Figure 32: Iron modulates mitochondrial functions and leads to cell death in Ras modulated cell types

Continued on following page.

Figure 32: Iron modulates mitochondrial functions and leads to cell death in Ras modulated cell types

A. T80, T80 + H-Ras, HEY, TOV112D, and TOV21G cells were treated with FAC for 48 hours and assessed for outer mitochondrial markers TOM20 and TOM70. TOM20 and 70 decreased in iron sensitive cells (T80 + H-Ras, HEY, TOV21G) and remained stable in T80 and TOV112D cell lines. **B.** We show increased ROS in presence of iron at 6 and 24 hours. This increase was shown in all cell lines surveyed. Measurements were performed using fluorescence reading via H_2DCFDA (DCF). Cells treated with hydrogen peroxide (H_2O_2) were utilized as a positive control for ROS. **C.** To determine if ROS activity was related to loss of the outer mitochondrial membrane markers, mitotracker Red ROS was utilized to detect changes in mitochondrial activity at 48 hours in T80 and HEY cell lines. **D.** Use of MAPK inhibitor U0126, reversed the decrease of TOM20 and TOM70 that occurred as a result of FAC treatment. **E.** Mitochondrial Calcium Uniporter Channel inhibitor, Ru360, was utilized to inhibit iron from entering the mitochondria. Use of Ru360 reversed FAC mediated decreased of TOM20 and TOM70. **F.** Ru360 inhibitor rescued HEY cells from the cell viability effects of FAC treatment.

Discussion

In Chapter 4, we determined that iron-induced cell death was correlated to Ras mutation/overexpression. However, we did not elucidate the signaling events downstream of Ras/MAPK leading to iron induced cell death. We hypothesized that activation of AKT and ERK may lead to induction of the translational control pathway and thus activation of cell death markers. Our findings suggest that overexpression of Ras leads to the activation of the translational control pathway upon treatment with FAC. However, inhibition of this pathway with siRNA or an MNK inhibitor, did not lead to dramatic reversal of cell death.

Ras/MAPK dependent cell death response we observed in our cell via iron treatment resembled the newly observed cell death mechanism known as ferroptosis. This mechanism resembles necrosis but is specifically mediated by intercellular iron. We utilized Ferr-1, a previously identified inhibitor of ferroptosis, but failed to observe any significant reversal of cell

death. While this suggests that the mechanism of cell death observed is not identical to the ferroptosis mechanisms reported by Dixon and colleagues [3] , it does not dismiss it all together. As stated, the response we observed was markedly similar to ferroptosis. Further, the mechanism of Ferr-1 inhibition was not fully elucidated in previous papers. It was previously determined that ferrostatin did not interact with the Ras/MAPK pathway nor does it chelate iron particles [3]. The only specific function observed was its ability to reduce ROS implicating its antioxidative capabilities [3]. It is possible that the inhibitor is selective for specific cell types or takes advantage of an iron regulatory process not involved in ovarian cells.

In Chapter 4, we successfully showed that Ras mutation/overexpression to be critical to iron-induced cell death. The question lingering was what signaling pathways were activated downstream of. We hypothesized Ras may influence the iron regulatory pathway by modulating absorption, retention, storage, or a combination of all three systems. We found that iron regulating proteins (CD71, ferritin, DMT-1, ferroportin, and hepcidin) were not modulated due to Ras mutation expression (see Figure 30). Further, the translational regulation of these proteins (IRP1/2) was also not critical in inducing cell death. Interestingly, the loss of IRP1 and IRP2 led to a reduction in cell survival in untreated HEY cells implicating IRPs' role as a tumor promoter.

Similar to cellular iron regulation, the mitochondria also has means of importing, storing, and exporting iron. Interestingly, iron plays a critical role in regulating aconitase activity of IRP1 that is essential in the conversion of citrate to glutamate (in a three step process) [21]. One core regulator of iron mitochondrial regulation is frataxin. This protein is considered a tumor suppressor and has been identified to be modified in cancer cell types [19]. We were unable to detect frataxin with the antibodies currently available for western detection. As an alternative,

future investigations could quantify levels of mRNA via RT-PCR. Interestingly, we reported a marked decrease of OMM proteins, TOM20 and TOM70, in Ras sensitive cell lines (HEY, TOV21G, and T80 + H-Ras) (see Figure 32). This suggests that the iron regulation in the mitochondria is dysregulated in Ras mutated/overexpressing cell types possibly leading permeabilization. Further, mitotracker staining revealed that iron treatment modulates mitochondrial structure suggesting that this organelle plays a role in general iron regulation in ovarian cell lines. Perhaps the most striking data that we identified in this chapter was the response to inhibition of the calcium uniporter channel. Indeed, inhibition of this channel reversed the cell death effects of iron in HEY cells suggesting that iron sensitivity is directly linked to mitochondrial dysfunction in Ras mutated/overexpressing cell types (see Figure 32). Further, reversal of FAC induced LC3-II via Ru360 suggests the induction of autophagy could potentially be mitophagy (see Figure 32 and 33).

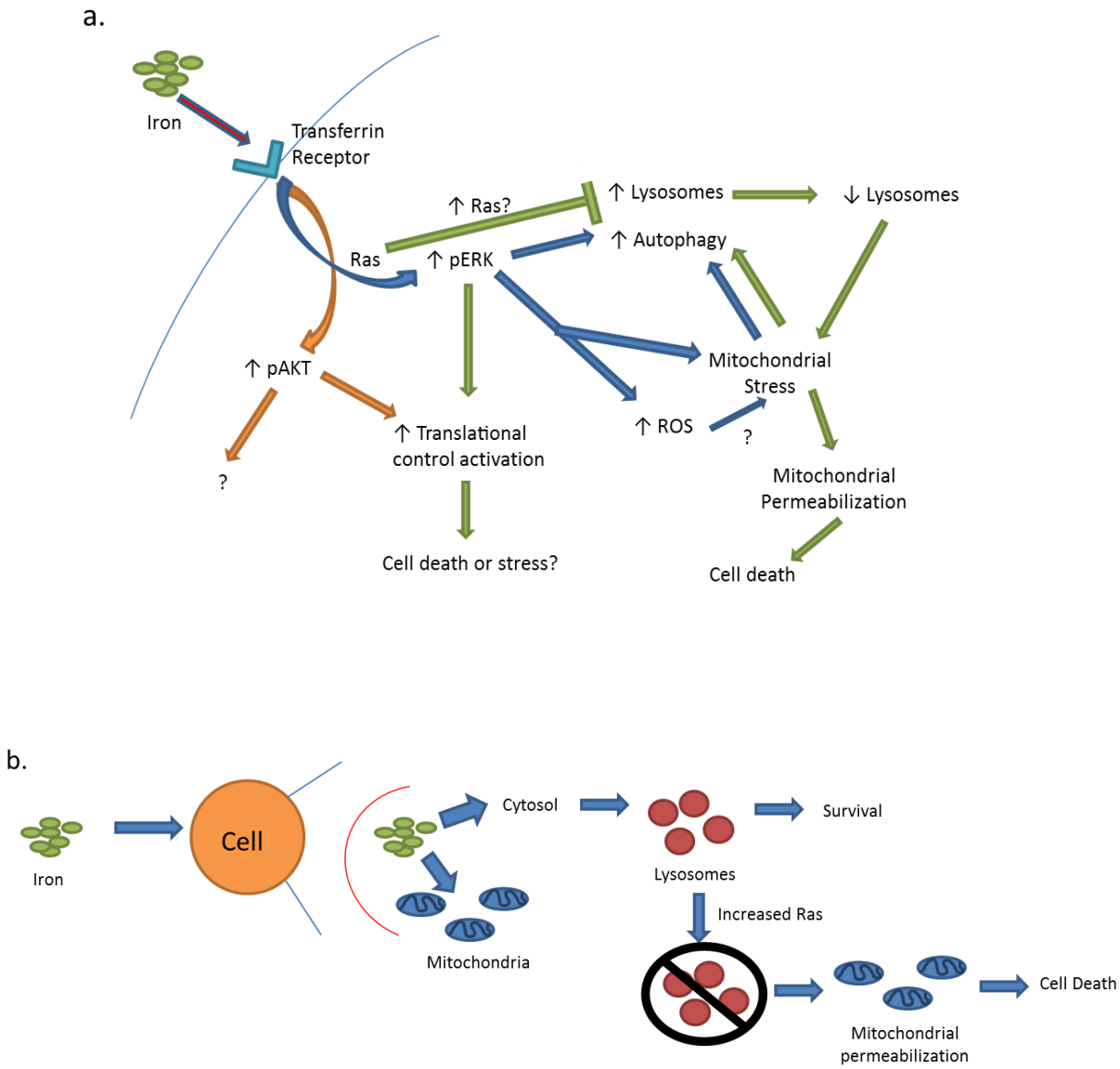

Figure 33: Model of signaling pathways that are activated by iron in gynecological cell types.

Continued on following page.

Figure 33: Model of signaling pathways that are activated by iron in gynecological cell types.
A. Iron enters the cell through the transferrin receptor leading to activation of p-AKT and p-ERK. Both pathways help to induce translational control activation leading to partial cell death. The other roles for activated AKT via iron treatment are yet unknown. Activation of the MAPK pathway induces autophagy and lysosomes. Further, iron treatment leads to mitochondrial stress and elevated ROS levels. Increased or mutated Ras may lead to decreased lysosome numbers (as seen in HEY cells). Loss of lysosomes may augment mitochondrial stress leading to mitochondrial permeabilization and cell death. **B.** Upon entering the cell, iron can be taken up by the lysosome to allow for protection and survival. However, in the presence of mutated/overexpressed Ras lysosomes are permeabilized. The lack of lysosomes as a result of activated Ras may result in mitochondrial permeabilization and cell death [21, 28, 29]. *Model created by Kyle Bauckman.

Acknowledgments

Protocols presented in Chapter 6 were designed with the guidance of Dr. Meera Nanjundan.

Chapter 7

Final Discussion and Future Directions

Overview

We present herein, an in-depth study of the role of iron response in gynecological cell lines. In Chapter 3, we developed a novel epithelial endometriotic lifespan extended cell line that can be utilized for intracellular iron research along with future mouse xenograft studies. Next, we investigated the effect of iron response on a panel of gynecological cell lines (Chapter 4). Intriguingly, we identified cell lines that contain Ras mutations or increased expression of Ras which were sensitive to iron. This sensitivity resulted in reduced cell viability and cell death in Ras specific cell lines. Iron activated multiple signaling pathways including AKT, MAPK, autophagy, and the translational control pathway (Chapters 4 and 6). Interestingly, inhibition of the MAPK/ERK pathway reversed iron-mediated reduction in cell viability with Ras sensitive cell lines.

Next, we investigated the effect of iron on ATP levels, adherence, migration, cell cycle, and ability to modulate anoikis. Chapters 4 and 5 explore these responses in gynecological cell types; we found that iron altered cell migration and cell cycle with little effect on cellular adherence. Further, cells grown under anchorage-independent conditions had reduced levels of cleaved PARP in the presence of iron. This suggests that iron antagonizes the apoptotic

response in detached cells thus promoting continued survival. Studies are currently ongoing to further elucidate the iron-induced mitochondrial response of gynecological cell types presented in this thesis. In Chapter 6, we provide evidence of mitochondrial permeabilization upon iron treatment leading to cell death in a Ras sensitive cell line (HEY, serous ovarian cell line).

Connection to Original Hypothesis

We hypothesized that continuous iron treatment would induce "normal" cells to grow, leading potentially to carcinoma-like characteristics. The work presented in this thesis uncovered a previously unknown iron response in gynecological cell lines. However, our findings superficially appear to contrast with our initial hypothesis and previously published iron/cancer publications [20, 25, 69]. Iron is a critical element essential for cell growth and beneficial to multiple cancer types including breast cancer and leukemia [20, 25]. Further, high iron exposure is linked to transformation of normal cells and increased toxicity [13, 20, 34, 70].

Iron is one of the most critical elements for survival; however, no mechanisms have been identified that would be responsible for eliminating iron from the body [25]. Many of the iron regulatory mechanisms in the cell are involved in import, export, utilization, and metabolic purposes [19, 25, 27]. Iron has been reported to increase ROS production which at constant levels could prove detrimental for organs (i.e. liver cirrhosis) and cell survival [20, 26, 70, 71, 130]. High iron levels have been shown to promote cell growth in a cancer cell system [25]. The mechanisms may be due to increased levels of transferrin receptor, HO-1, and proteins involved in iron regulation [25, 35, 65, 69, 154]. Advanced stages of cancer have also been correlated with increased risk of anemia suggesting the cancer cells are involved with increased uptake of iron from the microenvironment [27].

We hypothesized that "normal" gynecological cells maintained in an iron rich environment would elicit characteristics of an ovarian cancer tumor. Our studies presented in Chapter 4 compared "normal" cells vs. cells from different subtypes of ovarian cancer (serous carcinoma, clear cell, endometrioid). We expected ovarian cancer cell lines to exhibit increased proliferative capacity with iron while the "normal" cells would initially show increased cell stress. However, our serendipitous findings, reported in Chapter 4, identified an iron-induced Ras/MAPK dependent cell death mechanism. The focus of the thesis shifted from the role of iron in normal cells to elucidating the cell death response and mechanism in Ras mutated cell lines in response to iron. While the findings presented are novel, we now attempt to connect these findings with the original hypothesis. In the words of T.S Eliot, "the end of our exploring will be to arrive where we started and know the place for the first time [155]."

Our results presented in Chapter 4 conflict with data from previous reports and our proposed hypothesis on iron's transformative/proliferative properties [13, 20, 25, 34]. Our data suggests that iron may be beneficial to patients with ovarian cancer tumors (those containing Ras mutations). However, our observations may implicate a more intriguing event. In Chapter 3 we observed that long term iron treatment in HEY cells (K-Ras mutated serous carcinoma cell line) led to significant decrease in cell growth and increase in cell death. However, a small population of HEY cells would remain viable after 96 hours of treatment. These cells survived and apparently divided with continual exposure to iron beyond 96 hour leading to a fully confluent cell culture. This suggests that a small percentage of the HEY cells were resistant to iron-induced cell death. While it is not unusual for cancer cells to develop resistance to drug and chemical treatments, it is perhaps more alarming to observe the phenomenon with iron treatment. Indeed, this may be harmful rather than beneficial. Iron induces a very strong cell

death response toward ovarian cancer cells with Ras mutations. The rapid cell death response we observe in Ras mutated cancer cells may be a means of natural selection. Another possibility is that iron may be selecting for HEY cell populations lacking Ras mutations. The small population would then be unaffected by continued iron exposure thus promoting its growth. One could determine if this is occurring by sequencing K-Ras in the iron resistant population and identify if the mutation is still present.

We have also observed changes in the normal ovarian surface epithelial cell type, T80, and the epithelial endometriotic lifespan extended cell line (IE). T80 and IE cells displayed distinct morphological (spindle-like characteristics) changes upon treatment with iron. Though we observed changes in cell size, we did not detect changes in overall growth via crystal violet staining. This discrepancy may be due to the experimental technique utilized to assess cell viability. We performed crystal violet staining which stains protein but is not a direct measurement for proliferation. Thus, BrdU staining should be used to assess if the resistant cells are proliferating (in S phase). Our cell cycle analysis demonstrated G1 arrest utilizing whole cell populations. We may identify increases in S phase with the iron-resistant population.

In Vivo Response to Iron

The data presented in this thesis is exclusively *in vitro* based experiments. This allows a study of the mechanisms inducing iron cell death response; however, it does not provide data on the role of microenvironment in tumor development. As stated in Chapter 1, endometriotic cysts arise via retrograde movement of endometrial glands to the surface of the ovary [30, 33, 52]. These cysts contain elevated levels of heme which is proposed to transform the endometriotic tissue leading to the development of ovarian cancer [13, 40]. The surface of the ovary may be

exposed to high iron promoting cell stress leading to transformation [13, 40]. Unfortunately, the lack of precursor and early stage ovarian cancer specimens has made it challenging to support this idea. Thus, there is a lingering question of what precursor tissue/cells are leading to ovarian cancer development. Strong evidence suggests that ovarian cancer originates from the fallopian tube, the endometrial lining, as well as the surface of the ovary [13, 16, 46, 47].

Iron exposure may drive development of tumors from endometriotic cysts [13]. Indeed, in Chapter 6, we have shown that iron increased ROS; this could lead to cellular transformation by modulating cell signaling pathways [13, 20]. Excess iron (due to endometriotic cysts bursting and releasing iron into the microenvironment) could elicit cell stress to the ovary. This stress may lead to induction of an inflammatory response in the microenvironment. We propose that iron acts as a tumor initiator and the stress that is generated could potentially lead to transformation of the ovarian epithelial cells [89].

Interestingly, iron has similar characteristics to asbestos-mediated tumor development. Neither compound acts as a carcinogen but their ability to induce cell stress can lead to tumorigenesis nonetheless [20, 156]. It would be interesting to investigate ovarian cancer risk factors in women with high iron diets; no such study exists thus far.

As mentioned above (see **Connection to the Original Hypothesis** section), long term iron treatment eventually led to resistance in a subpopulation of cells. From an *in vivo* perspective, iron may destroy tissue leaving a denuded region that could be filled in by transformative cells. This behavior may allow for progression of a more aggressive tumor type *in vivo*. Iron may not result in massive cell death *in vivo* due to influence via the endocrine system. For example, hepcidin a small peptide hormone produced from the liver, promotes intercellular iron retention by degrading ferroportin which is involved in iron export [27, 69].

Further, hepcidin has been linked to increased iron levels in breast cancer in *in vivo* studies [27, 69]. The gynecological cell types we investigated had undetectable levels of hepcidin mRNA relative to HepG2 cells (liver carcinoma cells) which showed decreased levels of hepcidin mRNA with iron treatment (data not shown). This suggests that hepcidin does not contribute a large degree in iron regulation in the gynecological cell types we investigated. However, our hypothesis was that hepcidin would increase intercellular iron leading to iron toxicity in Ras mutated cancer cells. In Figure 34 and 35, we present a model describing development of ovarian cancer in the presence of iron and the *in vivo* response of Ras mutated ovarian cancer to iron.

Limitations

While our data strongly support our conclusions, we have not successfully answered the initial hypotheses. Each chapter was met with limitations and unanswered questions that we discuss below.

Chapter 3 focused on the development of a novel extended lifespan epithelial endometriotic cell line. Although we were successful in developing and characterizing such a cell line, we were unable to perform the many assays utilized in established cell lines due to its limited lifespan. The primary cells were challenging to immortalize as they were very sensitive to the retroviral infection process. This hindered the development of a SV40 Large T antigen / hTERT immortalized cell type. As a result, the passage number for the cell line was limited to around 20. As described in Chapter 2 (see Table 2), very few epithelial endometriotic cell lines are currently available. We hope that our continued efforts will eventually contribute a new cell

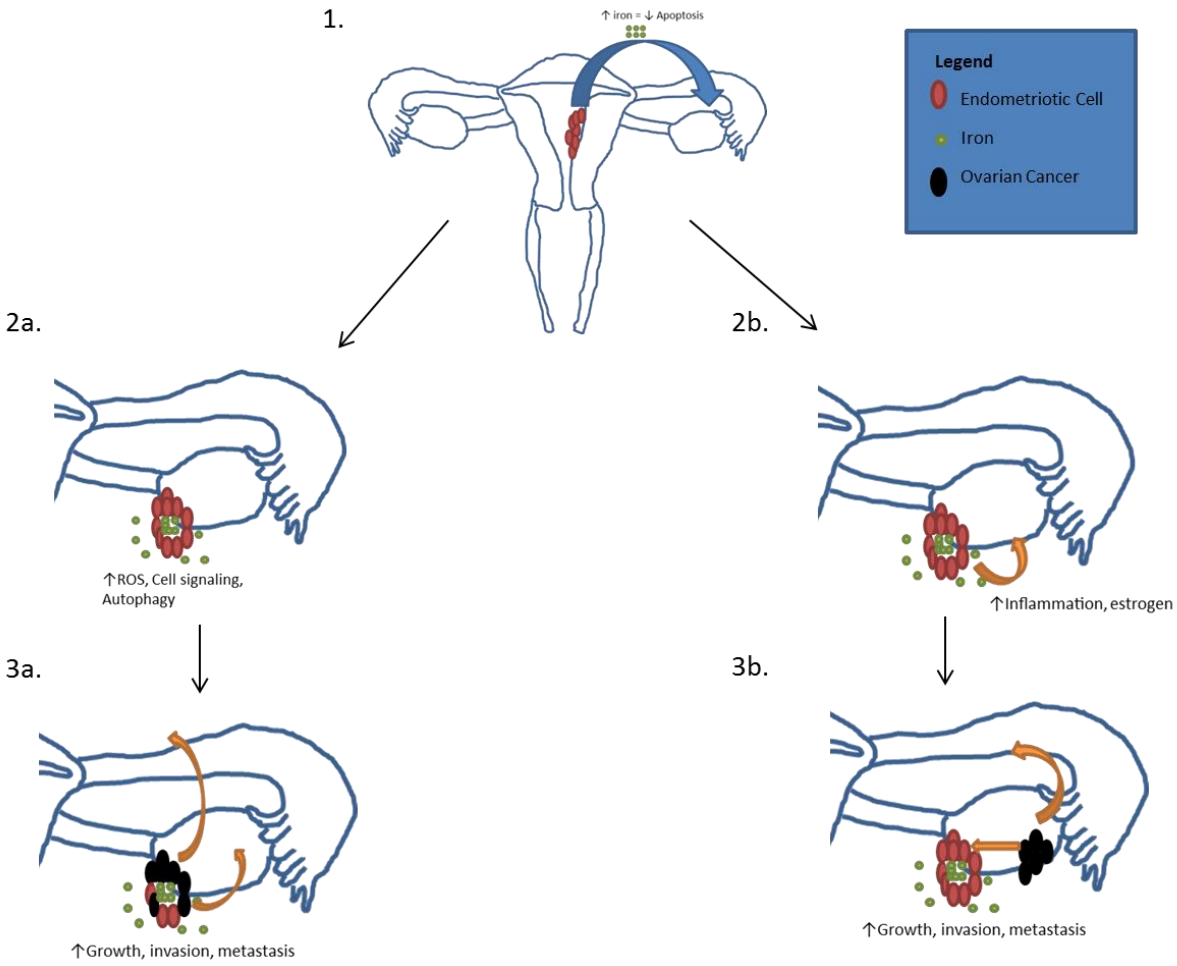

Figure 34: Role of Iron in Ovarian Cancer Initiation *in vivo*.
1. Endometrial glands (comprised of epithelial and stromal tissue) travel upward through the fallopian tube and attaches to the surface of the ovary leading to the development of an endometriotic cyst rich in iron. In Chapter 5, we demonstrate iron reduces anoikis (based on cleaved PARP decrease) (see Chapter 5, Figure 24). 2a. Endometriotic cysts containing iron rich heme form on the ovary. Iron rich heme present in the endometriotic cyst is released leading to increased ROS, cell signaling, and autophagy activation (see Chapters 4 and 6). 3a. Continual iron exposure transforms endometriotic epithelial cells to early stage tumors that eventually lead to invasion and metastasis. 2b/3b. Another pathway of tumorigenesis may stem from the content of endometriotic cysts influence on the surface of the ovary. Cyst burden may elicit an environment with inflammation (NK cells and macrophages) and hormone dysregulation (particularly estrogen) leading to transformation of ovarian tissue [13, 16, 18, 20, 30-33]. *Model created by Kyle Bauckman.

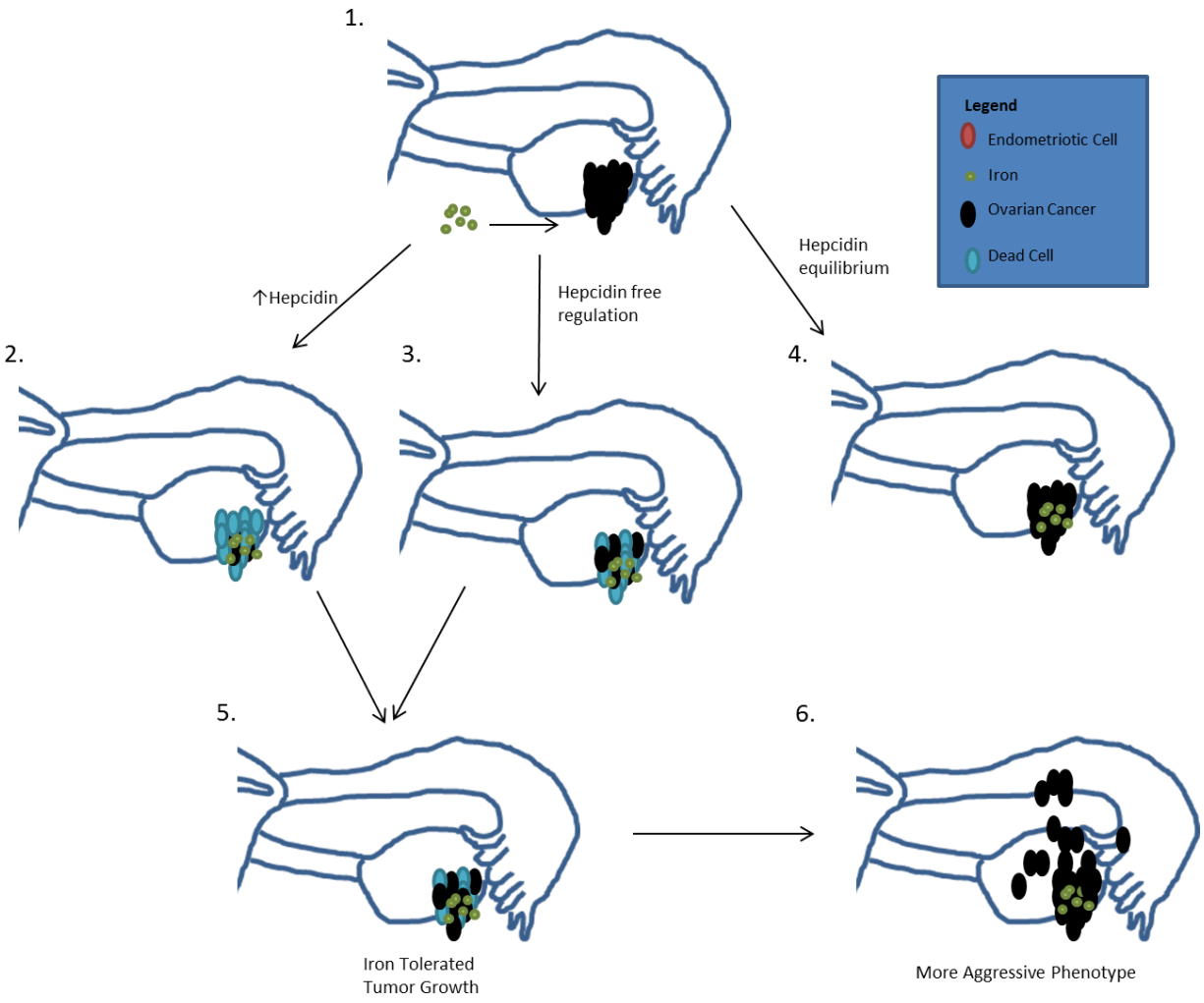

Figure 34: Model of Iron Influence in Ovarian Cancer Progression *in vivo*
1. Iron present in the microenvironment could influence ovarian cancer. This may lead to pathways 2 through 4. Pathway 2: if the tumor microenvironment has high levels of hepcidin, intercellular levels of iron would increase leading to high cell death in Ras mutated cell types. Pathway 3: Absence of hepcidin would also induce cell death response as seen *in vitro* (see Chapter 4). Pathway 4: Regulation of iron via equilibrium of hepcidin in the microenvironment may reduce the cell death effect observed. Pathway 5: Continual exposure to increased intercellular iron will lead to selection of cells tolerant to iron therefore to a potentially more aggressive/invasive tumor will develop (6.) [13, 25, 27, 28]. *Model created by Kyle Bauckman.

line to the field. We are presently characterizing and validating more endometriotic cell lines for future use. We have gained valuable knowledge in care and development of IE cells.

In Chapter 5, we observed a significant reduction of cell growth with Ras mutated or overexpressed cell types. We investigated multiple mechanisms of cell death; specifically in the HEY cell line we discovered marked iron induced necrotic activity (see Chapter 4, Figure 11). However, we were not successful in identifying the cell death behavior of the other Ras sensitive cell lines (TOV21G, T80 + H-Ras). We investigated multiple cell death mechanisms including apoptosis, necrosis, autophagy, and ferroptosis; however, these mechanisms did not appear to contribute to decreased cell viability observed in the TOV21G and T80 + H-Ras cell lines. Some of these shortcomings may be due to limitations in the experimental procedures performed. Although we did not observe cleaved PARP in iron-treated TOV21G cells using methods presented in Chapter 4, we do see slight increase of cleaved PARP in TOV21G cells treated with iron in data presented in Chapter 5. The protocol for analyzing cell death in Chapter 5 required collection of floating cells (not performed in any other western analysis presented in Chapter 4). Thus it is possible only the floating cells express cell death markers. Another possibility is apoptosis may be occurring via a caspase-independent mechanism [72]. Another dilemma arose with the ferroptosis inhibitor, ferrostatin. Our studies with the ferroptosis inhibitor demonstrated high toxicity indicating it was too potent for the selected gynecological cell lines (see Chapter 6, Figure 29). This does not indicate ferroptosis is not being induced, but simply that the inhibitor is too potent for the selected cell types. Future investigations should focus on finding alternate inhibitors for the ferroptosis process or alternatively screen for inhibitors that reverse the iron-induced cell death our studies delineate.

Elucidation of the signaling pathway induced by iron treatment proved the most challenging aspect of the project. The current literature related to iron and ovarian cancer is limiting and iron's role in ovarian cancer cell death is non-existent (excluding our recent publication). Multiple signaling pathways are activated via iron treatment; however, these events did not contribute to iron-induced cell death. This is logical considering that iron is a naturally occurring element in the cell and required for basic metabolic functions. We have identified that the cell death mechanism is Ras/MAPK dependent (see Chapter 4, Figure 16) and induces both lysosomal (see Chapter 4, Figure 16) and mitochondrial permeabilization (see Chapter 6, Figure 32). We also observed that the loss of mitochondria is directly linked to cell death induction in HEY cells (see Chapter 6, Figure 32).

Though we were successful in uncovering these important signaling pathways involved in iron- induced cell death, the links between these pathways has yet to be investigated. Some questions that arise include how does a Ras mutation influence lysosome and mitochondrial permeabilization? We attempted to determine if Ras mutations induced higher intake of iron, but technical issues prevented us from pursuing this. Future endeavors should focus on finding a method of accurately assessing intercellular iron intake.

Effort should also be placed in determining the kinetics of the iron-induced events. We have identified activation of pERK to occur early (1 hour or less) (see Chapter 4, Figure 16) which led to increased production of lysosomes at 24 hours (see Chapter 4, Figure 15). At the same time, mitochondrial stress was also observed at 24 hours followed by loss of outer mitochondrial markers at 48 hours (TOM20/70) (see Chapter 6, Figure 32). The remaining question is what is the specific cellular mechanism that can lead to the observed cell death? We propose that loss of lysosomes leads to increased mitochondrial stress and permeabilization or

vice versa. Western blots and flow cytometry assess the entire cell population and thus the overall trends; these methods may miss events occurring in smaller populations. For example, we observed lack of lysosome formation in necrotic HEY cell population treated with iron. However, in the resistant population, we noted abundant lysosomes present. It would be interesting to observe mitochondrial response in this population. Therefore, it may be advantageous to perform single cell, live imaging of HEY cells treated with iron. These cells could be tagged with lysotracker and a mitotracker and imaged over 48 hours to determine the specific chain of events leading to iron-induced cell death.

Summary of Future Directions and Proposed Specific Aims

The data presented in this thesis describes a novel discovery that we foresee to evolve into multiple future investigations (some of which are ongoing). The role of iron in ovarian tumor growth *in vivo* would be the core focus of the investigation. The cellular response to iron may drastically change with the addition of the microenvironment. The effect we observe *in vitro* may select for cells lacking Ras mutations and/or may promote a more aggressive phenotype. As stated, the limitation with IE cells (inability to expand cells beyond 20 passages) hinders experimental progress. Continued endeavors also include development of a more immortalized endometriotic cell line which would be useful for long term iron studies. We are currently in the process of immortalizing two primary endometriotic cell lines derived from the peritoneal cavity and ovary, respectively.

Finally, it is important to address the role of DFO on ovarian cancer growth. Treatment with DFO in gynecological cell lines induced high levels of cell death in the form of apoptosis (see Chapter 4, Figure 19). This response occurred with doses as low as 1 μM. This is

particularly impressive with consideration that typical doses of DFO range from 200-300 µM *in vivo [11]*. This suggests DFO may be an ideal drug for ovarian cancer treatment. The only negative detail is DFO is toxic to all gynecological cell types. This suggests *in vivo* treatment may lead to toxicity to all gynecological tissue.

Development and Characterization of Novel Endometriotic Cell Lines

Aim 1: Characterize additional primary endometriotic cell lines

1.1 : Determine if cells are stromal or epithelial

1.2 : Assesses markers of growth, survival, cell cycle, and EMT relative to existing ovarian cell types

Aim 2: Immortalize primary endometriotic cell line

2.1: Immortalize cells with hTERT

2.2: Characterize confirming immortalization and retention of similar proteomic profile expressed in primary cells.

Aim 3: Determine the role of autophagy in endometriotic cell survival

3.1: Inhibit autophagy and assess immortalized cell survival

Iron modulates cell survival in a Ras- and MAPK-dependent manner in ovarian carcinoma (in vivo)

Aim 1: Determine the influence of iron in mouse ovarian tumor models (Dinulescu's model [93])

1.1: Determine if cell death markers are present following iron treatment provided intratumorally.

1.2: Determine time of reoccurrence of tumor burden

Aim 2: Determine the phenotype and genotype of long term iron treated HEY cells

2.1: Is K-Ras mutation present in the resistant population (*In vitro*)?

2.2: *In vivo* mouse xenograft model using long term treated HEY cells to determine invasiveness, proliferative capacity, and metastatic potential.

Aim 3: Determine whether there is an association between high iron diet and ovarian cancer.

3.1: Determine if select populations of ovarian cancer patients can be classified according to their blood iron and/or tumor iron levels.

3.2: Assess whether increased iron intake increase ovarian cancer risk?

The cell death effect of DFO on ovarian cancer in vivo

Aim 1: Ovarian cancer mouse model studies

1.1 : Determine if DFO treatment reduces growth of ovarian tumors

1.2 : Determine lowest dose required for clearance of tumor burden

Aim 2: Phase 1 clinical trials of DFO on ovarian cancer patients

2.1: Treat with DFO with and without an iron limited diet to determine efficacy of drug

References Cited

1. Hou, J., et al., *Targeting Mnks for cancer therapy.* Oncotarget, 2012. **3**(2): p. 118-31.
2. Fortin, C.F., et al., *Translational control of human neutrophil responses by MNK1.* J Leukoc Biol, 2013. **94**(4): p. 693-703.
3. Dixon, S.J., et al., *Ferroptosis: an iron-dependent form of nonapoptotic cell death.* Cell, 2012. **149**(5): p. 1060-72.
4. Korch, C., et al., *DNA profiling analysis of endometrial and ovarian cell lines reveals misidentification, redundancy and contamination.* Gynecol Oncol, 2012. **127**(1): p. 241-8.
5. Bouquet de Joliniere, J., et al., *Human endometriosis-derived permanent cell line (FbEM-1): establishment and characterization.* Hum Reprod Update, 1997. **3**(2): p. 117-23.
6. Kniss, D.A. and T.L. Summerfield, *Discovery of HeLa Cell Contamination in HES Cells: Call for Cell Line Authentication in Reproductive Biology Research.* Reprod Sci, 2014.
7. Lopez, J., et al., *Normal and cancer stem cells of the human female reproductive system.* Reprod Biol Endocrinol, 2013. **11**: p. 53.
8. Borahay, M.A., et al., *Mullerian inhibiting substance suppresses proliferation and induces apoptosis and autophagy in endometriosis cells in vitro.* ISRN Obstet Gynecol, 2013. **2013**: p. 361489.
9. Gozzelino, R., V. Jeney, and M.P. Soares, *Mechanisms of cell protection by heme oxygenase-1.* Annu Rev Pharmacol Toxicol, 2010. **50**: p. 323-54.
10. Banerjee, P., et al., *The heme oxygenase-1 protein is overexpressed in human renal cancer cells following activation of the Ras-Raf-ERK pathway and mediates anti-apoptotic signal.* J Biol Chem, 2011. **286**(38): p. 33580-90.
11. Porter, J.B., et al., *Recent insights into interactions of deferoxamine with cellular and plasma iron pools: Implications for clinical use.* Ann N Y Acad Sci, 2005. **1054**: p. 155-68.
12. Ying, T.H., et al., *Association of p53 and CDKN1A genotypes with endometriosis.* Anticancer Res, 2011. **31**(12): p. 4301-6.
13. Yamaguchi, K., et al., *Contents of endometriotic cysts, especially the high concentration of free iron, are a possible cause of carcinogenesis in the cysts through the iron-induced persistent oxidative stress.* Clin Cancer Res, 2008. **14**(1): p. 32-40.
14. Xiao, W., A. Awadallah, and W. Xin, *Loss of ARID1A/BAF250a expression in ovarian endometriosis and clear cell carcinoma.* Int J Clin Exp Pathol, 2012. **5**(7): p. 642-50.
15. Wiegand, K.C., et al., *ARID1A mutations in endometriosis-associated ovarian carcinomas.* N Engl J Med, 2010. **363**(16): p. 1532-43.
16. Tokokuni, Y.Y.a.S., *Endometriosis-Associated Ovarian Cancer: The Role of Oxidative Stress* in *Endometriosis- Basic Concepts and Current Research Trends*, K. Chaudhury, Editor. 2012, Intech: Intech.

17. McConechy, M.K., et al., *Ovarian and endometrial endometrioid carcinomas have distinct CTNNB1 and PTEN mutation profiles.* Mod Pathol, 2013.
18. Lai, C.R., et al., *Ovarian cancers arising from endometriosis: A microenvironmental biomarker study including ER, HNF1ss, p53, PTEN, BAF250a, and COX-2.* J Chin Med Assoc, 2013.
19. Anderson, C.P., et al., *Mammalian iron metabolism and its control by iron regulatory proteins.* Biochim Biophys Acta, 2012. **1823**(9): p. 1468-83.
20. Valko, M., et al., *Free radicals, metals and antioxidants in oxidative stress-induced cancer.* Chem Biol Interact, 2006. **160**(1): p. 1-40.
21. Richardson, D.R., et al., *Mitochondrial iron trafficking and the integration of iron metabolism between the mitochondrion and cytosol.* Proc Natl Acad Sci U S A, 2010. **107**(24): p. 10775-82.
22. Kirches, E., et al., *Dual role of the mitochondrial protein frataxin in astrocytic tumors.* Lab Invest, 2011. **91**(12): p. 1766-76.
23. Institute, N.C. *http://www.cancer.gov/*. 2013.
24. Klionsky, D.J., et al., *Guidelines for the use and interpretation of assays for monitoring autophagy.* Autophagy, 2012. **8**(4): p. 445-544.
25. Torti, S.V. and F.M. Torti, *Iron and cancer: more ore to be mined.* Nat Rev Cancer, 2013. **13**(5): p. 342-55.
26. Nadadur, S.S., K. Srirama, and A. Mudipalli, *Iron transport & homeostasis mechanisms: their role in health & disease.* Indian J Med Res, 2008. **128**(4): p. 533-44.
27. Ganz, T. and E. Nemeth, *Hepcidin and iron homeostasis.* Biochim Biophys Acta, 2012. **1823**(9): p. 1434-43.
28. Bauckman, K.A., et al., *Iron modulates cell survival in a Ras- and MAPK-dependent manner in ovarian cells.* Cell Death Dis, 2013. **4**: p. e592.
29. Kurz, T., J.W. Eaton, and U.T. Brunk, *The role of lysosomes in iron metabolism and recycling.* Int J Biochem Cell Biol, 2011. **43**(12): p. 1686-97.
30. Siufi Neto, J., et al., *Cellular, Histologic, and Molecular Changes Associated with Endometriosis and Ovarian Cancer.* J Minim Invasive Gynecol, 2013.
31. Seidman, J.D., *The presence of mucosal iron in the fallopian tube supports the "incessant menstruation hypothesis" for ovarian carcinoma.* Int J Gynecol Pathol, 2013. **32**(5): p. 454-8.
32. Pratt, J.H. and W.R. Shamblin, *Spontaneous rupture of endometrial cysts of the ovary presenting as an acute abdominal emergency.* Am J Obstet Gynecol, 1970. **108**(1): p. 56-62.
33. Ogawa, S., et al., *Ovarian endometriosis associated with ovarian carcinoma: a clinicopathological and immunohistochemical study.* Gynecol Oncol, 2000. **77**(2): p. 298-304.
34. Yamaguchi, K., et al., *Identification of an ovarian clear cell carcinoma gene signature that reflects inherent disease biology and the carcinogenic processes.* Oncogene, 2010. **29**(12): p. 1741-52.
35. Defrere, S., et al., *Iron overload enhances epithelial cell proliferation in endometriotic lesions induced in a murine model.* Hum Reprod, 2006. **21**(11): p. 2810-6.
36. Boyraz, G., et al., *Ovarian carcinoma associated with endometriosis.* Eur J Obstet Gynecol Reprod Biol, 2013. **170**(1): p. 211-3.

37. Baldi, A., M. Campioni, and P.G. Signorile, *Endometriosis: pathogenesis, diagnosis, therapy and association with cancer (review).* Oncol Rep, 2008. **19**(4): p. 843-6.
38. Fukunaga, M., et al., *Ovarian atypical endometriosis: its close association with malignant epithelial tumours.* Histopathology, 1997. **30**(3): p. 249-55.
39. Heaps, J.M., R.K. Nieberg, and J.S. Berek, *Malignant neoplasms arising in endometriosis.* Obstet Gynecol, 1990. **75**(6): p. 1023-8.
40. Lim, D. and E. Oliva, *Precursors and pathogenesis of ovarian carcinoma.* Pathology, 2013. **45**(3): p. 229-42.
41. Kim, A., et al., *Therapeutic strategies in epithelial ovarian cancer.* J Exp Clin Cancer Res, 2012. **31**: p. 14.
42. Bookman, M.A., *First-line chemotherapy in epithelial ovarian cancer.* Clin Obstet Gynecol, 2012. **55**(1): p. 96-113.
43. Engel, J., et al., *Moderate progress for ovarian cancer in the last 20 years: prolongation of survival, but no improvement in the cure rate.* Eur J Cancer, 2002. **38**(18): p. 2435-45.
44. Ricci, F., M. Broggini, and G. Damia, *Revisiting ovarian cancer preclinical models: implications for a better management of the disease.* Cancer Treat Rev, 2013. **39**(6): p. 561-8.
45. Abdul Razak, A.R., et al., *Chemotherapy for malignant germ cell ovarian cancer in adult patients with early stage, advanced and recurrent disease.* Cochrane Database Syst Rev, 2011(3): p. CD007584.
46. Vang, R., M. Shih Ie, and R.J. Kurman, *Fallopian tube precursors of ovarian low- and high-grade serous neoplasms.* Histopathology, 2013. **62**(1): p. 44-58.
47. Salvador, S., et al., *The fallopian tube: primary site of most pelvic high-grade serous carcinomas.* Int J Gynecol Cancer, 2009. **19**(1): p. 58-64.
48. Gibson, S.B., *Autophagy in clear cell ovarian cancer, a potential marker for hypoxia and poor prognosis?* J Pathol, 2012.
49. Brinton, L.A., et al., *Cancer risk after a hospital discharge diagnosis of endometriosis.* Am J Obstet Gynecol, 1997. **176**(3): p. 572-9.
50. Brooks, J.J. and J.E. Wheeler, *Malignancy arising in extragonadal endometriosis: a case report and summary of the world literature.* Cancer, 1977. **40**(6): p. 3065-73.
51. Medicine, A.S.o.R., *Endometriosis: A Guide for Patients.* 2012.
52. Razzaghi, M.R., *endometriosis*, in *Endometriosis- Basic Concepts and Current Research Trends*, K. Chaudhury, Editor. 2012, Ingen: Ingen.
53. Sampson, J.A., *Metastatic or Embolic Endometriosis, due to the Menstrual Dissemination of Endometrial Tissue into the Venous Circulation.* Am J Pathol, 1927. **3**(2): p. 93-110 43.
54. Yamamoto, S., et al., *Cumulative alterations of p27-related cell-cycle regulators in the development of endometriosis-associated ovarian clear cell adenocarcinoma.* Histopathology, 2010. **56**(6): p. 740-9.
55. Treloar, S.A., et al., *Genomewide linkage study in 1,176 affected sister pair families identifies a significant susceptibility locus for endometriosis on chromosome 10q26.* Am J Hum Genet, 2005. **77**(3): p. 365-76.
56. Bois, F.Y. and B. Eskenazi, *Possible risk of endometriosis for Seveso, Italy, residents: an assessment of exposure to dioxin.* Environ Health Perspect, 1994. **102**(5): p. 476-7.

57. Jacques, S.M. and W.D. Lawrence, *Endometrial adenocarcinoma with variable-level myometrial involvement limited to adenomyosis: a clinicopathologic study of 23 cases.* Gynecol Oncol, 1990. **37**(3): p. 401-7.
58. Kucera, E., et al., *Malignant changes in adenomyosis in patients with endometrioid adenocarcinoma.* Eur J Gynaecol Oncol, 2011. **32**(2): p. 182-4.
59. Kato, N., S. Sasou, and T. Motoyama, *Expression of hepatocyte nuclear factor-1beta (HNF-1beta) in clear cell tumors and endometriosis of the ovary.* Mod Pathol, 2006. **19**(1): p. 83-9.
60. Grechukhina, O., et al., *A polymorphism in a let-7 microRNA binding site of KRAS in women with endometriosis.* EMBO Mol Med, 2012. **4**(3): p. 206-17.
61. Stewart, C.J., et al., *KRAS mutations in ovarian low-grade endometrioid adenocarcinoma: association with concurrent endometriosis.* Hum Pathol, 2012. **43**(8): p. 1177-83.
62. Sripetchwandee, J., et al., *Blockade of mitochondrial calcium uniporter prevents cardiac mitochondrial dysfunction caused by iron overload.* Acta Physiol (Oxf), 2013.
63. Sripetchwandee, J., et al., *Mitochondrial calcium uniporter blocker effectively prevents brain mitochondrial dysfunction caused by iron overload.* Life Sci, 2013. **92**(4-5): p. 298-304.
64. Schulz, T.J., et al., *Induction of oxidative metabolism by mitochondrial frataxin inhibits cancer growth: Otto Warburg revisited.* J Biol Chem, 2006. **281**(2): p. 977-81.
65. Lee, P.J., et al., *Overexpression of heme oxygenase-1 in human pulmonary epithelial cells results in cell growth arrest and increased resistance to hyperoxia.* Proc Natl Acad Sci U S A, 1996. **93**(19): p. 10393-8.
66. Kao, T.W., et al., *Associations between serum total bilirubin levels and functional dependence in the elderly.* Intern Med J, 2012. **42**(11): p. 1199-207.
67. Novotny, L. and L. Vitek, *Inverse relationship between serum bilirubin and atherosclerosis in men: a meta-analysis of published studies.* Exp Biol Med (Maywood), 2003. **228**(5): p. 568-71.
68. Koeppen, A.H., *Friedreich's ataxia: pathology, pathogenesis, and molecular genetics.* J Neurol Sci, 2011. **303**(1-2): p. 1-12.
69. Pinnix, Z.K., et al., *Ferroportin and iron regulation in breast cancer progression and prognosis.* Sci Transl Med, 2010. **2**(43): p. 43ra56.
70. Reid, T.M., D.I. Feig, and L.A. Loeb, *Mutagenesis by metal-induced oxygen radicals.* Environ Health Perspect, 1994. **102 Suppl 3**: p. 57-61.
71. Dixon, S.J. and B.R. Stockwell, *The role of iron and reactive oxygen species in cell death.* Nat Chem Biol, 2013. **10**(1): p. 9-17.
72. Kroemer, G., et al., *Classification of cell death: recommendations of the Nomenclature Committee on Cell Death 2009.* Cell Death Differ, 2009. **16**(1): p. 3-11.
73. Coates, J.M., J.M. Galante, and R.J. Bold, *Cancer therapy beyond apoptosis: autophagy and anoikis as mechanisms of cell death.* J Surg Res, 2010. **164**(2): p. 301-8.
74. Giannoni, E., et al., *Redox regulation of anoikis: reactive oxygen species as essential mediators of cell survival.* Cell Death Differ, 2008. **15**(5): p. 867-78.
75. Guadamillas, M.C., A. Cerezo, and M.A. Del Pozo, *Overcoming anoikis--pathways to anchorage-independent growth in cancer.* J Cell Sci, 2011. **124**(Pt 19): p. 3189-97.
76. Frisch, S.M. and H. Francis, *Disruption of epithelial cell-matrix interactions induces apoptosis.* J Cell Biol, 1994. **124**(4): p. 619-26.

77. Westhoff, M.A. and S. Fulda, *Adhesion-mediated apoptosis resistance in cancer.* Drug Resist Updat, 2009. **12**(4-5): p. 127-36.
78. Choi, J., et al., *The role of autophagy in human endometrium.* Biol Reprod, 2012. **86**(3): p. 70.
79. Kenific, C.M., A. Thorburn, and J. Debnath, *Autophagy and metastasis: another double-edged sword.* Curr Opin Cell Biol, 2010. **22**(2): p. 241-5.
80. Chen, Y. and D.J. Klionsky, *The regulation of autophagy - unanswered questions.* J Cell Sci, 2011. **124**(Pt 2): p. 161-70.
81. Spowart, J.E., et al., *The Autophagy Protein LC3A Correlates with Hypoxia and is a Prognostic Marker of Patient Survival in Clear Cell Ovarian Cancer.* J Pathol, 2012.
82. Wu, W., P. Liu, and J. Li, *Necroptosis: an emerging form of programmed cell death.* Crit Rev Oncol Hematol, 2012. **82**(3): p. 249-58.
83. Degterev, A., et al., *Identification of RIP1 kinase as a specific cellular target of necrostatins.* Nat Chem Biol, 2008. **4**(5): p. 313-21.
84. Louandre, C., et al., *Iron-dependent cell death of hepatocellular carcinoma cells exposed to sorafenib.* Int J Cancer, 2013. **133**(7): p. 1732-42.
85. Iizuka, M., et al., *Chemical assay of iron in ovarian cysts: a new diagnostic method to evaluate endometriotic cysts.* Gynecol Obstet Invest, 1998. **46**(1): p. 58-60.
86. Kuohung, W., et al., *Characteristics of patients with endometriosis in the United States and the United Kingdom.* Fertil Steril, 2002. **78**(4): p. 767-72.
87. Kobayashi, H., et al., *Risk of developing ovarian cancer among women with ovarian endometrioma: a cohort study in Shizuoka, Japan.* Int J Gynecol Cancer, 2007. **17**(1): p. 37-43.
88. Hu, Q., et al., *Homozygous deletion of CDKN2A/2B is a hallmark of iron-induced high-grade rat mesothelioma.* Lab Invest, 2010. **90**(3): p. 360-73.
89. Shigetomi, H., et al., *Molecular mechanisms linking endometriosis under oxidative stress with ovarian tumorigenesis and therapeutic modalities.* Cancer Invest, 2012. **30**(6): p. 473-80.
90. Suzuki, S., et al., *MR findings of ruptured endometrial cyst: comparison with tubo-ovarian abscess.* Eur J Radiol, 2012. **81**(11): p. 3631-7.
91. D'Hooghe, T.M., et al., *Nonhuman primate models for translational research in endometriosis.* Reprod Sci, 2009. **16**(2): p. 152-61.
92. Tirado-Gonzalez, I., et al., *Endometriosis research: animal models for the study of a complex disease.* J Reprod Immunol, 2010. **86**(2): p. 141-7.
93. Dinulescu, D.M., et al., *Role of K-ras and Pten in the development of mouse models of endometriosis and endometrioid ovarian cancer.* Nat Med, 2005. **11**(1): p. 63-70.
94. Mariani, M., et al., *The selective vitamin D receptor agonist, elocalcitol, reduces endometriosis development in a mouse model by inhibiting peritoneal inflammation.* Hum Reprod, 2012. **27**(7): p. 2010-9.
95. Cheng, C.W., et al., *Activation of mutated K-ras in donor endometrial epithelium and stroma promotes lesion growth in an intact immunocompetent murine model of endometriosis.* J Pathol, 2011. **224**(2): p. 261-9.
96. Yamanaka, A., et al., *Primate model research for endometriosis.* Tohoku J Exp Med, 2012. **226**(2): p. 95-9.
97. Mayr, D., et al., *Does endometriosis really have premalignant potential? A clonal analysis of laser-microdissected tissue.* FASEB J, 2003. **17**(6): p. 693-5.

98. Smith, D.M., et al., *Arsenic trioxide induces a beclin-1-independent autophagic pathway via modulation of SnoN/SkiL expression in ovarian carcinoma cells.* Cell Death Differ, 2010. **17**(12): p. 1867-81.
99. Tan, T.H., J. Wallis, and A.J. Levine, *Identification of the p53 protein domain involved in formation of the simian virus 40 large T-antigen-p53 protein complex.* J Virol, 1986. **59**(3): p. 574-83.
100. Lilyestrom, W., et al., *Crystal structure of SV40 large T-antigen bound to p53: interplay between a viral oncoprotein and a cellular tumor suppressor.* Genes Dev, 2006. **20**(17): p. 2373-82.
101. Yang, G., et al., *Knockdown of p53 combined with expression of the catalytic subunit of telomerase is sufficient to immortalize primary human ovarian surface epithelial cells.* Carcinogenesis, 2007. **28**(1): p. 174-82.
102. Dive, C., et al., *Considerations for the use of plasma cytokeratin 18 as a biomarker in pancreatic cancer.* Br J Cancer, 2010. **102**(3): p. 577-82.
103. Fortier, A.M., E. Asselin, and M. Cadrin, *Keratin 8 and 18 loss in epithelial cancer cells increases collective cell migration and cisplatin sensitivity through claudin1 up-regulation.* J Biol Chem, 2013. **288**(16): p. 11555-71.
104. Lu, Y.M., et al., *Suppression of HER-2 via siRNA interference promotes apoptosis and decreases metastatic potential of SKOV3 human ovarian carcinoma cells.* Oncol Rep, 2013. **29**(3): p. 1133-9.
105. Liu, J., et al., *A genetically defined model for human ovarian cancer.* Cancer Res, 2004. **64**(5): p. 1655-63.
106. Del Bufalo, D., et al., *Involvement of hTERT in apoptosis induced by interference with Bcl-2 expression and function.* Cell Death and Differentiation, 2005. **12**(11): p. 1429-1438.
107. Nims, R.W., et al., *Short tandem repeat profiling: part of an overall strategy for reducing the frequency of cell misidentification.* In Vitro Cell Dev Biol Anim, 2010. **46**(10): p. 811-9.
108. Choi, J., et al., *Differential induction of autophagy by mTOR is associated with abnormal apoptosis in ovarian endometriotic cysts.* Mol Hum Reprod, 2013.
109. Kimura, T., et al., *Chloroquine in cancer therapy: a double-edged sword of autophagy.* Cancer Res, 2013. **73**(1): p. 3-7.
110. Guo, J.Y. and E. White, *Autophagy is required for mitochondrial function, lipid metabolism, growth and fate of KRAS (G12D) -driven lung tumors.* Autophagy, 2013. **9**(10).
111. Strohecker, A.M. and E. White, *Autophagy promotes -driven lung tumorigenesis by preserving mitochondrial metabolism.* Autophagy, 2013. **10**(2).
112. Yamada, T., et al., *Role of oxidative stress in vinorelbine-induced vascular endothelial cell injury.* Free Radic Biol Med, 2010. **48**(1): p. 120-7.
113. Oexle, H., E. Gnaiger, and G. Weiss, *Iron-dependent changes in cellular energy metabolism: influence on citric acid cycle and oxidative phosphorylation.* Biochim Biophys Acta, 1999. **1413**(3): p. 99-107.
114. Wu, Y. and R.M. Brosh, Jr., *DNA helicase and helicase-nuclease enzymes with a conserved iron-sulfur cluster.* Nucleic Acids Res, 2012. **40**(10): p. 4247-60.
115. Williams, R., et al., *Pathogenic implications of iron accumulation in multiple sclerosis.* J Neurochem, 2012. **120**(1): p. 7-25.

116. Ma, Y.S., et al., *Response to the increase of oxidative stress and mutation of mitochondrial DNA in aging.* Biochim Biophys Acta, 2009. **1790**(10): p. 1021-9.
117. Hegde, M.L., et al., *Oxidative genome damage and its repair in neurodegenerative diseases: function of transition metals as a double-edged sword.* J Alzheimers Dis, 2011. **24 Suppl 2**: p. 183-98.
118. Reif, P., et al., *Rupture of endometriotic ovarian cyst causes acute hemoperitoneum in twin pregnancy.* Fertil Steril, 2011. **95**(6): p. 2125 e1-3.
119. Alcantara, D.D., et al., *Cellular responses induced in vitro by iron (Fe) in a central nervous system cell line (U343MGa).* Genet Mol Res, 2013. **12**(2): p. 1554-60.
120. Samouelian, V., et al., *Chemosensitivity and radiosensitivity profiles of four new human epithelial ovarian cancer cell lines exhibiting genetic alterations in BRCA2, TGFbeta-RII, KRAS2, TP53 and/or CDNK2A.* Cancer Chemother Pharmacol, 2004. **54**(6): p. 497-504.
121. Liu, G., et al., *Stanniocalcin 1 and ovarian tumorigenesis.* J Natl Cancer Inst, 2010. **102**(11): p. 812-27.
122. Fan, H.Y., et al., *Consequences of RAS and MAPK activation in the ovary: the good, the bad and the ugly.* Mol Cell Endocrinol, 2012. **356**(1-2): p. 74-9.
123. Klionsky, D.J., et al., *Guidelines for the use and interpretation of assays for monitoring autophagy in higher eukaryotes.* Autophagy, 2008. **4**(2): p. 151-75.
124. Komatsu, M., S. Kageyama, and Y. Ichimura, *p62/SQSTM1/A170: physiology and pathology.* Pharmacol Res, 2012. **66**(6): p. 457-62.
125. Moscat, J. and M.T. Diaz-Meco, *p62: a versatile multitasker takes on cancer.* Trends Biochem Sci, 2012. **37**(6): p. 230-6.
126. Ni, H.M., et al., *Dissecting the dynamic turnover of GFP-LC3 in the autolysosome.* Autophagy, 2011. **7**(2): p. 188-204.
127. Galluzzi, L., et al., *Guidelines for the use and interpretation of assays for monitoring cell death in higher eukaryotes.* Cell Death Differ, 2009. **16**(8): p. 1093-107.
128. Sturm, B., H. Goldenberg, and B. Scheiber-Mojdehkar, *Transient increase of the labile iron pool in HepG2 cells by intravenous iron preparations.* Eur J Biochem, 2003. **270**(18): p. 3731-8.
129. Nylandsted, J., et al., *Heat shock protein 70 promotes cell survival by inhibiting lysosomal membrane permeabilization.* J Exp Med, 2004. **200**(4): p. 425-35.
130. Uchiyama, A., et al., *Translocation of iron from lysosomes into mitochondria is a key event during oxidative stress-induced hepatocellular injury.* Hepatology, 2008. **48**(5): p. 1644-54.
131. Wei, L., et al., *Altered regulation of Src upon cell detachment protects human lung adenocarcinoma cells from anoikis.* Oncogene, 2004. **23**(56): p. 9052-61.
132. Liu, B., et al., *Cyclooxygenase-2 inhibitors induce anoikis in osteosarcoma via PI3K/Akt pathway.* Med Hypotheses, 2012. **79**(1): p. 98-100.
133. Ma, Z., et al., *p66(Shc) restrains Ras hyperactivation and suppresses metastatic behavior.* Oncogene, 2010. **29**(41): p. 5559-67.
134. Debnath, J., *p66(Shc) and Ras: controlling anoikis from the inside-out.* Oncogene, 2010. **29**(41): p. 5556-8.
135. Anger, D.L., et al., *Tyrosine receptor kinase B (TrkB) protein expression in the human endometrium.* Endocrine, 2007. **31**(2): p. 167-73.

136. Hong, J.H., et al., *Iron promotes the survival and neurite extension of serum-starved PC12 cells in the presence of NGF by enhancing cell attachment.* Mol Cells, 2003. **15**(1): p. 10-9.
137. He, X., et al., *Downregulation of HtrA1 promotes resistance to anoikis and peritoneal dissemination of ovarian cancer cells.* Cancer Res, 2010. **70**(8): p. 3109-18.
138. Caneba, C.A., et al., *Pyruvate uptake is increased in highly invasive ovarian cancer cells under anoikis conditions for anaplerosis, mitochondrial function, and migration.* Am J Physiol Endocrinol Metab, 2012. **303**(8): p. E1036-52.
139. Page, V., et al., *BAG-1 p29 protein prevents drug-induced cell death in the presence of EGF and enhances resistance to anoikis in SKOV3 human ovarian cancer cells.* Biochem Biophys Res Commun, 2005. **328**(4): p. 874-84.
140. Rubinstein, A.D. and A. Kimchi, *Life in the balance - a mechanistic view of the crosstalk between autophagy and apoptosis.* J Cell Sci, 2012. **125**(Pt 22): p. 5259-68.
141. Sundqvist, J., et al., *Expression of adhesion, attachment and invasion markers in eutopic and ectopic endometrium: a link to the aetiology of endometriosis.* Hum Reprod, 2012. **27**(9): p. 2737-46.
142. Somigliana, E., et al., *Adhesion prevention in endometriosis: a neglected critical challenge.* J Minim Invasive Gynecol, 2012. **19**(4): p. 415-21.
143. Kaminskyy, V.O., et al., *Suppression of basal autophagy reduces lung cancer cell proliferation and enhances caspase-dependent and -independent apoptosis by stimulating ROS formation.* Autophagy, 2012. **8**(7): p. 1032-44.
144. Wu, D. and A.I. Cederbaum, *Inhibition of autophagy promotes CYP2E1-dependent toxicity in HepG2 cells via elevated oxidative stress, mitochondria dysfunction and activation of p38 and JNK MAPK.* Redox Biol, 2013. **1**(1): p. 552-565.
145. Gandesiri, M., et al., *DAPK plays an important role in panobinostat-induced autophagy and commits cells to apoptosis under autophagy deficient conditions.* Apoptosis, 2012. **17**(12): p. 1300-15.
146. Zhu, X., et al., *Autophagy stimulates apoptosis in HER2-overexpressing breast cancers treated by lapatinib.* J Cell Biochem, 2013. **114**(12): p. 2643-53.
147. Somigliana, E., et al., *Endometrial ability to implant in ectopic sites can be prevented by interleukin-12 in a murine model of endometriosis.* Hum Reprod, 1999. **14**(12): p. 2944-50.
148. Ye, Q., et al., *ERK and AKT signaling cooperate to translationally regulate survivin expression for metastatic progression of colorectal cancer.* Oncogene, 2013.
149. Zhang, Y. and X.F. Zheng, *mTOR-independent 4E-BP1 phosphorylation is associated with cancer resistance to mTOR kinase inhibitors.* Cell Cycle, 2012. **11**(3): p. 594-603.
150. Gallagher, P.J. and E.K. Blue, *Post-translational regulation of the cellular levels of DAPK.* Apoptosis, 2013.
151. Martelli, A., et al., *Clinical data and characterization of the liver conditional mouse model exclude neoplasia as a non-neurological manifestation associated with Friedreich's ataxia.* Dis Model Mech, 2012. **5**(6): p. 860-9.
152. Wheater, M.J., P.W. Johnson, and J.P. Blaydes, *The role of MNK proteins and eIF4E phosphorylation in breast cancer cell proliferation and survival.* Cancer Biol Ther, 2010. **10**(7): p. 728-35.
153. Chang, C.C., et al., *Simvastatin downregulates the expression of hepcidin and erythropoietin in HepG2 cells.* Hemodial Int, 2013. **17**(1): p. 116-21.

154. Tauber, S., et al., *Transcriptome analysis of human cancer reveals a functional role of heme oxygenase-1 in tumor cell adhesion.* Mol Cancer, 2010. **9**: p. 200.
155. Eliot, T.S., *Collected poems, 1909-1935*. 1936, New York,: Harcourt. 220 p.
156. Barlow, C.A., et al., *The role of genotoxicity in asbestos-induced mesothelioma: an explanation for the differences in carcinogenic potential among fiber types.* Inhal Toxicol, 2013. **25**(9): p. 553-67.

Appendix

Request for reproduction of article for thesis: The paper titled "Iron modulates cell survival in a Ras- and MAPk- dependent manner in ovarian cells" is represented in Chapter 4 of the thesis presented herein [28].

Jones, Verity [V.Jones@nature.com]

Actions
To: Bauckman, Kyle A.
Cc:'CDDisease' [cell.death.disease@uniroma2.it];
Vickerstaff, Rebecca [R.Vickerstaff@nature.com]

Wednesday, January 22, 2014 5:30 AM

Dear Kyle,

Many thanks for your enquiry, which was forwarded on by the *Cell Death & Disease* editorial office.

As an author, you have the right to use this manuscript and figures, as per the licence-to-publish you signed before publication:

Ownership of copyright in the article remains with the Authors, and provided that, when reproducing the Contribution or extracts from it, the Authors acknowledge first and reference publication in the Journal, the Authors retain the following non-exclusive rights:

a) To reproduce the Contribution in whole or in part in any printed volume (book or thesis) of which they are the author(s).

b) They and any academic institution where they work at the time may reproduce the Contribution for the purpose of course teaching.

c) To post a copy of the Contribution as accepted for publication after peer review (in Word or Tex format) on the Authors' own web site or institutional repository, or the Authors' funding body's designated archive, six months after publication of the printed or online edition of the Journal, provided that they also give a hyperlink from the Contribution to the Journals web site.

d) To reuse figures or tables created by them and contained in the Contribution in other works created by them.

I hope this helps – please don't hesitate to contact me if I can be of any further assistance.

Best wishes,
Verity

Verity Jones
Publishing Assistant (Academic Journals)
nature publishing group

The Macmillan Campus
4 Crinan Street,
London ¦ N1 9XW

Tel: +44 (0)207 843 4877
Fax: +44 (0)207 843 4839

Email: v.jones@nature.com

Da: "Bauckman, Kyle A." <Kyle.Bauckman@moffitt.org>
Data: martedì 21 gennaio 2014 15.24
A: Cell Death and Disease <cell.death.disease@uniroma2.it>, Rebecca Vickerstaff <R.Vickerstaff@nature.com>
Oggetto: RE: Request for reproduction of article for thesis

Hello, I just wanted to follow up with my request below. I am writing to request permission to reproduce a version of the paper entitled " Iron modulates cell survival in a Ras- and MAPk- dependent manner in ovarian cells" for my doctoral thesis. I am the primary author of this paper. The article appear in cell death and disease April 18th 2013 (PMCID: PMC3668627). I would greatly appreciate it if you could email your decision to Kyle.Bauckman@moffitt.org.

Thank-you for your time and assistance
-Kyle

_____

About the Author

Kyle attended the University of Florida for his undergraduate degree in Zoology. He worked in a marine biology lab focused on horseshoe crab reproductive behavior until his graduation in 2009. Afterwards, he attended the University of South Florida to earn his PhD in cancer biology. Kyle worked in the lab of Dr. Meera Nanjundan and focused on endometriosis and ovarian cancer.